COUPLED HEAT AND MOISTURE TRANSFER IN UNSATURATED SOIL FOR THE MODELING OF SHALLOW HORIZONTAL GROUND LOOPS

By

Ray Wu

A thesis submitted in partial fulfillment of the requirements for the degree of

MASTER OF SCIENCE
(GEOLOGICAL ENGINEERING)

At the
UNIVERSITY OF WISCONSIN-MADISON
2013

Coupled Heat and Moisture Transfer in Unsaturated Soil for the Modeling of Shallow Horizontal Ground Loops

_____	_____
Student Name	**Campus ID Number**

Approved

_____

date

James M. Tinjum

Assistant Professor

EXECUTIVE SUMMARY

Ground-source heat pump systems with shallow horizontal ground loops can be used to extract or reject heat from the ground to heat and cool residential and commercial buildings. Compared to traditional heating and air conditioning systems, these ground-source heat pump systems are more energy efficient and cost effective to operate. However, major barriers, such as high initial capital costs and lack of consumer confidence in the benefits of the system, continue to limit increased implementation. These barriers are, in part, attributed to the conservative design of the ground loop.

The design principles of geothermal ground loops are straightforward; however, system design is complicated by the numerous design parameters necessary to calculate the length of ground loop. Previous studies have suggested that the most influential design parameter is the thermal conductivity of the soil surrounding the ground loop. In current state-of-practice, conservative and constant thermal properties of the ground formation into which the ground loop will be installed are often estimated or assumed. As a consequence, the ground loop may be oversized and the entire system may be inefficient and more costly to install and operate. The use of conservative and constant thermal properties of soil is justified in that the properties can be difficult and prohibitively expensive to measure. However, the use of constant soil properties is unrepresentative of actual conditions since the behavior of soil is expected to vary temporally and spatially during operation of the ground loop. Furthermore, the use of conservative soil properties is disadvantageous because oversized ground loops are expected to adversely impact the performance and economic competitiveness of ground-source heat pump systems.

In this study, models based on two-dimensional, finite element methods were developed to simulate coupled heat and moisture flow during operation of a shallow horizontal ground loop. To improve modeling of coupled heat and moisture transfer, constitutive relationships that define

variable behavior of soil, the thermal conductivity dryout curve (i.e., thermal conductivity as a function of water content) and soil-water characteristic curve (i.e., suction as a function of water content), were experimentally determined and coupled for use in the models. Six models were performed for three different backfill soils simulated with either variable soil properties or the conventional method of using constant soil properties. Simulation results provide information about the spatial and temporal profiles of ground temperature and water content during one year of operating a ground loop.

Furthermore, an equation to calculate the required length of ground loop for a certain heat pump capacity and coefficient of performance was derived. The equation was used to calculate the length of ground loop using results obtained from each model simulation. Models simulated with variable soil properties resulted in lengths of ground loop that were 25% to 50% shorter than models simulated with conservative and constant soil properties. The difference in ground loop lengths also suggests that accurately predicting the thermal conductivity of soil surrounding the ground loop could save thousands of dollars. In situations where the thermal conductivity of soil is greatly improved from the thermal conductivity of native soil or a conservative estimate, the additional costs associated with enhancing or measuring soil thermal conductivity are compensated by significant reductions of the length of ground loop. The use of coupled thermal conductivity dryout curves and soil-water characteristic curves provides a more realistic representation of thermo-hydro behavior of soil surrounding shallow horizontal ground loops as well as improved design parameters for calculating the length of the ground loop.

ACKNOWLEDGEMENTS

I would like to especially thank my advisor, Professor James Tinjum, for his invaluable advice and endless support during my graduate studies and as an undergraduate researcher. Thank you for the confidence you had in me. Your guidance, mentorship, patience, constructive criticism, and flexibility were essential for this work to be completed. Moreover, your generosity of time and resources are greatly appreciated. I owe much of my success, inside and outside of academics, to you.

I would also like to express my gratitude to my thesis committee members, Professors Dante Fratta and Bill Likos. Thank you for providing opinions and suggestions for the improvement of my knowledge and experience and for challenging me to think from different perspectives. I consider myself extremely fortunate to have had the opportunity to work with the inspirational mentors on my committee. Additionally, I would like to thank Professor Craig Benson for introducing me to the geological engineering discipline and offering guidance when it was needed.

Special thanks are due to my fellow research group colleagues Jun Yao and Hyunjun Oh for their help in the laboratory as well as their ideas and suggestions that helped improve my work. I sincerely enjoyed collaborating with both of you. More thanks are due to Xiaodong Wang, the geotechnical laboratory manager, for his advice and assistance in developing and setting up the apparatus used in my research. I thank Jim Zhang and Robert Thode of SoilVision Systems Ltd., for their assistance with modeling shallow horizontal ground loops using SVFlux and SVHeat. The results and conclusions expressed herein are solely those of the author, and do not necessarily represent the policies or opinions of SoilVision Systems.

I am extremely grateful to my family for their constant source of support and encouragement. I would also like to thank all my friends, and particularly my fellow geo-

colleagues for their support and keeping the office entertaining. My sincere appreciation extends to all who have aided and encouraged me during my time at the University of Wisconsin-Madison.

TABLE OF CONTENTS

LIST OF FIGURES

LIST OF TABLES

1. INTRODUCTION

In recent decades, ground-source heat pump (GSHP) systems have received considerable attention as an energy efficient technology for residential and commercial heating and cooling. Approximately 50,000 GSHP systems are sold each year in the United States (Do and Haberl, 2010). As one of the fastest growing applications of alternative energy, a primary appeal of GSHP systems is their efficiency and widespread geographic applicability. GSHP systems are efficient because the geothermal exchange occurs through the sustainable transfer of stored thermal energy. GSHP systems can also be implemented worldwide because the ground acts as an effective thermal source and sink. Natural ground temperatures become relatively stable with increasing depth and are closer to room temperature (e.g., 20 °C) than air temperature during the year.

Noteworthy recognition of the promising potential of GSHP systems was publicized during the late 20th century as government reports by the United States Environmental Protection Agency and Natural Resources Canada stated, respectively, that "GSHPs are the most energy efficient, environmentally clean, and cost-effective systems available" (US EPA, 1993) and that "There is unlikely to be a potentially larger mitigating effect on greenhouse gas emissions and the resulting global warming impact of buildings from any other current, market available single technology, than from GSHPs" (Caneta Research, 1999). In comparison to traditional heating, ventilation, and air conditioning (HVAC) systems, GSHP systems offer benefits of reduced greenhouse gas emissions, high reliability, low maintenance, and lower energy, operating, and life-cycle costs (Inalli and Esen, 2005; Tarnawski et al., 2009; Congedo et al., 2012). Despite these advantages, however, several barriers continue to hinder increased implementation of GSHP systems. Important barriers include the high initial capital costs of GSHP systems and the lack of consumer knowledge and/or confidence in GSHP system benefits (Hughes, 2008).

The high initial investment and lack of consumer confidence in GSHP systems are, in part, related to the design of the GSHP's ground loop. As shown in Table 1-1, the ground loop is generally the most expensive component of a GSHP system. Cane and Forgas (1991) estimated that the length of ground loops used in GSHP applications were oversized by about 10% to 30% in the North American market. The length of ground loops may still be oversized due to prevalent use of rule of thumbs (i.e., certain length of trench per quantity of load) and conservative estimates of subsurface properties (McQuay International, 2002; ASHRAE, 2007; Remund and Carda, 2009). Conservatively designed ground loops safeguard against worst-case scenarios but result in inefficient and uneconomical GSHP systems. Shallow horizontal ground loops have potential to provide an effective compromise between efficiency and cost if the thermal performance of the ground loop is improved and the material, installation, and operating costs are reduced. By improving the design of ground loops, GSHP systems can be optimized and have better performance and lower capital investments.

This thesis focuses on using energy geotechnics to improve the design of shallow horizontal ground loops. Energy geotechnics is an emerging discipline in which engineers and scientists employ principles of geotechnical engineering and the physical sciences of geology, physics, and chemistry for the advancement and design of energy-related systems, including renewables. In this study, the mechanisms and properties that govern thermal and hydraulic behavior of unsaturated soil are applied to predict coupled heat and moisture flow associated with operation of a shallow horizontal ground loop. More specifically, experimentally determined thermal conductivity dryout curves (TCDCs) and soil-water characteristic curves (SWCCs) were coupled in finite-element models to simulate temporal and spatial variations of soil surrounding horizontal ground loops. Results from the simulations were used to estimate the

required total length of ground loop attached to a GSHP system using a heat pump with nominal 10.55-kW capacity and coefficient of performance (COP) of 4. Changes in the required total length of ground loop as well as associated costs are compared between models that were simulated with a soil's TCDC versus similar models that were simulated with a conservative value of soil thermal conductivity (λ_{soil}).

Chapter 2 contains background information about GSHP systems, the importance of λ_{soil} and TCDCs, and methods for experimental determination of TCDCs. Chapter 3 discusses the selected materials, the methods used to determine material properties, and setup of a two-dimensional horizontal ground loop model based on finite-element analysis. Chapter 4 presents results and analysis of the model simulations. Chapter 5 summarizes conclusions drawn from model results and discusses recommended future work to improve modeling of shallow horizontal ground loops. In the appendices, a draft of an ASTM International standard for experimental determination of thermal resistivity dryout curves (TRDCs) is included (Appendix A); a discussion on testing λ_{soil} at elevated temperatures is included (Appendix B); and an overview of finite-modeling with SVOffice is presented (Appendix C).

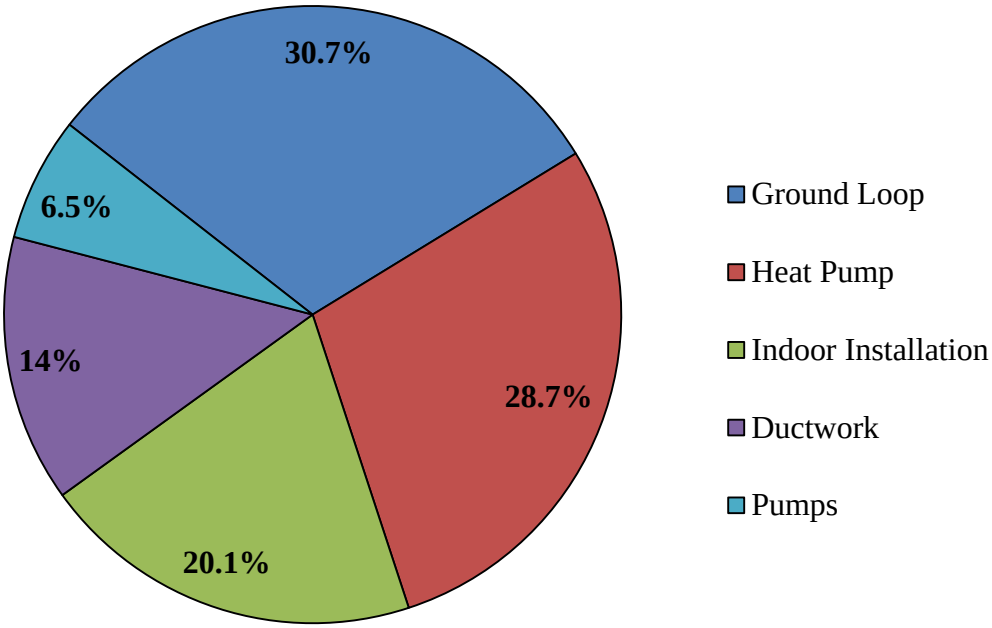

Figure 1-1. Component costs of a GSHP system using a heat pump with 10.55 kW capacity (adapted from Kavanaugh et al., 1995). Ground loop costs include pipe installation and trenching. Heat pump costs include type of heat pump unit. Indoor installation costs include thermostats, auxiliary heat, wiring, unit connections, non-loop related labor, overhead, and profit. Ductwork costs include duct system installation. Pump costs include type of circulator pump.

2. BACKGROUND

The term GSHP is inclusive of a three-loop system that transfers heat between the space within a building and the ground (Figure 2-1). These loops include a distribution loop (i.e., ductwork) within the building to distribute the desired heating or cooling, a refrigeration loop (i.e., heat pump) typically housed in the lower level of a building to enhance the heat exchange between the other two loops, and a ground loop (i.e., geothermal heat exchanger) that is usually buried below the ground surface in a trench, borehole, or body of water to reject or extract heat to or from the ground, groundwater, or surface water. The design and operation of the ventilation ductwork and heat pump are well understood and efficient from a mechanical engineering perspective. However, the soil properties that influence the design of the ground loop are uncertain due to the complexity of soil thermal behavior (i.e., energy geotechnics).

The ground loop can be open or closed and arranged vertically or horizontally (Figure 2-2). The most commonly installed type of ground loops is the closed vertical heat exchanger (Curtis et al., 2005). In general, closed loops are preferred since the direct connection between the ground loop and subsurface in open loops presents environmental concerns such as groundwater contamination. Furthermore, the vertical configuration has been preferred because vertical heat exchangers have more efficient heat transfer performance and require a relatively smaller footprint. In contrast, horizontal heat exchangers require a larger footprint and are more susceptible to seasonal fluctuations (i.e., variable heat transfer performance), but may be cost effective because trench installation equipment is widely available and inexpensive compared to borehole drilling (ASHRAE, 2007). For smaller heat-load applications, such as residential and commercial heating and cooling, shallow vertical (e.g., < 50 m below ground surface (bgs)) or horizontal (e.g., < 2 m bgs) ground loops are used.

In the horizontal configuration, the ground loop is typically buried 1 m to 2 m bgs and a fluid (e.g., water or water/antifreeze mixture) is circulated within the loop, transferring heat from the ground to the ground loop or vice versa. The second law of thermodynamics places constraints upon the direction of heat transfer to and from the ground loop (i.e., heat naturally flows from higher temperature regions to colder temperature regions). As shown in Figure 2-3, the advantage of using the ground as a thermal source and sink is that at approximately five meters bgs, the ground temperature is relatively stable due to the high thermal inertia of soil (i.e., ability of soil to conduct and store heat), which attenuates temperature fluctuations and causes a time lag between climatic variations and the ground (Florides and Kalogirou, 2007). Therefore, in the winter, when the ground temperature is warmer than the air temperature, cooler fluid in the ground loop extracts heat from the warmer ground (i.e., heating mode). Conversely, in the summer, when the ground temperature is cooler than the air temperature, warmer fluid in the ground loop rejects heat to the cooler ground (i.e., cooling mode). However, ground temperature is not the only subsurface property necessary to quantify the heat transfer of ground loops.

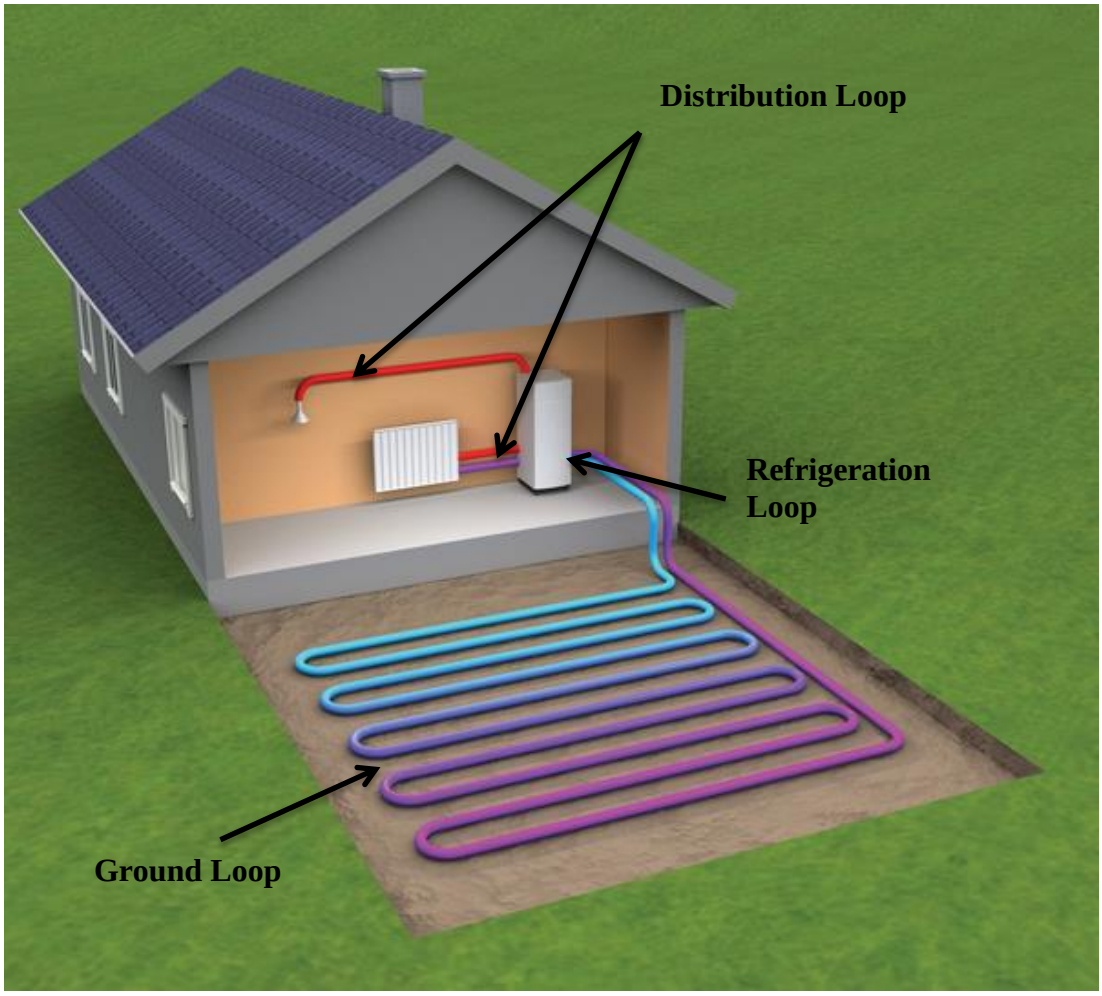

Figure 2-1. The GSHP system is a three-loop system consisting of a distribution, refrigeration, and ground loop (Ultimate Green Energy, 2013).

(a)

(b)

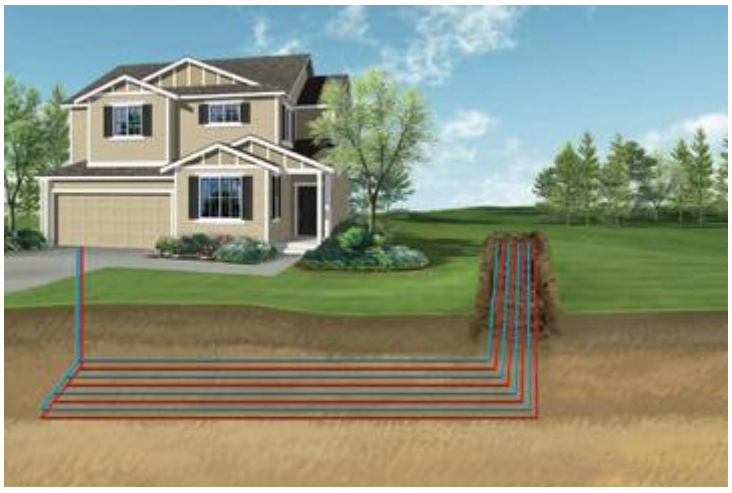

(c)

Figure 2-2. Common types of ground loops: (a) open, (b) closed horizontal, and (c) closed vertical (GeoComfort, 2013).

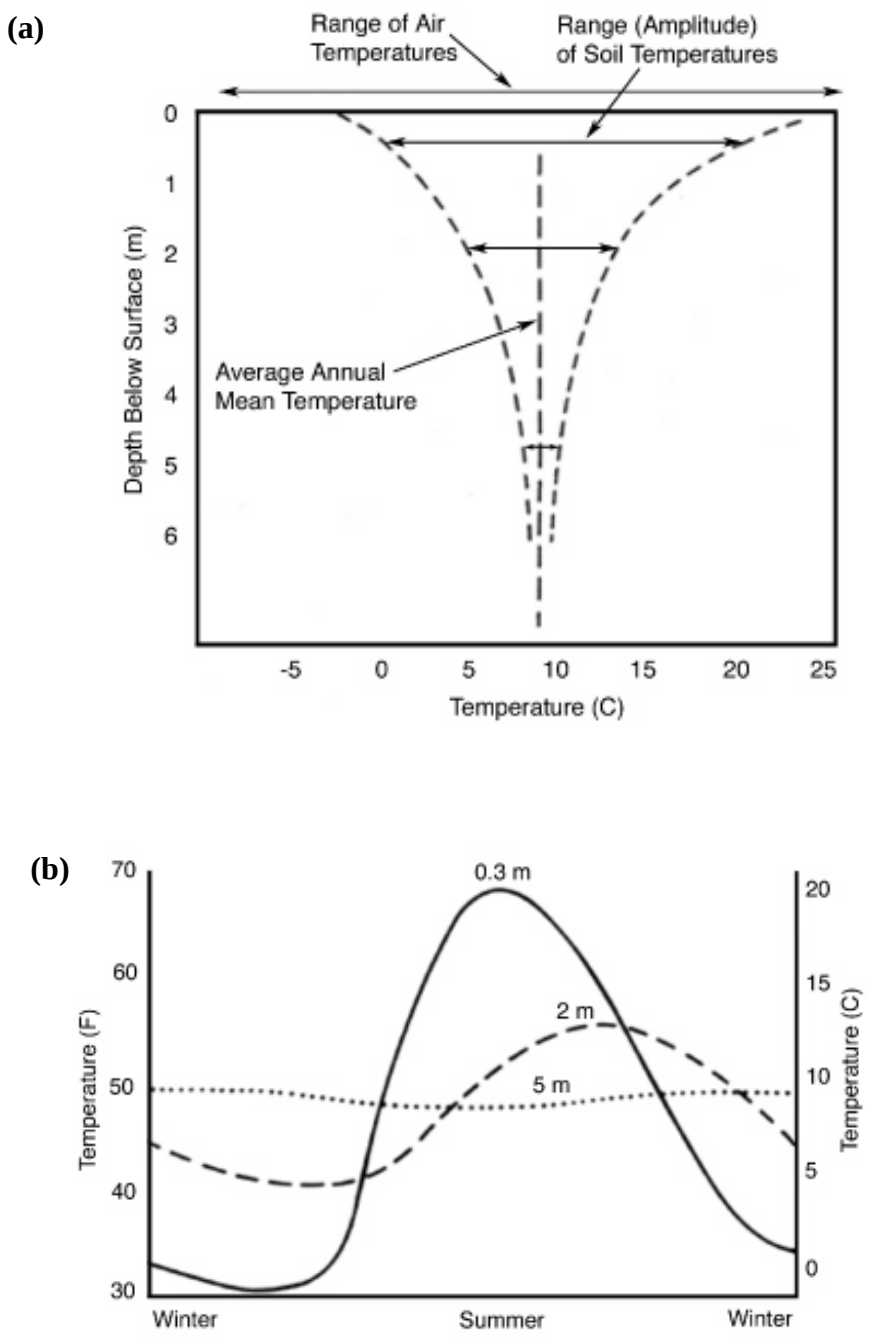

Figure 2-3. Examples of (a) depth dependence of annual range of ground temperatures and (b) annual variation of ground temperature with depth below ground surface (Williams and Gold, 1976).

2.1. Conductive Heat Transfer in Soil

The three primary mechanisms of heat transfer through soil are conduction, convection, and radiation. Conductive heat transfer occurs when kinetic energy is transferred through direct physical contact at the molecular level due to temperature gradients. Convective heat transfer occurs when kinetic energy is transported by the bulk movement of the pore fluid. Radiation heat transfer occurs when electromagnetic energy, such as solar radiation, is emitted from one object and is transmitted through another object. Of these heat transfer mechanisms, conduction generally dominates, convection is important only if there is a high flow rate of pore fluid (e.g., groundwater flow), and radiation is unimportant expect for surface soils (Farouki, 1981; Mitchell and Soga, 2005; Fredlund et al., 2012). Therefore, conductive heat transfer is typically the only heat transfer mechanism considered in engineering problems that involve heat transfer through soil. In conductive heat transfer, a single material variable, thermal conductivity (λ) is used to define the rate of heat conduction through the material. Fourier's Law of steady state heat conduction relates λ to the driving potential for heat flow is (one-dimensional):

$$\frac{\Delta Q}{\Delta t} = -\lambda A \frac{\Delta T}{\Delta x} \tag{2.1}$$

where ΔQ is the quantity of heat flow over a given time, Δt, A is the cross-sectional area, and ΔT is the temperature gradient over a given distance, Δx. Rearrangement of Fourier's Law provides a mathematical expression to define λ_{soil} as the quantity of heat transfer through a unit area of soil in a unit of time under a unit temperature gradient over a unit distance.

For non-steady state heat conduction, as in the case of GSHP systems, Fourier's Law of transient heat conduction is modified to include time-varying temperatures and thermal storage of the material (one-dimensional):

$$\frac{\partial T}{\partial t} = D\frac{\partial^2 T}{\partial x^2} \tag{2.2}$$

$$D = \frac{\lambda}{\rho c_p} \tag{2.2a}$$

where T is temperature, t is time, D is thermal diffusivity, ρ is density, and c_p is specific heat capacity at constant pressure. Another mechanism that contributes to the overall conductive heat transfer is latent heat transfer, the thermal energy required to change a substance from one state to another (e.g., transitions between states of solid, liquid, and gas). Multiphase pore fluid movement due to moisture and temperature gradients (i.e., evaporation or condensation of water) enhances λ_{soil} (Hansen et al., 1970; Su, 1981). The classical theory used to describe coupled heat and moisture flow was developed by Philip and de Vries (1957). The governing differential equation for moisture movement in porous materials under combined temperature and moisture gradients is given by:

$$\frac{\partial \theta}{\partial t} = \nabla(D_T \nabla T) + \nabla(D_\theta \nabla \theta) + \frac{\partial \mathrm{k}}{\partial t} \tag{2.3}$$

where θ is volumetric water content, D_T is thermal moisture diffusivity, ∇T is temperature gradient, D_θ is isothermal moisture diffusivity, $\nabla\theta$ is moisture content gradient, and k is hydraulic conductivity. In Eq. 2.3, the first right-hand side term represents liquid and vapor flow driven by temperature gradients, the second term represents liquid and vapor flow driven by moisture content gradients, and the third term represents liquid flow driven by gravity. In soil, the diffusivity terms account for both liquid and vapor phases and are functions of soil suction (ψ_{soil}), which is the thermodynamic potential of soil pore water. Liquid diffusivity dominates at high water contents, whereas vapor diffusivity dominates at low water contents. Philip and de Vries (1957) also derived an equation for heat conduction in soil with distillation effects induced by moisture migration:

$$C\frac{\partial T}{\partial t} = \nabla(\lambda_{soil}\nabla T) - L\nabla\left(D_{\theta_{vap}}\nabla\theta\right) \quad (2.4)$$

where C is volumetric heat capacity, L is latent heat of vaporization, and $D_{\theta_{vap}}$ is vapor diffusivity. To better account for changes of moisture content in the liquid and the vapor phase (i.e., when the liquid and vapor phase are of the same order of magnitude), an extension of Eq. 2.4 is discussed in de Vries (1958).

2.1.1. Factors influencing soil thermal conductivity

Although λ_{soil} generally only varies over one order of magnitude, λ_{soil} is challenging to measure because it is a function of soil composition, density, temperature, and water content. The dependency of λ_{soil} on these factors has been studied in geotechnical and soil science literature over many decades (Woodside and Messmer, 1961; Johansen, 1977; Sepaskhah and Boersma, 1979; Farouki, 1981; Salomone et al., 1984; Hopmans and Dane, 1986; Brandon and Mitchell, 1989; Campbell et al., 1994; Abu-Hamdeh and Reeder, 2000; Campbell, 2006; Woodward and Tinjum, 2012). However, there are limited physically based models to predict λ_{soil}. Since the database of λ_{soil} is still limited to specific soils, densities, temperatures, or water contents, an understanding of the expected behavior of λ_{soil} under various conditions is important.

An unsaturated soil is a type of porous material with multiple phases (i.e., solid, liquid and vapor). Since heat flows through a network of minerals, water, and air in unsaturated soils, the volume fractions and conductivities of the soil constituents (i.e., mineralogy, porosity, and degree of saturation) influence the overall λ_{soil}. de Vries (1963) observed that the ability of soil to transmit heat was a function of the relative proportions of its constituents and developed a model to estimate λ_{soil} based on a weighted sum calculation of the conductivities of the soil constituents:

$$\lambda = \frac{\sum_{i=1}^{n} k_i \lambda_i x_i}{\sum_{i=1}^{n} k_i \, x_i} \tag{2.5}$$

where n is the number of components, λ_i is the thermal conductivity of each component, x_i is the volume fraction of each component, and k_i is the volume of each component. The values for k_i can be computed if the soil particles are assumed to be of ellipsoidal shape and are far enough that they do not influence each other:

$$k_i = \frac{1}{3}\sum_{i=1}^{n}[1 + \left(\frac{\lambda_l}{\lambda_0} - 1\right) g_i]^{-1} \tag{2.6}$$

where λ_l is the thermal conductivity of dry particles, λ_0 is the thermal conductivity of the continuous fluid phase (i.e., air or water), and g_i represents the shape factors for each component considered as an ellipsoid. de Vries (1963) also proposed an $\lambda_{apparent}$ term to capture the thermal conductivity of dry air (λ_a) and latent heat transport within the pores of soil:

$$\lambda_{apparent} = \lambda_a + \lambda_v \tag{2.7}$$

where λ_v is the thermal conductivity of vapor movement and is proportional to relative humidity (h) and thermal conductivity of saturated vapor ($\lambda_v{}^s$):

$$\lambda_v = h\lambda_v{}^s \tag{2.8}$$

Further, h and $\lambda_v{}^s$ can be calculated by:

$$\psi = -\frac{RT}{v_{wo}\omega_v}\ln(h) \tag{2.9}$$

$$\lambda_v{}^s = \frac{LDP}{RT(R - P_w^s)}\frac{dP_w^s}{dT} \tag{2.10}$$

where ψ is suction, v_{wo} is the specific volume of water, ω_v is the molecular mass of water vapor, L is latent heat of vaporization, R is the universal gas constant, D is the vapor diffusion coefficient; P is the total pressure equal to the summation of atmospheric and vapor pressure; P_w^s

is the saturated vapor pressure, and T is temperature. The de Vries model is often referenced as a theoretical basis for estimating λ_{soil}.

In general, solids transfer heat better than liquids and liquids better than gases because conductive heat transfer depends on the proximity of physical contacts at the molecular level (i.e., particles are closer together in solids). In terms of solid particles, coarse-grained soils generally exhibit higher λ_{soil} than fine-grained soils. Among the diverse set of potential minerals in soil, quartz is the most prevalent mineral and has high λ. In contrast, the clay minerals of fine-grained soils have low λ, about two-thirds less than quartz. For all other minerals, λ generally varies within one order of magnitude between 1 W/m-K to 10 W/m-K (Côté and Konrad, 2005). Besides minerals, air and water usually comprise the remainder of the soil's composition. Although water has a lower λ than minerals, the presence of water is extremely important because the λ of water is two orders of magnitude greater than the λ of air. Therefore, in terms of soil constituents alone, a saturated soil made of quartz will have the highest λ_{soil} and conductive heat transfer. A list of typical λ values for common soil constituents is shown in Table 2-1.

The density of soil has a significant influence on λ_{soil}. Dry density of soil increases as void space is reduced (i.e., decreased porosity and void ratio). The increase in soil dry density can enhance λ_{soil} in several ways: (1) increased physical contact between solid particles improves heat flow paths, (2) higher λ of solid particles replace lower λ of air, (3) reduced hydraulic permeability retains absorbed water, and (4) limited vegetation root growth prevents removal of water from the soil (Salomone et al., 1984; Brandon and Mitchell 1989; Abu-Hamdeh and Reeder, 2000). The density of soil can be modified through a variety of densification techniques such as dynamic loading, vibrating (best for sand), rolling, and kneading. Brandon and Mitchell (1989) noted that some sands compacted wet and then dried to a lower water content had

significantly higher λ_{soil} than when compacted initially at the lower water content, indicating the initial compaction water content also greatly influenced λ_{soil}.

Temperature influences λ_{soil} because thermal properties of soil constituents are temperature dependent. The effect of increasing temperature on the λ of soil minerals versus the λ of liquids and gases is opposite of each other. With the exception of feldspars, crystalline minerals in soil exhibit a decrease in λ with increasing temperature. In contrast, the λ of water and gases increase with increasing temperature (Van and Winterkorn, 1959). Since elevated temperatures increase the kinetic energy of water and gas molecules, molecular collisions are more frequent and conductive heat transfer increases. Additionally, water can absorb heat through rupture of hydrogen bonds; the frequency of hydrogen bond ruptures increases with increasing temperature (Brandon and Mitchell, 1989). In unsaturated soils, the net effect of opposing λ between minerals versus liquids and gases is an overall increase in λ_{soil} with increasing temperature (Sepashka and Boersma, 1979; Campbell et al., 1994; Hiraiwa and Kasubuchi, 2000; and Smits et al., 2012).

In Section 2.2, heat from moisture movement in porous materials under combined temperature and moisture gradients was referred to as latent heat transfer. In moist soil at room temperature (e.g., 20 °C), 10% to 20% of the total heat transport is as latent heat through the pores (Campbell, 2006). At higher temperatures, latent heat transfer becomes a more important mechanism since water gains potential to evaporate (i.e., liquid water immediately evaporates at 100 °C). However, the contributions of enhanced latent heat transfer are generally limited to an intermediate range of saturation ($0.1 < S < 0.6$) because there needs to be enough liquid water to evaporate, sufficient air-water interfacial surfaces for evaporation and condensation, and enough air space for vapor movement (Smits et al., 2012). For GSHP systems, the effects of elevated

temperature on λ_{soil} are not expected to be significant since building heating and cooling applications are categorized as low-temperature (generally < 32 °C) applications (ASHRAE, 2007). A more detailed discussion of elevated temperature effects on λ_{soil} is presented in Appendix B.

Although λ_{soil} is dependent on mineralogy, density, and temperature, these conditions are often relatively constant in a specific soil. However, water content (i.e., gravimetric water content (w), volumetric water content (θ), or degree of saturation (S)) can be highly variable and can have the most significant effect on λ_{soil}. Figure 2-4 illustrates the importance of degree of saturation on λ_{soil}. In soil, conductive heat transfer occurs through solid particle contacts and continuous pore fluid phases. Heat conduction in fully dry soil is limited to the physical contact between grains and the corresponding preferential cross-sectional area (i.e., effective flow area) for heat flow is small (Figure 2-4a). On the other hand, heat conduction in fully saturated soil is maximized as the effective flow area is widened to incorporate the addition of the continuous liquid phase (Figure 2-4d). In the unsaturated range between and dry and saturated soil, heat conduction increases with increasing saturation and widening of the effective flow area (Figures 2-4b and 2-4c).

Table 2-1. λ of common materials in soils (adapted from Côté and Konrad, 2005).

Material	λ (W/m-K)
Air (20 °C)	0.024
Water (20 °C)	0.60
Ice (0 °C)	2.24
Quartz	7.69
Feldspars	1.98
Calcite	3.59
Dolomite	5.51
Mica	2.75
Chlorite	5.15
Olivine	4.10
Clay Minerals	2.90
Organic Matter	0.25

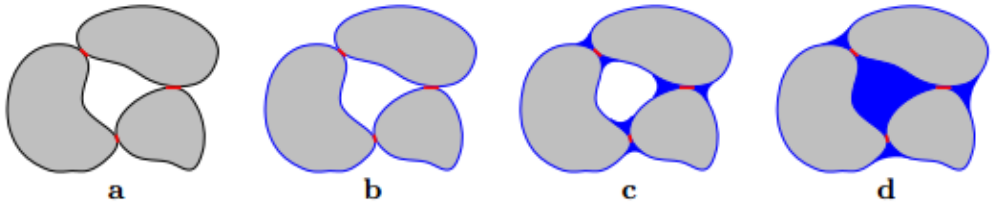

Figure 2-4. λ_{soil} as a function of water content in a coarse-grained soil. Greater heat conduction can occur when the effective flow area (i.e., sum of physical particle contacts (red area) and continuous fluid phase (blue area)) is larger. Increasing saturation occurs from left to right, completely dry (a) to saturated (d). The fully dry soil in (a) would be expected to have low λ_{soil} and the fully saturated soil in (d) would be expected to have high $\lambda_{soil.}$ (Roth, 2012).

2.1.2. The thermal conductivity dryout curve (TCDC)

The relationship between λ_{soil} and water content is referred to as the thermal conductivity dryout curve (TCDC). In general, the TCDC exhibits a nonlinear shape as shown in Figure 2-5a. Typically, four distinct regions of moisture-dependent λ_{soil} behavior are seen over a full range of saturation on a TCDC: (I) a nearly horizontal linear slope between $0.6 < S < 1.0$, (II) a mild change and shallowly dipping slope between $0.1 < S < 0.6$, (III) an abrupt change and steeply dipping slope between $0.05 < S < 0.1$, and (IV) a modest change and less steeply dipping slope at $S < 0.03$ (Smits et al., 2009; Tarnawski et al., 2013).

As shown in Figure 2-5b, each of these regions correlates with the presence and location of water at certain saturations. At high water content (region I), the water phase is continuous and physically connected such that the effective flow area is large and λ_{soil} is high. The small change in λ_{soil} within this region indicates that the influence of air is trivial. As water content decreases (region II), water is displaced by air and the water phase becomes disconnected (i.e., pendular form). As the effective flow area shrinks, λ_{soil} gradually decreases. As water content continues to decrease (region III) beyond the knee of the TCDC, known as the critical water content (θ_{crit}) or residual water content (θ_r), only small water bridges connect grain particles and λ_{soil} decreases significantly as the effective flow area diminishes. Finally, at extremely low water content well below the residual water content (region IV), the water phase is essentially absent and only exists as thin films around solid particles. The effective flow area essentially becomes the physical contact between particles and λ_{soil} approaches its minimum.

Since λ_{soil} varies significantly with water content, comparisons of λ_{soil} under varying conditions are often reported in terms of TCDCs. A comparison between various soil compositions, soil densities, and temperatures are shown in terms of TCDCs in Figures 2-6, 2-7,

and 2-8, respectively. As discussed in Section 2.1.1., λ_{soil} is greater for soils with higher quartz content (Figure 2-6), density (Figure 2-7), and temperature (Figure 2-8). In all figures, differences in soil composition, density, or temperature were more significant at water contents between the residual water content and full saturation.

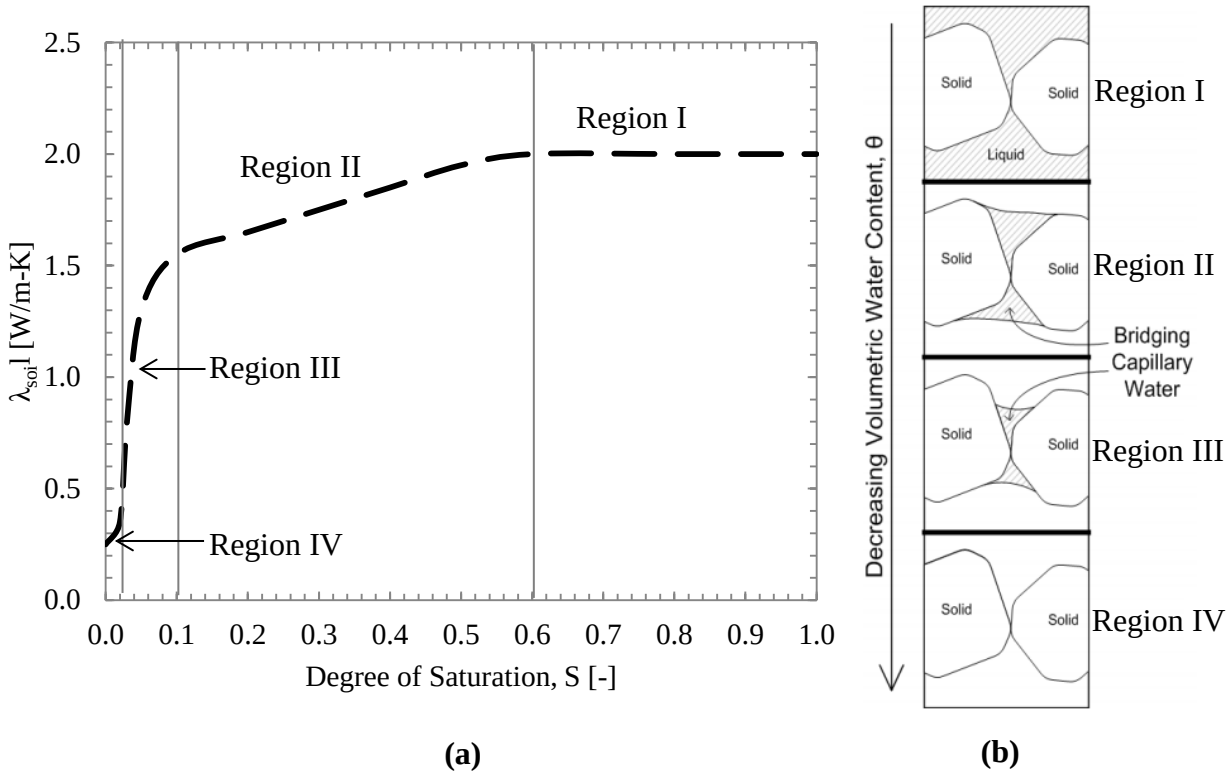

Figure 2-5. (a) Example TCDC with four distinct regions and (b) visualization of water contents that correlate each region (Salomone and Kovacs, 1983).

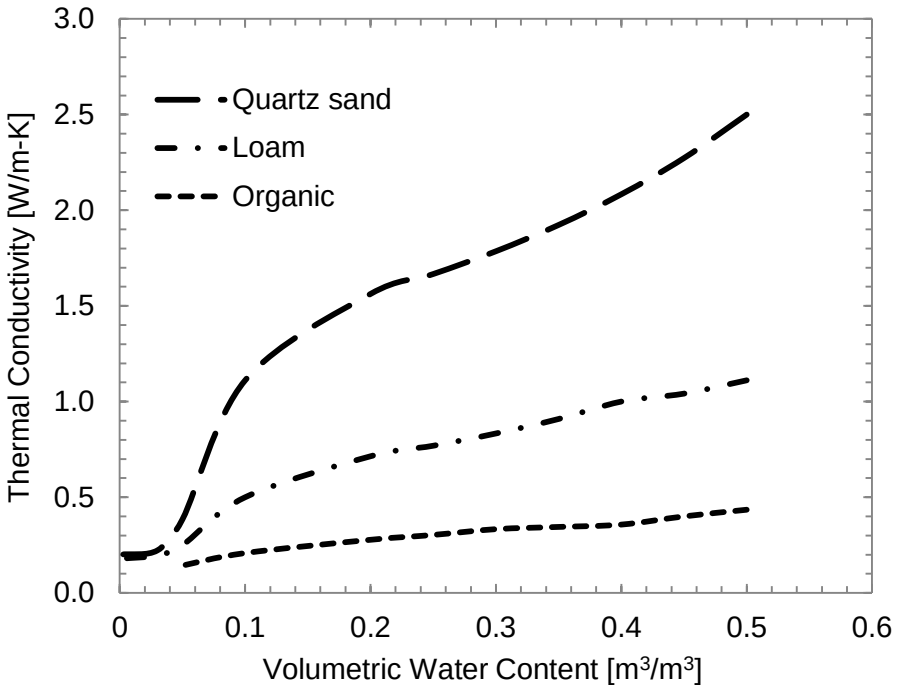

Figure 2-6. Effect of soil composition and water content on λ_{soil} (adapted from Campbell, 2006).

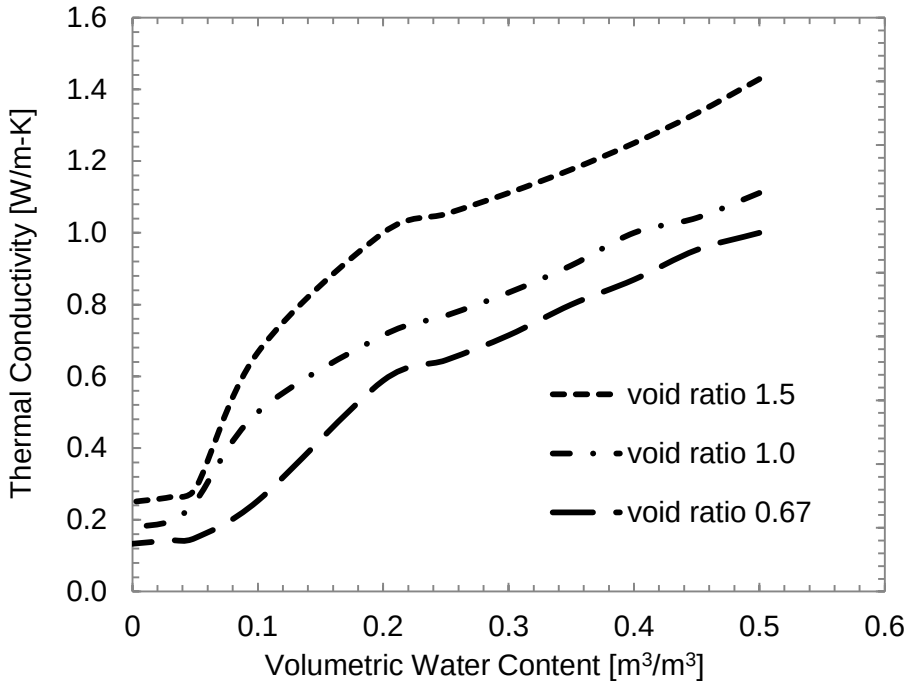

Figure 2-7. Effect of density (void ratio) and water content on λ_{soil} for a loam soil (adapted from Campbell, 2006).

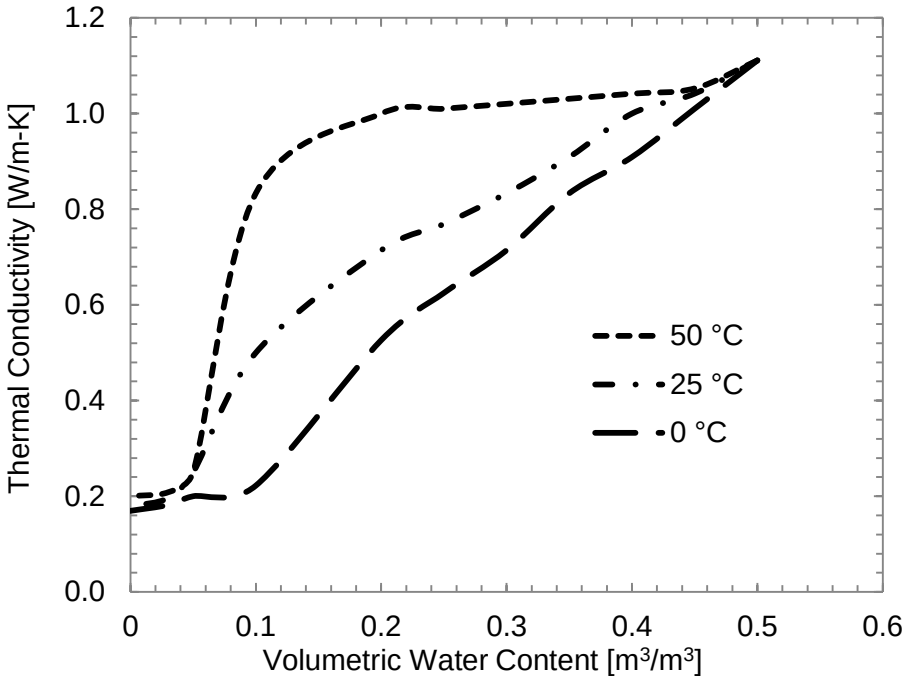

Figure 2-8. Effect of temperature and water content on λ_{soil} for a loam soil (adapted from Campbell, 2006).

2.1.3. Using the TCDC in the design of horizontal ground loops

The design principles of horizontal ground loops are straightforward, but complicated by the numerous parameters that are required to determine the length of the ground loop. To calculate the length of the ground loop, knowledge of the following parameters are required: the arrangement of the horizontal trenches, specifications of the heat pump (i.e., heating capacity, flow rate, electrical demand, and efficiency), thermal properties of the soil and heat exchanger pipe, fluid flow rate in the ground loop, ground temperature, and geographic climate. Within the past decade, a number of experimental and numerical modeling studies have been conducted to determine the effect of these parameters on the performance of horizontal ground loops (e.g., Florides and Kalogirou, 2007; Esen et al., 2007; Demir et al., 2009; Pulat et al., 2009; Chiasson, 2010; Wu et al., 2010; Benazza et al., 2011; Congedo et al., 2012; Chong et al., 2013). A significant conclusion among Demir et al. (2009), Pulat et al. (2009), and Congedo et al. (2012) was that the λ_{soil} surrounding the ground loop was the most influential design parameter.

A constant and uniform λ_{soil} was selected for model simulations in those studies. However, λ_{soil} is expected to vary during operation of the ground loop. The water content of the backfill will change spatially and temporally depending on the soil hydraulic properties, groundwater table (GWT) fluctuations, and climatic variations. Therefore, a variable λ_{soil} value would better characterize unsaturated soil conditions.

One practical solution is to incorporate TCDCs to model the size and performance of horizontal ground loops. As discussed in Section 2.1.2., the TCDC for a soil defines the relationship between water content (w, θ, or S) and λ, and thus quantifies the moisture-dependent thermal behavior of soil. To determine the water content in response to changing environmental conditions, another constitutive relationship is necessary. The retention of water in unsaturated

soil can be predicted from the soil-water characteristic curve (SWCC), which defines the relationship between moisture content and ψ_{soil}. Furthermore, to predict the rate of water movement, the SWCC can be used to estimate the hydraulic conductivity curve, which defines the relationship between moisture content and hydraulic conductivity. The TCDC and SWCC are characteristic functions for a given soil, and when coupled, govern the transport of heat and moisture. With various model estimation and experimental techniques available (e.g., Fredlund and Xing, 1994; Agus and Schanz, 2005; Côté and Konrad, 2005; Likos et al., 2012; Woodward et al., 2013) as well as a growing base of literature with published values (e.g., Campbell et al., 1994; Leij et al., 1996; Smits et al., 2010; Krishnapillai and Ravichandran, 2012), TCDCs and SWCCs are now relatively easy to acquire experimentally or from literature and be useful for modeling coupled heat and moisture flow present in the operation of shallow horizontal ground loops.

2.2. Experimental Determination of the TCDC

Methods for determining the SWCC of soil have been well-established (e.g., ASTM D6836-02), but no internationally recognized standard exists for determining the TCDC of soil. A single measurement of λ_{soil} can be done according to the ASTM *Standard Method for Determination of Thermal Conductivity of Soil and Soft Rock by Thermal Needle Probe Procedure* (ASTM D5334-08) or the IEEE *Guide for Soil Thermal Resistivity Measurements* (IEEE 442-1981). Both of these standards utilize the probe method in which a single thermal probe measurement is used to determine the λ_{soil} of a specimen. However, neither of the standards provides instructions for generating the TCDC, which requires multiple measurements of λ_{soil} at varying water contents. There are various techniques available to produce TCDCs that include estimation models (e.g., Campbell et al., 1994; Tarnawski et al., 2000; Côté and Konrad,

2005), laboratory procedures based on probe methods (e.g., Smits et al., 2010; Likos et al., 2012; Woodward et al., 2013), and the steady-state guarded-heat plate (GHP) method (Farouki, 1981; Reid, 2005). Among the laboratory methods, Mitchell and Kao (1978) determined that the probe method was the most advantageous for soil in terms of experiment ease, short testing duration, and measuring λ_{soil} during transient conditions.

2.2.1. Probe methods

Use of the probe method for determining λ_{soil} is well documented (Sepaskhah and Boersma; 1979; Farouki 1981; Salomone et al., 1984; Brandon and Mitchell, 1989; Bristow et al., 1994; Abu-Hamdeh et al., 2001; Woodward et al., 2013). The probe method uses the line heat source theory to relate the temperature rise of an infinite, linear, and constant heat source within an infinite, homogeneous, isotropic medium to λ. An analytical solution of this relationship was presented in Carslaw and Jaeger (1959):

$$T = -\frac{q}{4\pi\lambda} E_i\left(-\frac{r^2}{4\alpha t}\right) \tag{2.11}$$

where T is temperature rise, q is heat input rate, E_i is the exponential integral, r is radial distance from probe, α is thermal diffusivity, and t is time. By expanding the exponential integral and using a linear least squares computation to determine the slope of a line (*s*) relating T and ln(t), λ can be determined by:

$$\lambda = \frac{q}{4\pi s} \tag{2.12}$$

A thermal probe consists of a heater wire that supplies a constant heat input rate (q) and a thermocouple to measure temperature. When inserted into a soil specimen, the probe provides a constant heat input rate to heat the soil for a period of time (t_h) and then the heat input is turned off to allow the soil to cool for an equivalent amount of time ($t_c = t_h$). During this entire time (t =

$t_h + t_c$), the thermocouple monitors the temperature response of the probe, which reflects the rate at which heat is conducted away from the probe through the soil. A schematic graph of the typical temperature response during heating with respect to the natural logarithm of time is shown in Figure 2-9. For Eq. 2.13 to be applicable, only temperature-time data that can be fitted with a straight line is used. Nonlinear data before and after the data fitted with a straight line are typically ignored since early-time data includes contact resistance (e.g., resistance of heat at the interface between the surfaces of the probe and soil) and transient effects (e.g., temperature drift), and late-time data includes moisture migration and finite boundary effects (e.g., specimen is not infinitely large) (ASTM 5334-08 and IEEE 442-1981).

Beyond GSHP applications, λ_{soil} is an important design parameter for numerous other engineering applications related to heat transfer through soil (e.g., underground nuclear waste disposal, thermo-active structures, and buried utilities). Pending the application, λ_{soil} may be presented as thermal resistivity (ρ_{soil}), the inverse of λ_{soil}. Generally, ρ_{soil} is used in the design of power cables where electrical engineers prefer to think in terms of a material's ability to resist heat flow (i.e., analogous to electrical resistance). However, the use of λ_{soil} is usually preferred because λ_{soil} is better for statistical analysis (Campbell, 2012). For example, if the range of λ_{soil} is between zero and one, then the range of ρ_{soil} is between infinity and one. Furthermore, the average of this range for λ_{soil} is one-half, which would correctly predict an average heat flow of one-half, whereas the average for ρ_{soil} is infinity, which would incorrectly predict zero heat flow. Thus, λ_{soil} is often determined and mathematically manipulated and then the reciprocal of λ_{soil} is taken if ρ_{soil} is desired.

Four different techniques for experimentally determining TCDCs using the probe method have been employed in practice. Generally, the key difference between techniques is the

preparation of the specimen or the drying process used to obtain λ_{soil} measurements at various water contents. The single-specimen and multiple-specimen methods are the simplest to conduct, but more informative results are obtained from the stage-drying and automated hanging column methods. A more complete description of these four methods in terms of ρ_{soil} is presented in Appendix A.

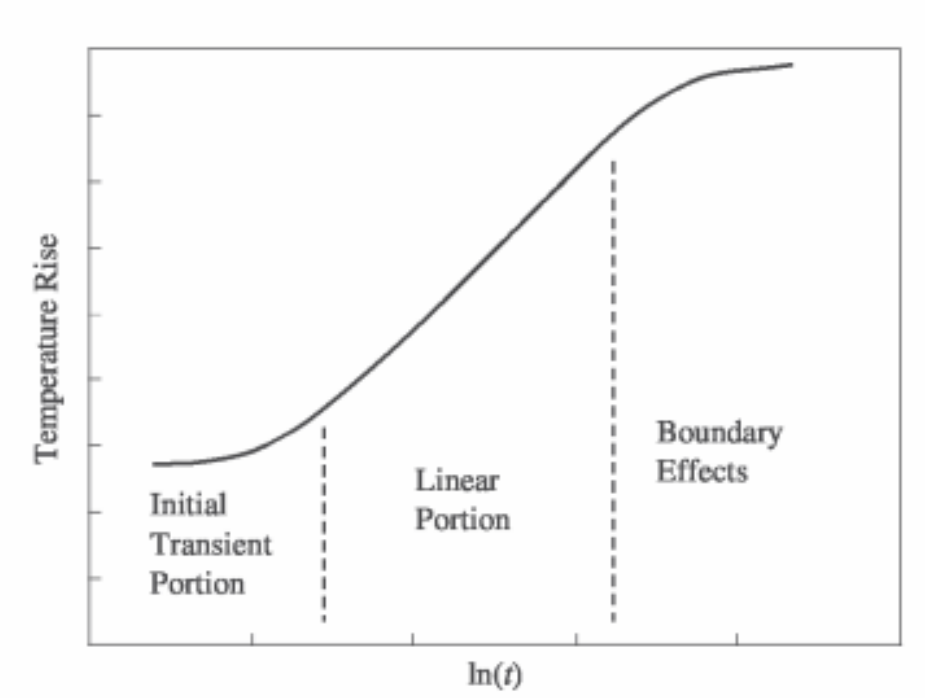

Figure 2-9. Typical probe method testing temperature response with time. Only the linear portion of the curve is used to calculate λ_{soil} (Hanson et al., 2004).

2.2.2. Single-specimen

The single-specimen method can be considered as an extension of the single measurement procedure in ASTM D5334-08. A single specimen is obtained from an undisturbed soil sample or recompacted to a desired density. The specimen is saturated and placed on a balance, as shown in Figure 2-10a. A thermal probe is inserted through the vertical axis of the specimen. Weight and λ_{soil} measurements are taken at certain time intervals as the specimen air dries (i.e., evaporation to the laboratory atmosphere). In general, a frequency of two readings per day is appropriate (Likos et al., 2012). Gravimetric water content is determined from the difference in weight measurements and the TCDC is plotted. The main advantages of this method are that undisturbed specimens can be used and all measurements are done on the same specimen. The two disadvantages of this method are that drying is very slow (i.e., longer time to obtain TCDC), particularly for fine-grained soils that retain water well, and the weight measurements provide an average water content of the specimen. For example, as illustrated in Figure 2-10b, the average water content of the specimen is not truly representative of the actual water content at the location of the λ_{soil} measurement along the length of the thermal probe since soil specimens do not dry uniformly from moisture migration due to gravity or evaporation. Therefore, the λ_{soil} corresponding to the average water content may actually be lower than the actual water content since the thermal probe was measuring λ_{soil} in a drier portion of the specimen (Woodward et al., 2013).

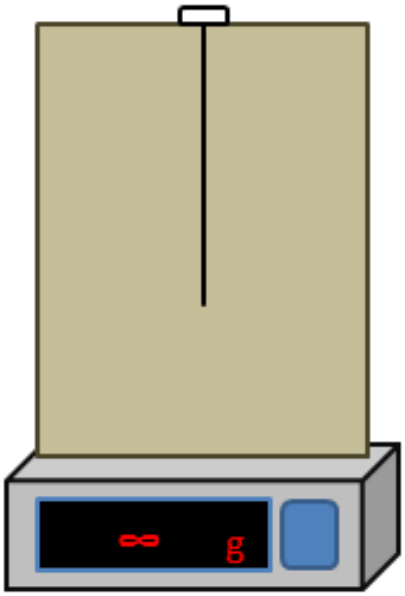

(a)

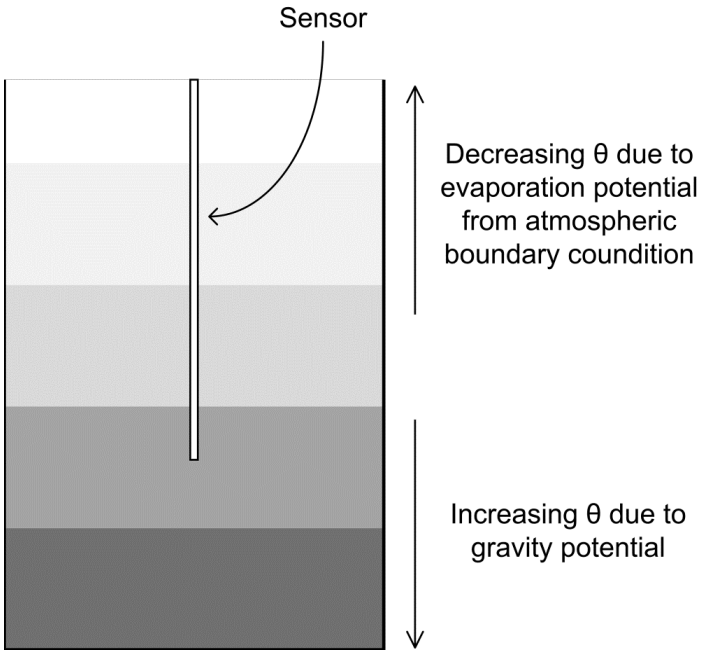

(b)

Figure 2-10. (a) Single-specimen testing involves air drying of a soil specimen placed on a balance so that λ_{soil} and weight measurements can be made at certain time intervals. (b) Non-uniform drying of soil results in λ_{soil} measurements that do not correspond with actual water content measurements (Woodward et al., 2013).

2.2.3. Multiple-specimen

One approach to address the lengthy time of the single-specimen method is to use the multiple-specimen method. Typically, a minimum of five specimens are prepared to identical dry densities but various water contents so that weight and λ_{soil} measurements can be taken quickly to generate the TCDC (Figure 2-11). However, appropriate care must be taken in preparing multiple specimens since specimen variability (i.e., soil fabric, density, or water content) induces errors in λ_{soil} measurements. Similar to the single-specimen method, the thermal probe is inserted through the vertical axis of the specimen. The multiple-specimen method also shares the same average-based gravimetric water content issues as the single-specimen method. Despite these disadvantages, the multiple-specimen method is still a practical method and, in conjunction with the single-specimen method, is possibly the most commonly used method in industry today.

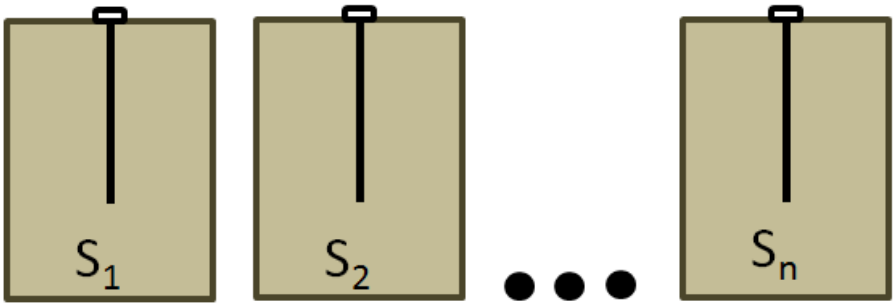

Figure 2-11. Multiple-specimen testing involves preparing multiple soil specimens to identical dry densities but various water contents. Rather than waiting for a single specimen to dry, λ_{soil} measurements are made to specimens that are compacted to specific water contents.

2.2.4. Stage-drying

The stage-drying method was developed to address the issue of using average-based water contents and provides quantification of water redistribution throughout the specimen (Woodward et al., 2013). Three identical specimens are compacted to a specified density and water content. On day zero, these specimens are weighed to verify density and water content consistency between specimens. Additionally, a thermal probe is inserted horizontally into the top, middle, and bottom thirds of each specimen to measure initial λ_{soil} values (Figure 2-12). All three specimens are placed in a 50 °C oven to accelerate drying time. One specimen is removed after 24 hours, 3 days, and 10 days of oven drying for subsequent λ_{soil} measurements at the same top, middle, and bottom locations. Different oven-drying intervals may be used depending on the soil type (e.g., sand specimens may only need a maximum of six days of oven drying). After λ_{soil} measurements have been completed, each specimen is deconstructed to collect soil samples from each measurement location for water content determination. The TCDC is constructed with all three specimens on a single plot. The primary advantage of the stage-drying procedure is that the λ_{soil} measurements correspond to location specific water content measurements. The disadvantages of this method are that induced errors from specimen variability exist and the rather large specimen size necessary to allow three horizontal measurements requires additional material and time for specimen preparation and drying. The larger volume of soil increases the thermal inertia of specimen and the specimen becomes more resistant to changes in temperature (i.e., oven drying).

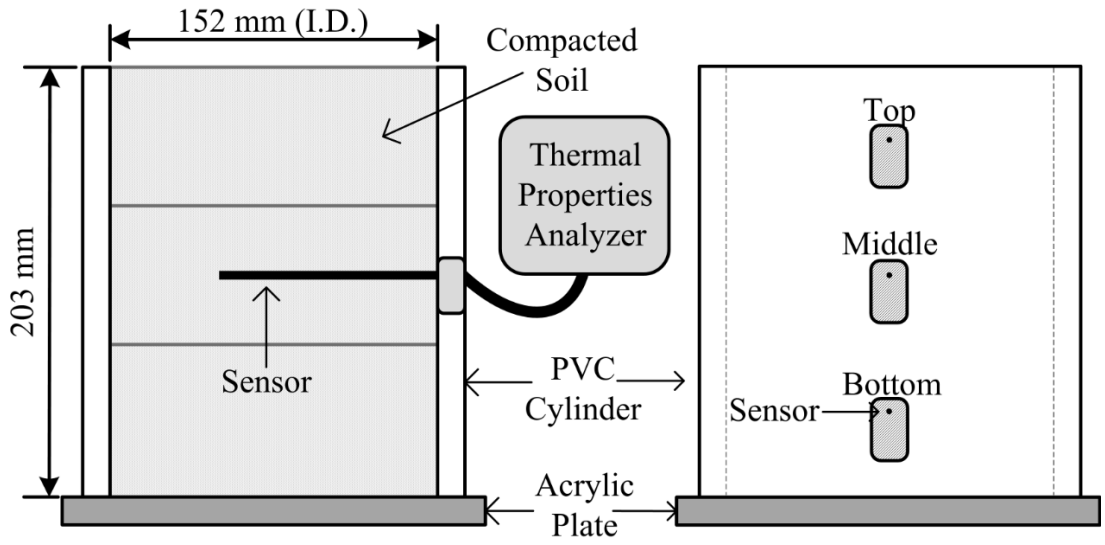

Figure 2-12. Stage-drying testing involves larger specimens that accommodate three horizontal measurements of λ_{soil} at the top, middle, and bottom thirds of the specimen. The specimen is deconstructed after λ_{soil} measurements to collect soils samples at the location of the λ_{soil} measurements to determine location-specific water content (Woodward et al., 2013).

2.2.5. Automated hanging column

The automated hanging column method is typically used for sands since the apparatus utilizes a tensiometer that is capable of measuring suctions up to the cavitation pressure of water under atmospheric conditions (i.e., ~70 kPa). As shown in Figure 2-13, soil is packed into a Tempe cell embedded with a dielectric moisture content sensor, temperature probe, tensiometer, and dual-needle thermal probe. Pore water is allowed to rise or drain through the specimen as the measurement devices collect water content, temperature, suction, and λ_{soil} data. Once the specimen is completely dry, soil samples in the vicinity of the sensors are collected and weighed to verify moisture conditions. The main advantages of the automated Tempe cell are that both the TCDC and SWCC are determined at the same soil conditions and data can be collected at small time increments (e.g., every one minute).

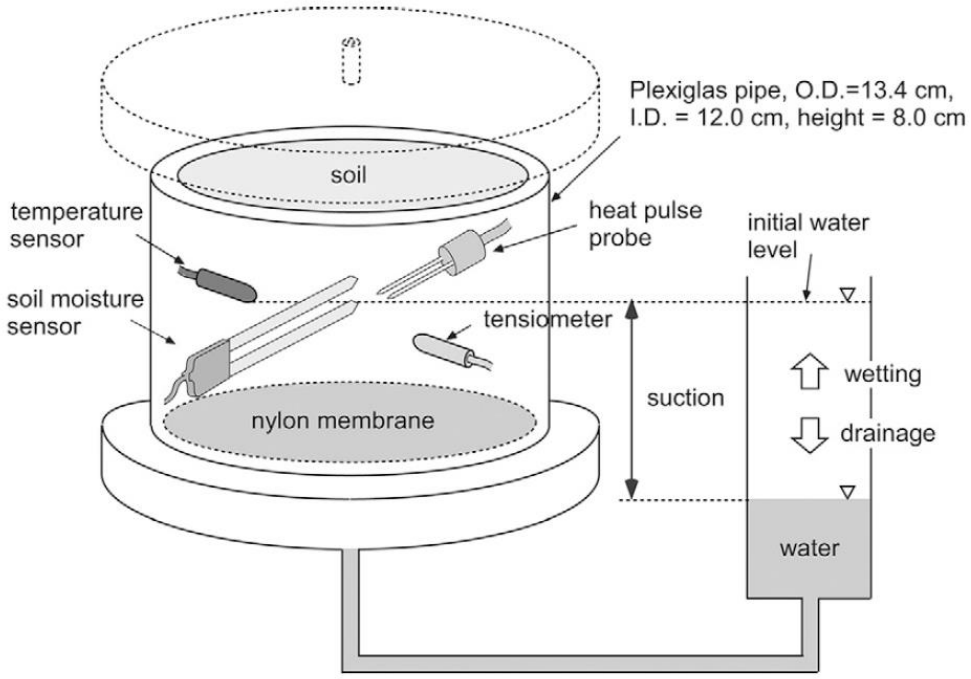

Figure 2-13. Components of an automated hanging column setup. During testing, pore water is allowed to drain or rise through the specimen based on the location of the initial water level in the hanging column reservoir. Temperature, water content, suction and λ_{soil} are continuously monitored at set intervals (Smits et al., 2010).

3. MATERIALS AND METHODS

3.1. Selected Backfill

In the design of geothermal grounds loop, designers have some control over the factors that influence λ_{soil}. Generally, designers have most control over soil type and density since the type of soil can be selected and compacted to a desired density and initial water content. A key criterion for selecting a backfill soil is its thermal properties and behavior. Locally available or native soil is the preferred choice since additional labor and costs to remove soil and import new soil are avoided. However, in situations where the native soil has unfavorable thermal properties, manufactured thermal sands may be imported. Thermal sands typically consist of well-graded quartz sand and limestone screenings that have favorable thermal properties (λ_{quartz} = 8 W/m-K > λ_{fines} = 2.9 W/m-K > λ_{water} = 0.6 W/m-K >> λ_{air} = 0.024 W/m-K). The addition of a small percentage (i.e., 5% to 10%) of non-swelling clay or silt to retain absorbed moisture can further improve the thermal characteristics of the sand (Van and Winterkorn, 1959; Jorgensen, 2012).

For the model analysis of a ground loop, three quartz-rich sands–hereby referred to as soil A, B, and C–were selected as backfill. Grain-size distribution (ASTM D422-63), standard Proctor compaction (ASTM D698-12), and X-ray diffraction techniques were performed to determine physical characteristics of the soils, as shown in Table 3-1. The three soils were compacted to approximately 90% maximum dry unit weight to determine TCDCs and SWCCs using the automated hanging column method (Section 2.2.5). The automated hanging column method was selected because the SWCC and TCDC were known to be measured at the same density, temperature, and water content. Furthermore, small time increments were used to collect many measurements such that the modeling program would not have to estimate large interpolations between measurements. The TCDC and SWCC were obtained during a drying

process as pore water was allowed to drain through the specimen along an initial drainage path. Figure 3-1 shows measured TCDCs and SWCCs of each soil in terms of saturation.

A key feature is the residual saturation (SWCC) or the critical saturation (TCDC) located at the knee of the curves (Figure 3-1). In the TCDC, the critical saturation defines the point at which an incremental decrease in saturation will result in a significant decrease in λ_{soil}. Likewise, in the SWCC, the residual saturation defines the point at which an incremental decrease in saturation will require much greater ψ. Knowledge of the residual saturation is important because it is an indicator of thermal instability. Dry soil conditions around the ground loop occur from moisture migration due to thermal and hydraulic gradients and continued drying below the critical saturation results in significant reductions of λ_{soil} (Hartley and Black, 1981). If the developed dry zone persistently inhibits dissipation of heat from the ground loop, a thermal runaway condition (i.e., an increase in temperature changes conditions in a way that causes a further increase in temperature) may ensue (Campbell and Bristow, 2007). Even though the critical saturation provides a benchmark for thermal stability, there is still a wide range of saturations ($\sim 0.3 < S < 1.0$) where higher λ_{soil} exists.

Table 3-1. Physical characteristics of selected backfill.

Soil	USCS[1] ID	D_{10}[2] [mm]	Quartz [%]	Fines [%]	$\gamma_{dry,max}$[3] [kN/m^3]
A	SP	0.18	69.1	0.57	17.89
B	SP	0.13	77.4	2.0	18.55
C	SW	0.13	78.2	3.13	19.53

[1]USCS = Unified Soil Classification System (ASTM D2487-11)
[2] D_{10} = soil particle diameter at 10% finer (ASTM D422-63)
[3] $\gamma_{dry,max}$ = maximum dry unit weight (ASTM D698-12)

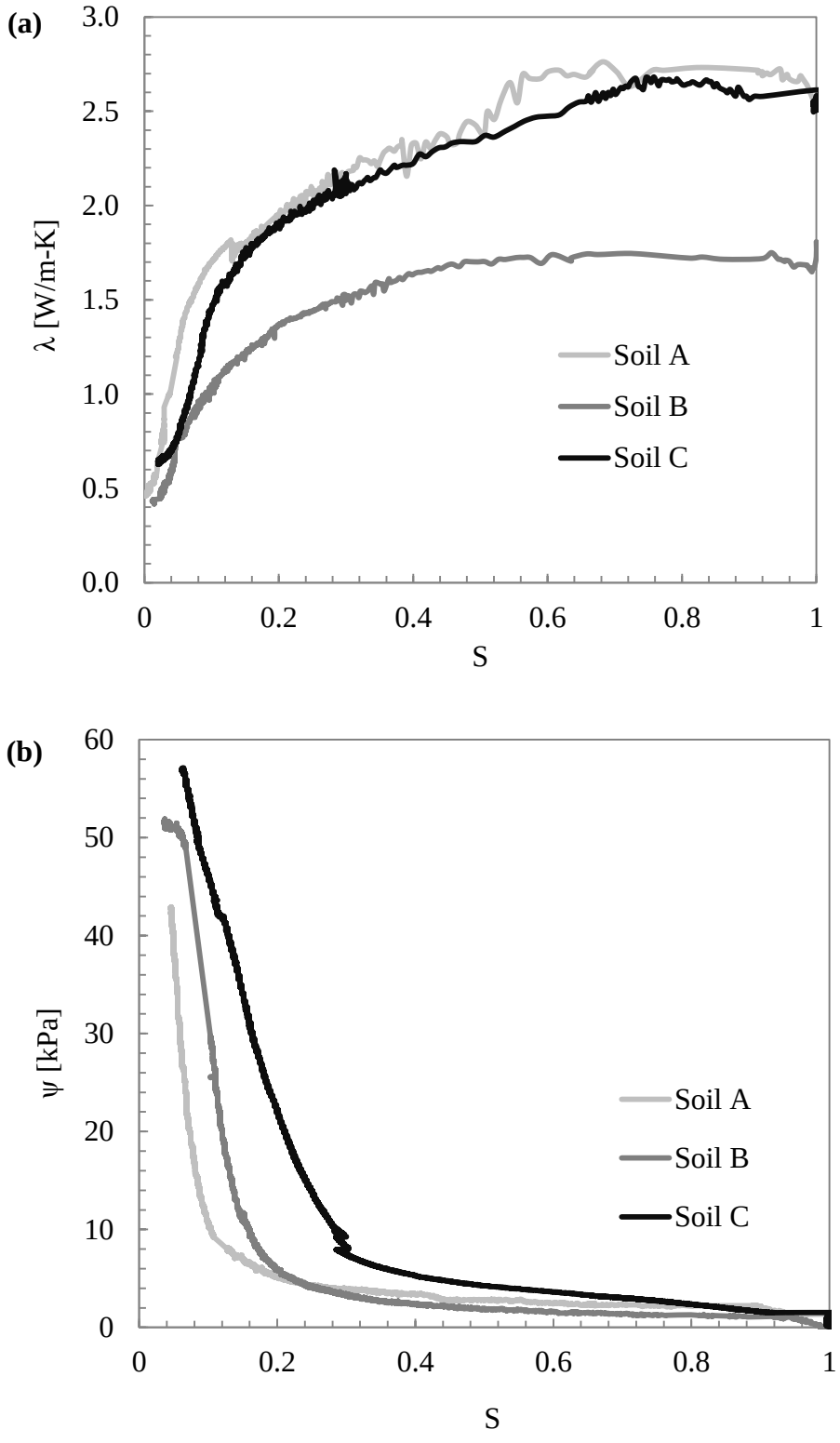

Figure 3-1. (a) TCDCs and (b) SWCCs of the backfill soils.

3.2. Calculating the Length of Ground Loop

A simplified estimation of the required total length of ground loop for a given heat pump capacity and COP can be derived from an energy balance on the GSHP system and differential element shown in Figure 3-2. The thermal resistance approach is analogous to the Neher-McGrath (1957) method used to model heat transfer mechanisms in underground cable installations for calculating cable ampacity. Based on known values of the heat pump capacity (Q_{hp}), COP or energy efficiency ratio (EER), fluid flow rate (m_w), and entering water temperature (EWT = $T_{w,out}$), the heat exchanger load (Q_{hx}) and leaving water temperature (LWT = $T_{w,in}$) can be determined by:

$$COP = \frac{Q_{hp}}{Q_{hp} - Q_{hx}} \tag{3.1}$$

$$EER = \frac{Q_{hp}}{Q_{hx} - Q_{hp}} \tag{3.2}$$

$$Q_{hx} = m_w \, c_{wp} \, \Delta T_w \tag{3.3}$$

where c_{wp} is the specific heat capacity of the fluid at constant pressure and ΔT_w is the temperature difference of the fluid ($\Delta T_w = T_{w,out} - T_{w,in}$ = EWT - LWT). The rate of heat transferred per unit length between the heat exchanger fluid (T_w) and ground (T_g) can be determined by:

$$Q = \frac{(T_g - T_w)}{R_{total}} \tag{3.4}$$

Depending on whether the ground loop is used to extract or reject heat, Q may be positive (i.e., heating mode) or negative (i.e., cooling mode). Assuming a horizontal pipe with inner diameter (D_i) and outer diameter (D_o) buried at a certain depth (d), the total thermal resistance (R_{total}) is

the sum of resistances (i.e., inverse of conductivity) from fluid convection (R_{conv}), pipe conduction (R_{pipe}), and soil conduction (R_{soil}):

$$R_{conv} = \frac{1}{h_w \, \pi \, D_i} \tag{3.5}$$

$$R_{pipe} = \frac{\ln\left(\frac{D_o}{D_i}\right)}{2\pi \, \lambda_{pipe}} \tag{3.6}$$

$$R_{soil} = \frac{1}{S \, \lambda_{soil}} \tag{3.7}$$

In Eq. 3.5, the properties of the fluid necessary to determine the heat transfer coefficient (h_w) are evaluated at the average fluid temperature (T_{avg}) since variations with temperature are not significant (Incropera et al., 2006). The Nusselt number (Nu) and Gnielinski correlation (Eq. 3.9) can be used to determine h_w:

$$T_{avg} = \frac{T_{w,in} + T_{w,out}}{2} \tag{3.8}$$

$$Nu = \frac{h_w \, D_i}{k_w} = \frac{(f/8)(Re - 1000)P_r}{1 + 12.7(f/8)^{1/2}(Pr^{2/3} - 1)} \tag{3.9}$$

$$f = (0.79 \ln(R_e) - 1.64)^{-2} \tag{3.10}$$

where k_w is the thermal conductivity of the fluid, f is the Darcy friction factor, Re is the Reynolds number (i.e., ratio of inertial to viscous forces), and Pr is the Prandtl number (i.e., ratio of momentum to thermal diffusivity). The Gnielinski correlation is valid for $0.5 \leq Pr \leq 2000$ and $3000 \leq Re \leq 5 \times 10^6$ (Incropera et al., 2006). For the design of a horizontal ground loop, the circulating fluid flow rate and pipe diameter are chosen to maintain turbulent flow (i.e., Re > 4000) to enhance heat transfer (i.e., higher Re yields higher Nu and h_w) In Eq. 3.6, λ_{pipe} is the thermal conductivity of the heat exchanger pipe which is typically made of high-density

polyethylene (HDPE). In Eq. 3.7, S is a conduction shape factor for a horizontally buried cylinder (Incropera et al., 2006):

$$S = \frac{2\pi}{\ln\left[\left(\frac{2d}{D_o}\right) + \sqrt{\left(\frac{2d}{D_o}\right)^2 - 1}\right]} \tag{3.11}$$

An energy balance on the differential element, where Q_{hx} = Q produces the differential heat transfer is:

$$dQ = m_w\, c_{wp}\, dT_w = \frac{(T_g - T_w)}{R_{total}}\, dx \tag{3.12}$$

By separation of variables, integration, and application of boundary conditions shown in Figure 3-2 ($T = T_{w,out}$ at $x = 0$ and $T = T_{w,in}$ at $x = L$), the total ground loop length (L) is determined by:

$$L = m_w\, c_{wp}\, R_{total} \ln\left[\frac{(T_{w,in} - T_g)}{(T_{w,out} - T_g)}\right] \tag{3.13}$$

At constant m_w and ΔT_w, the two variables that are subject to change from coupled moisture and heat flow are λ_{soil} (which is incorporated in R_{total}) and T_g. From Eq. 3.13, a change in λ_{soil} and T_g results in a change of the total length of the ground loop. Generally, the lowest expected λ_{soil} value (i.e., greatest soil resistance during long-term operation of the ground loop) is chosen as an input to calculate the length of the ground loop. In current state-of-practice, a conservative and constant value of λ_{soil} is often estimated or assumed for the ground formation into which the ground loop will be installed (ASHRAE, 2007; Remund and Carda, 2009). However, an improved approach to determine the total length of the ground loop is to use variable λ_{soil} values that characterize unsaturated soil behavior to simulate actual operating conditions (i.e., spatially and temporally varying moisture content and temperature).

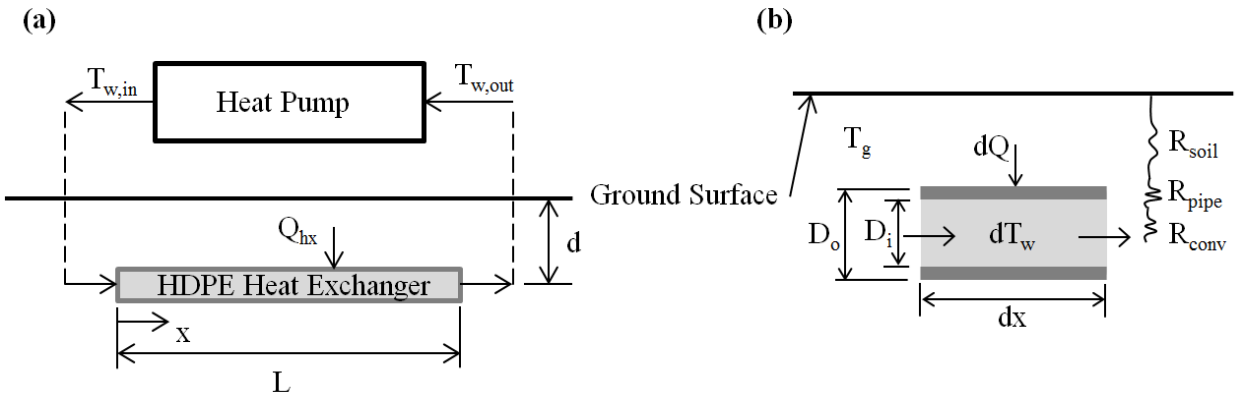

Figure 3-2. (a) Simple GSHP system schematic and (b) ground loop differential element.

3.3. Shallow Horizontal Ground Loop Model

A two-dimensional (2D) cross-sectional modeling domain was evaluated to compare the thermal performance of a horizontal ground loop in a two-pipe trench configuration (Figure 3-3). The 2D cross-section approach is reasonable if the cross-section is taken through the mid-section of the trench along the direction of fluid flow (Chiasson, 2010). Furthermore, the 2D approach provides the benefit of reduced computational time. The SVHeat and SVFlux programs of SVOffice were used to perform the model analysis. The SVHeat program allowed for the input of material TCDCs. Additionally, the SVFlux program allowed for the input of material SWCCs and was used to fit the SWCCs with the van Genuchten (1980) equation to estimate the hydraulic conductivity curve.

The model domain was 6-m wide by 6-m deep with an initial groundwater table (GWT) located 2.5-m bgs. The size of the domain was assumed to be sufficiently large to encompass the expected thermally disturbed area from operation of the ground loop. Native soil was simulated as a sandy loam. The thermal and hydraulic properties of the sandy loam were derived from Abu-Hamdeh and Reeder (2000) and Leij et al. (1996), respectively. Due to symmetry, zero-flux boundary conditions (BC) were applied to the left and right side of the domain. The top surface boundary was defined by daily air temperature and precipitation. Approximated air temperature and precipitation data (Figure 3-4a) were used to reduce computational time. The domain was assumed to be deep enough for the bottom boundary temperature to remain constant at 10 °C, which is the approximate groundwater temperature of northern continental United States (ASHRAE, 2007). Furthermore, the bottom boundary was defined by varying total head values to simulate a fluctuating GWT (Figure 3-4b). Since several databases were used to obtain climatic data, the precipitation and GWT data are not perfectly coupled. However, using both

precipitation and fluctuating GWT conditions more accurately represents possible mechanisms for moisture migration.

A 1-m-wide by 2-m-deep trench was centered within the model domain at the ground surface. Two parallel SDR-11 (32-mm nominal diameter) HDPE pipes were buried 1.97-m deep in the trench and separated along the x-axis by 0.8 m to minimize the effects of thermal resistance (i.e., R_{soil}). The HDPE pipes were modeled as constant temperature elements equivalent to the average of the design EWT as suggested in ASHRAE (2007) and the LWT calculated by Eq. 3.3. This average temperature (e.g., T_{avg} = -2.8 °C in heating and T_{avg} = 29 °C in cooling for a heat pump with 10.55 kW capacity and COP of 4) was also used to specify thermophysical properties of the fluid and determine the convective heat transfer coefficient from forced convection in turbulent pipe flow (Eq. 3.9). As suggested in Remund and Carda (2009), a mixture of water and 20% by volume propylene glycol antifreeze was used since design temperatures were expected to fall below the freezing point of water.

Modifications of the governing partial differential equations for coupled moisture (Eq. 2.4) and heat (Eq. 2.5) flow used in SVOffice are Eq. 3.14 and Eq. 3.15, respectively:

$$\frac{\partial}{\partial y}\left[\left(\frac{\left(k_y^w + k^{vd}\right)}{\gamma_w}\right)\frac{\partial u_w}{\partial y} + k_y^w + k_{12}\frac{\partial T}{\partial y}\right] = \frac{\partial \Theta_u}{\partial t} + \frac{\rho_i}{\rho_w}\frac{\partial \Theta_i}{\partial t} \tag{3.14}$$

where $$k_{12} = \frac{k^{vd}(-u_w)}{\gamma_w(274.15 + T)} \tag{3.14a}$$

$$k^{vd} = \gamma_w \frac{\omega_v u_v^{soil}}{\rho_w R(T + 273.15)}\frac{D^{v*}}{\rho_w} \tag{3.14b}$$

$$\frac{\partial}{\partial y}\left[\left(\frac{\left(L_f k_y^w + L_v k^{vd}\right)}{\gamma_w}\right)\frac{\partial u_w}{\partial y} + k_{22}\frac{\partial T}{\partial y} + L_f k_y^w\right] - C_w q_y^w \frac{\partial T}{\partial y} = (C + L_f m_2^i)\frac{\partial T}{\partial t} \qquad (3.15)$$

$$\text{where } k_{22} = \lambda + (L_v + L_f)k_{12} \qquad (3.15a)$$

where k_y^w is hydraulic conductivity; k^{vd} is the water vapor conductivity by diffusion within the air phase, ω_v is the molecular weight of water vapor; u_v^{soil} is the soil-water vapor pressure; R is the universal gas constant, D^{v*} is the vapor diffusivity through soil; T is temperature; u_w is the pore water pressure; γ_w is the unit weight of water; Θ_u is the volumetric water content; Θ_i is the volumetric ice content; ρ_w is water density; ρ_i is ice density; y is elevation; t is time; L_f is the mass latent heat of fusion of water; L_v is the volumetric latent heat of water vaporization; C_w is the volumetric heat capacity of water; q_y^w is the water flow flux; C is the volumetric heat capacity of soil; and m_2^i is the slope of the soil-freezing characteristic curve. Terms that involve ice properties were set to zero since frozen conditions were not considered. Additional discussion and other forms of general partial differential equations used to describe coupled heat and moisture flow specific to SVHeat and SVFlux are presented in Thode and Zhang (2009). An overview of modeling with SVOffice is presented in Appendix C.

Although SVOffice is a reputable geotechnical and hydrological software used by industry consulting firms, additional model verification measures were performed to verify the model's accuracy and credibility. An iterative process was used to isolate, test, and improve boundary conditions in basic models to confirm that the outputs of these models were consistent with analytical solutions or experimental results. For instance, basic models of steady-state heat transfer from a single ground loop simulated only in SVHeat were conducted first to confirm that results matched analytical solutions for steady-state heat conduction (Eq. 2.1). Likewise, simple

models of steady-state groundwater flow and capillary rise simulated only in SVFlux were conducted first to confirm that results matched experimentally measured results. Accurate steady-state models were advanced to transient models in a stepwise manner. The final 2D model of a shallow horizontal ground loop was built upon advancement of these simple models.

Two simulations were performed for each of the three backfill sands. In each case, one simulation used the soil's measured TCDC in the simulation and the other used a conservative value of λ_{soil}. Since soils A and B had similar TCDCs, a constant value of 0.7 W/m-K was selected for the conservative analysis. For soil C, a constant value of 0.8 W/m-K was selected. Each simulation was performed for 365 d beginning on the 1st of January to encompass a heating mode followed by cooling mode and returning to heating mode. The ground loop was simulated to operate in the heating mode or cooling mode during measured heating degree days (e.g., 253 d when the average air temperature is greater than the reference temperature, T_{ref} = 18.33 °C) and cooling degree days (e.g., 112 d when the average air temperature is less than T_{ref}). For each simulation, the initial thermal condition was a uniform T_g = 7.78 °C. Initial hydraulic conditions were prescribed from the initial groundwater table location and corresponding partially saturated soil resulting from equilibrium capillary rise. The SVFlux and SVHeat programs were fully coupled and performed simultaneously during simulation to determine transient moisture and temperature profiles of the ground. The computational time for each simulation was between 4 h and 6 h.

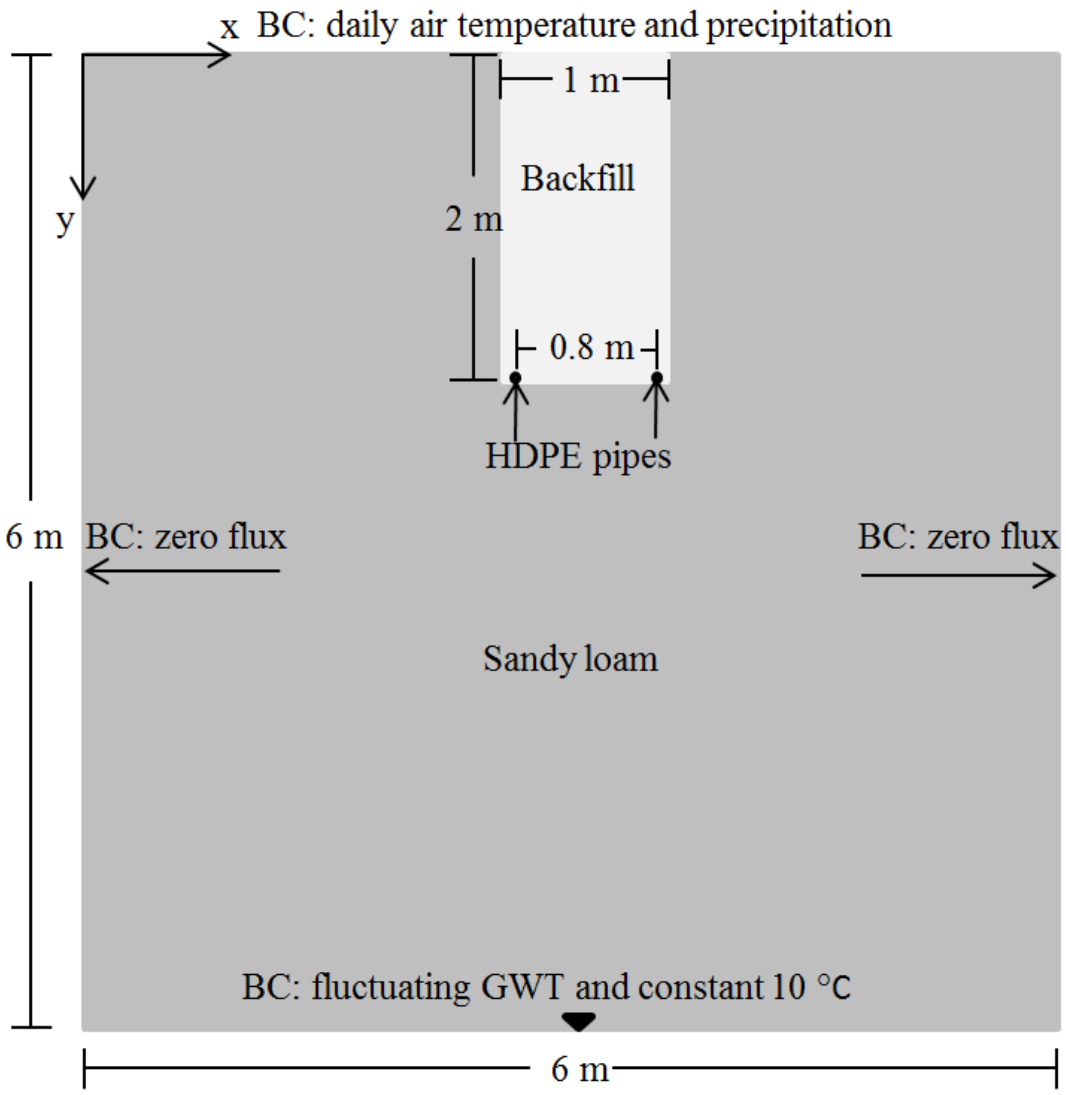

Figure 3-3. Geometry and boundary conditions (BC) of shallow horizontal ground loop model.

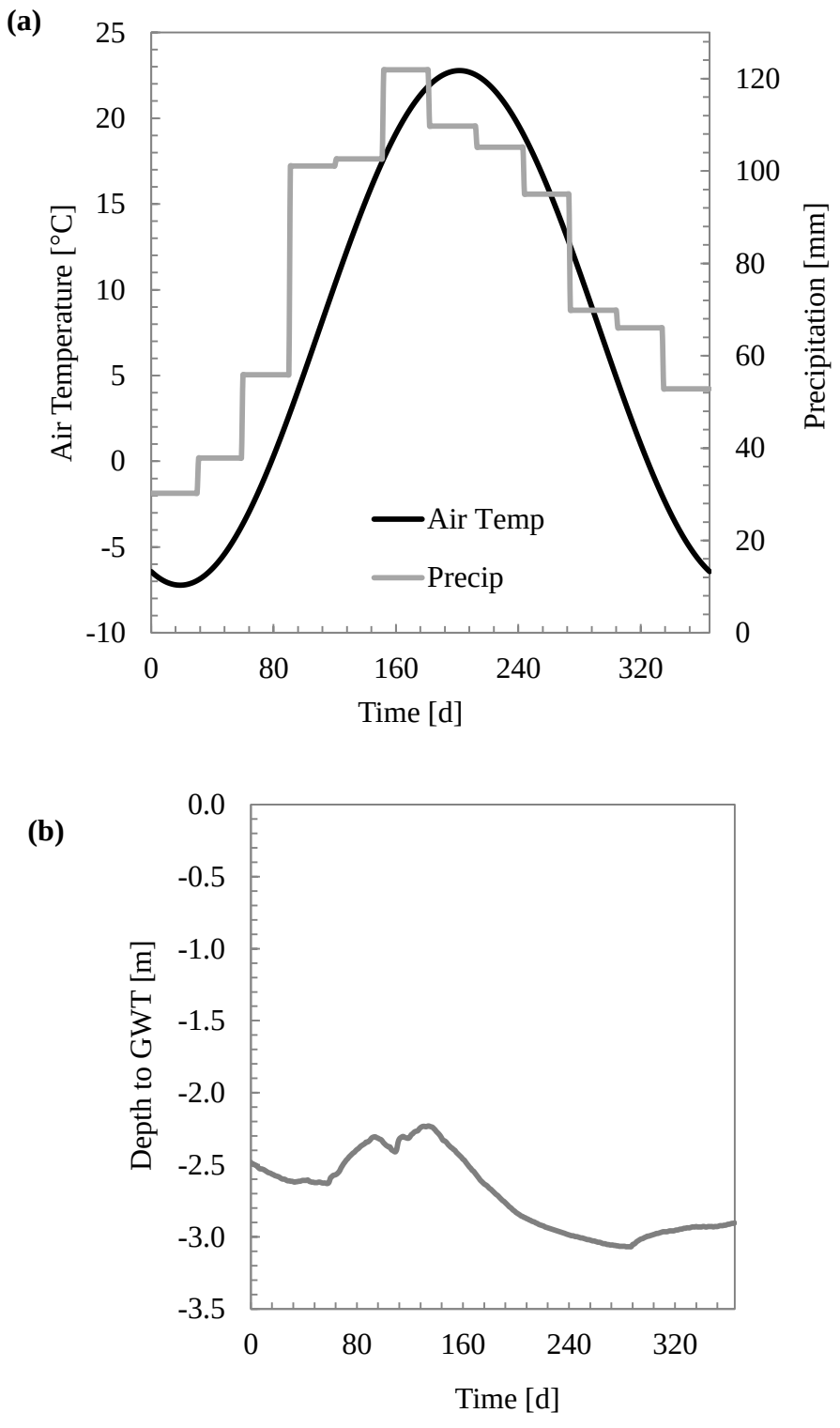

Figure 3-4. (a) Daily air temperature and precipitation used for top BC and (b) depth to GWT bgs for bottom BC.

4. RESULTS AND DISCUSSION

4.1. Simulation Results

Soil moisture varied spatially and temporally due to precipitation infiltration from the top of the trench and a fluctuating GWT near the bottom of the trench. Figure 4-1a shows the volumetric water content (θ) time series for soil C at five observation points (0.67, 1.30, 1.98, 2.30, and 2.67 m bgs) along the y-axis (Figure 3-3) through the middle of the model domain. Similar results were also obtained for soils A and B. Figure 4-1b shows the θ-time series for all simulations at an observation point equivalent to the depth of the ground loop (1.98 m bgs) within the trench. For all soils, the trend of the θ-time series closely followed the increase and decrease of precipitation as well as rise and fall of the GWT (Figure 3-4), suggesting that the amount of precipitation and location of GWT have a significant influence on *in situ* moisture conditions. The initial θ as well as ensuing θ from capillary effects were dictated by the soil's SWCC (Figure 3-1b). The initial θ is important because it may be the lowest θ at a given location if there are constant contributions from precipitation and capillary rise. For all simulations, the lowest observed θ (i.e., driest condition) was within the trench and was equal to θ_r. However, the use of the van Genuchten (1980) model may have forced the driest condition to be θ_r since the van Genuchten fit is asymptotic at θ_r and does not go to zero.

Figure 4-2a shows the λ-time series at the same five observation points for soil C as in Figure 4-1a. Likewise, Figure 4-2b shows the λ-time series at the same observation point for all simulations as in Figure 4-1b. Since soils A and B had the same constant λ_{soil} value, only one curve for both soils is shown in Figure 4-2b. As dictated by the TCDC (Figure 3-1a), the spatial and temporal variation of λ followed the same trends as θ. Even though the 2.30 m and 2.67 m observation points were closer to the GWT, the λ_{soil} of the sandy loam was inherently lower than

the λ_{soil} of the backfill. The backfill closest to the ground loops was able to maintain relatively high λ_{soil} due to precipitation infiltration and capillary rise effects from the GWT. As a consequence, the conservative and constant λ_{soil} values were about half of the λ_{soil} values predicted in the simulations using the soil's measured TCDC.

Figure 4-3 shows θ contour plots overlain with average water flux vectors for soil C at 120 d, midway through the first heating mode. Similar results were also obtained for soils A and B. The size of vectors indicates the magnitude of water flux (i.e., larger arrow indicates greater water flux). The magnitude of water flux was less in models simulated with TCDCs (Figure 4-3a) and greater in models simulated with a constant λ_{soil} (Figure 4-3b). The circular zones delineated by the water flux vectors around the ground loops indicate that water was not moving towards the ground loops but rather around the ground loops. These circular zones represent developing areas of dry soil caused by excessive thermally induced moisture migration moving water away from the ground loops. Drying conditions developed faster in models simulated with a constant λ_{soil} since the constant λ_{soil} value was about half of the λ_{soil} predicted by using the TCDC (Figure 4-2b). With lower λ_{soil} around the ground loops, heat does not dissipate as effectively and more water is driven away. In other words, under continuous operation of the ground loop, the dry soil will continue to reduce in λ_{soil}, inhibit dissipation of heat from the ground loop, and prevent resupplying of water to the area around the ground loop. As illustrated in Figure 4-3, more water was retained in the trench for the simulation modeled with the TCDC compared to the simulation modeled with constant λ_{soil}.

Figure 4-4 shows ground temperature contour plots for soil C at the end of 365 days when the simulation finished in the heating mode. Only half of the domain is shown due to symmetrical conditions. Similar results were also obtained for soils A and B. In models

simulated with TCDCs, the temperature contours were farther apart (i.e., steeper temperature gradients) and the overall temperature profile was more widespread (e.g., 10 °C temperature contour is lower in Figure 4-4a than 4-4b), which was expected since heat transfer between the ground and ground loop is more effective at higher λ_{soil}. Temperature contours located closest to the ground loop also showed that in the simulations using TCDCs, the ground temperatures closest to the ground loop were colder (and were also hotter in the cooling mode). At the end of one year of operation, the greatest difference between ground temperature contours obtained from models simulated with a TCDC versus a constant λ_{soil} was about 0.2 m.

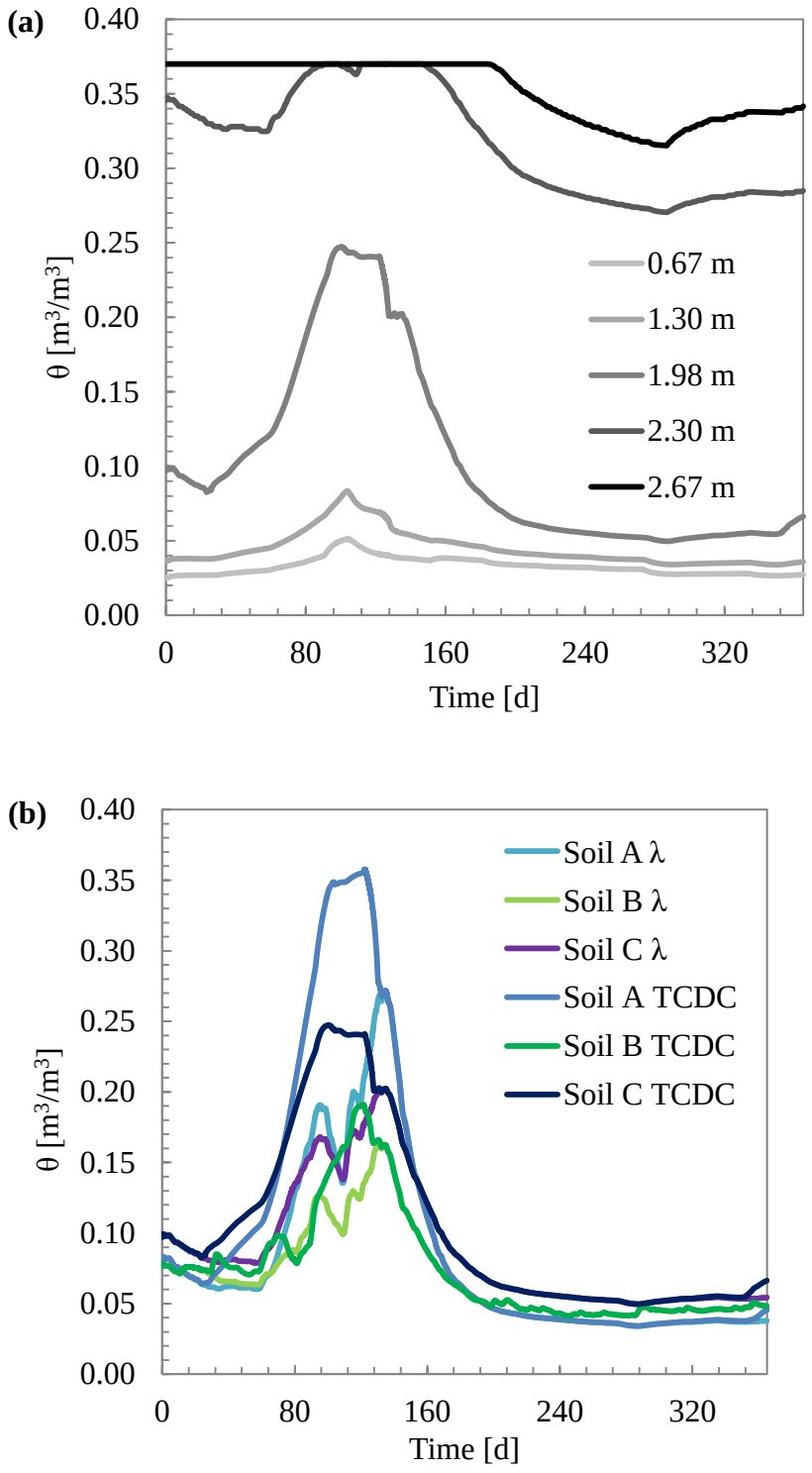

Figure 4-1. Daily θ (a) at five observation points along the y-axis for one simulation and (b) at 1.98 m bgs for all simulations. Curves labeled with λ represent simulations modeled with constant λ_{soil}.

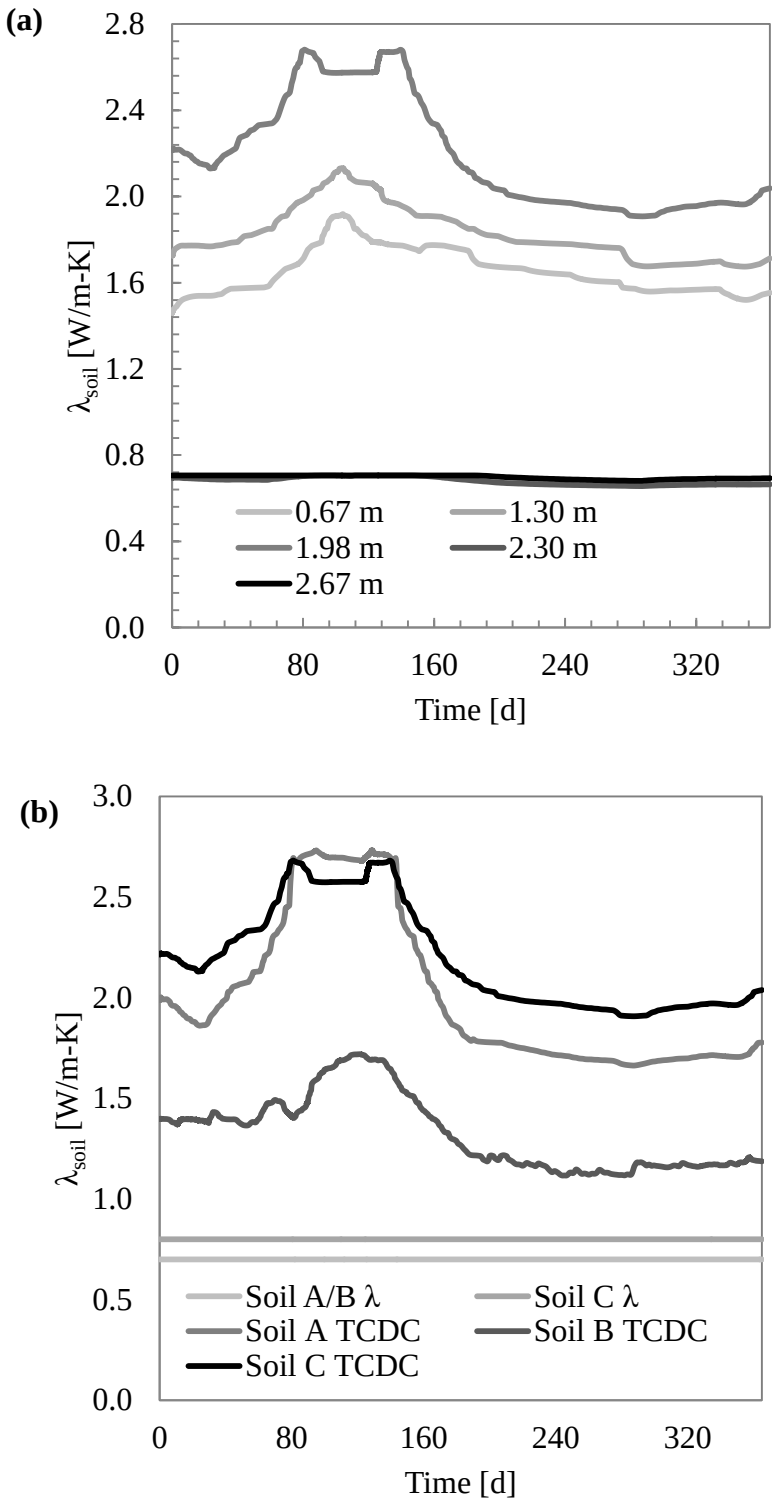

Figure 4-2. Daily λ (a) at five observation points spaced along the y-axis for one simulation and (b) at 1.98 m bgs for all simulations. Curves labeled with λ represent simulations modeled with constant λ_{soil}.

(a)

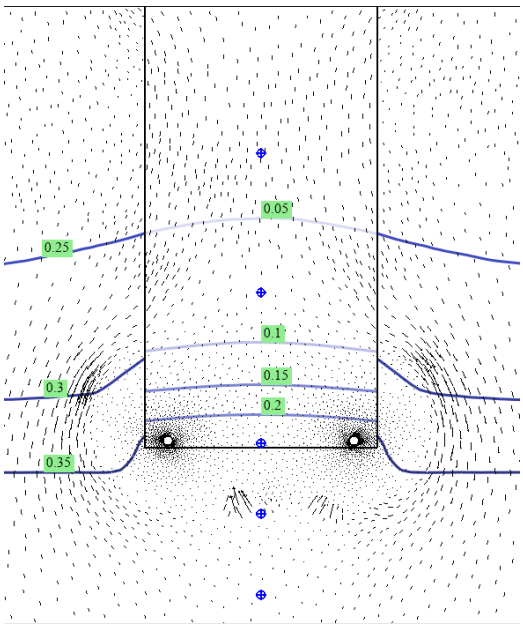

(b)

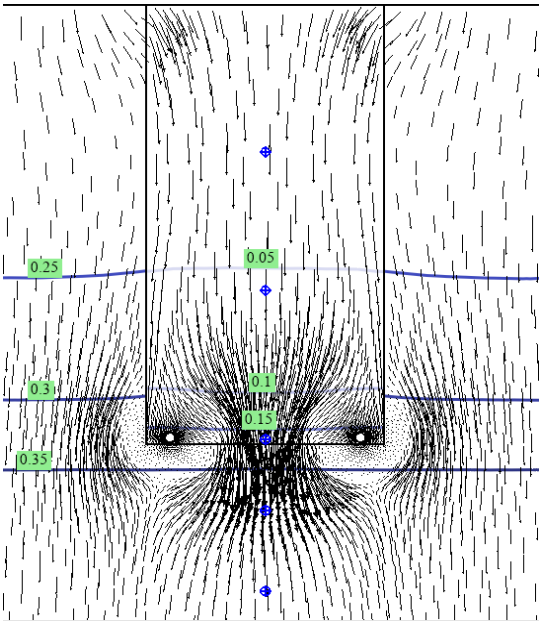

Figure 4-3. Water content contour profiles with water flux vectors after 120 days of simulation for soil C: (a) simulation modeled with TCDC and (b) simulation modeled with constant λ_{soil}. Contour labels are in θ. The size of the vectors indicates the magnitude of water flux.

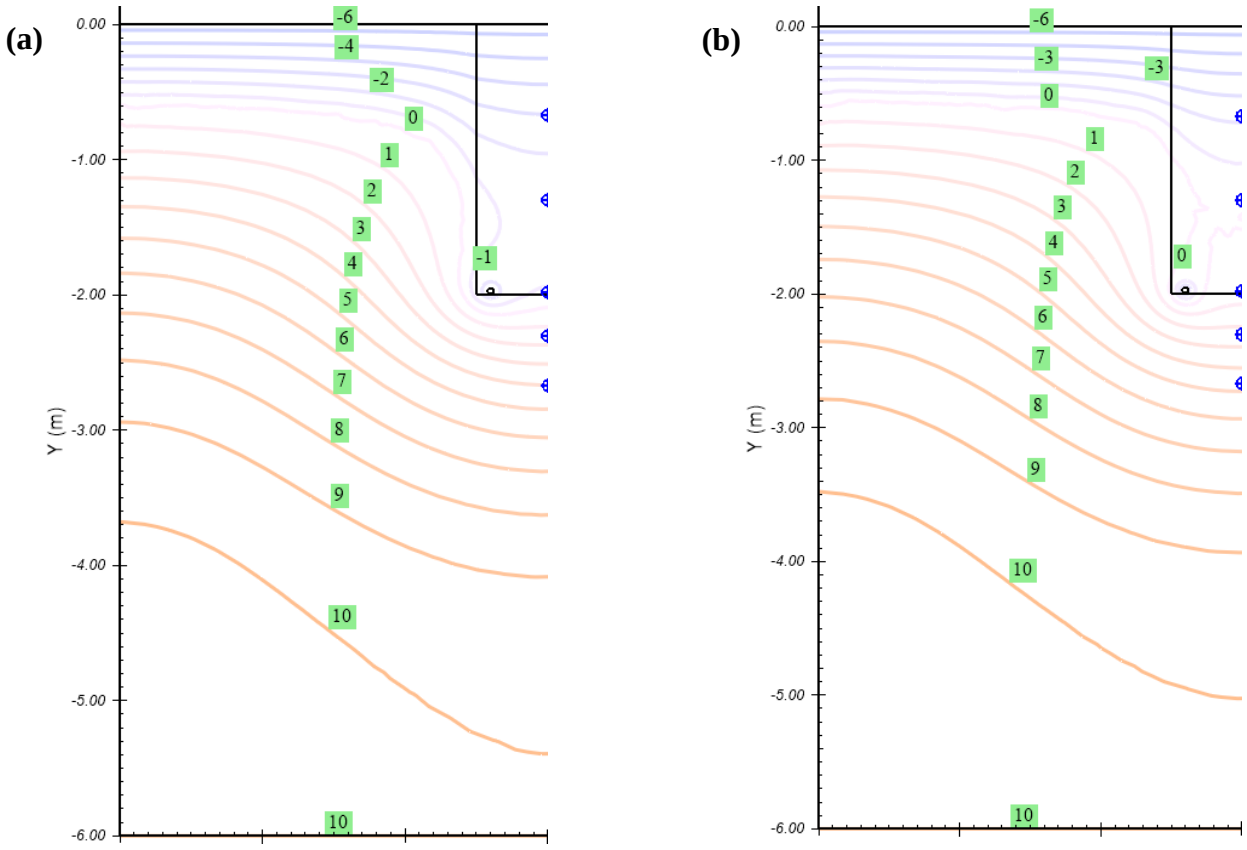

Figure 4-4. Ground temperature contour profiles after 365 days of simulation for soil C: (a) simulation modeled with TCDC and (b) simulation modeled with constant λ_{soil}. Contour labels are in °C.

4.2. Length of Ground Loop

The required length of ground loop was calculated using Eq. 3.13 for each simulation based on the input data in Table 4-1. Preliminary calculations indicated that the length of the ground loop required for the heating mode was longer than the required length for the cooling mode. Therefore, the lowest observed value of λ_{soil} at the depth of the ground loop (i.e., 1.98-m bgs) and average ground temperature during the heating mode were used (Table 4-2).

Since λ_{soil} is in the denominator of the R_{total} term in Eq. 3.13, a lower λ_{soil} value increases R_{total} and thus the length of the ground loop. Figure 4-5 presents the total length of ground loop required for each soil and indicates that differences in λ_{soil} had a significant effect on the total length of ground loop. Soils simulated with conservative and constant λ_{soil} (i.e., soils A(λ), B(λ), and C(λ)) had λ_{soil} values one-half to one-third lower than λ_{soil} values predicted by soils simulated with variable soil properties (i.e., A(TCDC), B(TCDC), and C(TCDC)). The length of ground loop was 25% to 50% longer for soils simulated with a conservative λ_{soil} value rather than a TCDC.

Table 4-1. Fixed input parameters used to calculate the total length of the ground loop in the heating mode.

Parameter	Value	Dimension
Heat pump capacity	10.55	[kW]
Heat pump COP	4	[-]
EWT	-1.11	[°C]
m_w	0.584	[kg/s]
Re (turbulent flow check)	4767	[-]
D_o	0.048	[m]
λ_{pipe}	0.48	[W/m-K]

Table 4-2. λ_{soil} and T_g used to calculate the total length of the ground loop.

Soil (TCDC or λ) →	A (λ)	A (TCDC)	B (λ)	B (TCDC)	C (λ)	C (TCDC)
λ_{soil} [W/m-K]	0.7	1.7	0.7	1.1	0.8	1.9
T_g [°C]	2.82	2.47	3.26	2.60	2.70	2.51

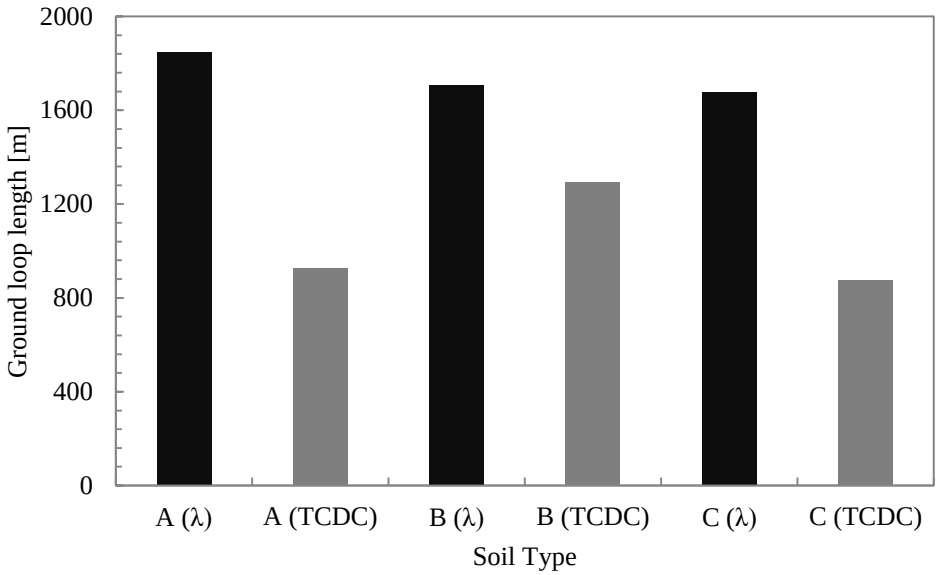

Figure 4-5. Required length of ground loop for each simulated soil. Columns labeled with λ represent simulations modeled with constant λ_{soil}.

4.3. Cost Considerations

The differences in total length of ground loop calculated in Section 4.2 suggest that significant cost implications may result, depending on the choice of input of the thermal properties of the backfill soil. Having a higher λ_{soil} results in shorter ground loops, but there are additional costs for measuring or increasing λ_{soil}. To be useful and worthwhile, the benefits of measuring λ_{soil} to avoid using conservative values or importing thermal backfill, increasing compaction, or adding water to the soil (i.e., moisture conditioning) to increase λ_{soil} must outweigh the costs. A simple analysis of costs related to the ground loop (Table 1-1) was conducted to determine whether the reduction in length of ground loop offset the extra costs from improving λ_{soil}.

Typical costs for HDPE piping, trenching, importing thermal backfill, increased compaction, moisture conditioning, and geotechnical lab testing are presented in Table 4-3. A base-case scenario using the same ground loop configuration and model geometry show in Figure 3-3 was used as a reference to compare each simulated model. The base case assumed that the ground loop was placed in native soil (i.e., sandy loam). Additionally, the base case assumed a conservative λ_{soil} value and had the longest length of ground loop. In this simple cost analysis, only HDPE piping and trenching costs were included as contributions to the total cost. However, the length of ground loop would also affect the pump costs (Table 1-1) since a longer loop requires additional energy to circulate a fluid to overcome frictional losses.

In comparison, the total cost for scenarios A(λ), B(λ), and C(λ) composed of HDPE piping, trenching, and importing thermal backfill costs. The total cost for soils A(TCDC), B(TCDC), and C(TCDC) composed of HDPE piping, trenching, importing thermal backfill costs, and one-time fee for geotechnical lab testing to determine the soil's SWCC and TCDC. In

general, geotechnical laboratory testing is costly due to expensive instrumentation and laboratory technician time. However, the SWCC and TCDC do not necessarily have to be experimentally determined as estimation models that rely on more easily measured properties (e.g., mineralogy, porosity, and dry density) can also be used. The difference in total cost (ΔCost) was determined by subtracting the total cost of the base case scenario from the total cost of each scenario.

The breakdown of costs between scenarios is shown in Table 4-4. The relative difference in λ_{soil} had a significant influence on the total cost. The imported soils A(λ), B(λ), and C(λ) had greater total costs (i.e., ΔCost increased by over $5000) than the base case because the improvement in λ_{soil} was only an increase of 0.1 W/m-K to 0.2 W/m-K, but the additional costs for that improvement were large. However, if λ_{soil} is more accurately predicted as in imported soils A(TCDC), B(TCDC), and C(TCDC), then there are significant cost savings. For example, soil B(TCDC) predicted λ_{soil} that was double the value for λ_{soil} of the base case and the total cost between scenarios was about the same (i.e., improved λ_{soil} from using TCDC offset cost of measuring TCDC). Furthermore, soils A(TCDC) and C(TCDC) predicted λ_{soil} that was triple the value of λ_{soil} for the base case and the total costs were decreased by over $5000 (i.e., improved λ_{soil} from using TCDC significantly reduced pipe length and costs). Additional cost analyses may also be conducted to evaluate the cost implications of increased compaction or moisture conditioning, but additional testing and modeling would need to be performed to determine λ_{soil} and ground temperature values. These results indicate that using conservative λ_{soil} values can result in overly expensive ground loops and that there may be a certain increase in λ_{soil} necessary to offset costs that were used to improve λ_{soil}.

Table 4-3. Cost estimates of ground loop installation expenses and techniques used to improve λ_{soil} (Kavanaugh et al., 1995; Jorgensen, 2012; Cooper Testing Laboratory, 2013).

Item	Unit	Unit Cost
HDPE piping	[$/m]	3
Trenching	[$/m]	20
Importing thermal backfill	[$/m]	12
90% compactive effort	[$/m]	2
Moisture conditioning	[$/m]	13
Geotechnical Lab Testing	[$]	3000

Table 4-4. Comparison of total cost estimates between base case and simulated soil scenarios. Larger differences in λ_{soil} with respect to the base case result in greater cost savings.

Scenario	λ_{soil} [W/m-K]	T_g [°C]	Pipe Length [m]	Total Cost	ΔCost
Base Case	0.6	3.0	2060	$26,780	$0
A (λ)	0.7	2.8	1850	$35,150	$8,370
A (TCDC)	1.7	2.5	926	$20,594	-$6,186
B (λ)	0.7	3.3	1708	$32,452	$5,672
B (TCDC)	1.1	2.6	1295	$27,605	$825
C (λ)	0.8	2.7	1679	$31,901	$5,121
C (TCDC)	1.9	2.5	878	$19,682	-$7,098

5. CONCLUSIONS AND RECOMMENDATIONS

5.1. Summary of Findings

Six finite element models were performed to predict the thermal response of three different backfill soils simulated with variable or constant soil properties. The results of the models were used to calculate the length of ground loop required for a heat pump with 10.55-kW capacity and COP of 4. The use of conservative and constant λ_{soil} values grossly underestimated the λ_{soil} predicted by using coupled TCDCs and SWCCs. As a consequence, the length of ground loop was 25% to 50% shorter when coupled TCDCs and SWCCs were used. The reduction in length of ground loop also indicated that using coupled TCDCs and SWCCs was worthwhile because better predictions of λ_{soil} can result in higher λ_{soil} where cost savings from a shorter loop can offset additional costs from measuring or improving λ_{soil}. The significant influence of λ_{soil} on the design of the ground loop was consistent with findings of previous studies.

The effect of using coupled TCDCs and SWCCs to predict the moisture-dependent thermal behavior of soil was significant in these scenarios, but may not be as drastic in other situations. Nonetheless, these simulations showed that TCDCs and SWCCs improve modeling of coupled heat and moisture flow in shallow horizontal ground loops and have potential use in the design of the ground loop. The SWCC is used to determine changes in soil moisture in response to temporal hydraulic and thermal gradients from climatic variations and ground loop operation. Furthermore, by coupling the TCDC, λ_{soil} and the thermal response of the surrounding soil are determined. By using SWCCs and TCDCs, the effects of water movement are incorporated and the thermal properties of the ground are more accurately predicted.

In extremely arid or wet climates, where soil moisture is not expected to vary over a wide range, a constant λ_{soil} representative of the dry or saturated condition may serve as a suitable

design parameter for calculating the length of the ground loop in shallow horizontal GSHP systems. However, in regions where precipitation is common or the GWT may be in proximity to the ground loop, the SWCC and TCDC are necessary to accurately model conditions. Even in scenarios where the actual operating conditions of the ground loop can be defined by a constant λ_{soil}, modeling with SWCCs and TCDCs can be used to evaluate other possible scenarios. For instance, rain collection systems (i.e., rain barrels) and drip/soak hoses are relatively inexpensive and could be installed with the ground loop. A simulation using the soil's SWCC and TCDC could predict the effect of installing an irrigation system (i.e., similar to moisture addition from precipitation) on the length of the ground loop and provide information on whether installing an irrigation system is cost effective. These comparative scenarios are significant because the length of ground loop directly impacts capital costs. Instead of using conservative estimates of thermal and hydraulic properties of soils, knowledge of temporal thermal and hydraulic behavior of the backfill and native soil can be used to calculate the length of the ground loop with more confidence and reduce capital costs associated with conservatism.

5.2. Future Study Considerations

Far more can be done with the results obtained from coupled heat and moisture flow modeling of unsaturated soil surrounding geothermal ground loops. The following recommendations are suggested for the continuation of this study:

1) Improving the model. The numerical models in this study can be improved, especially in terms of improving simplified boundary conditions. In the current models, the soil-atmosphere boundary condition was defined by approximated temperature and precipitation data. However, evaporation, net radiation, wind speed, and snow cover should also influence moisture migration. Since SWCCs and TCDCs can capture

moisture migration effects, using the most realistic climate boundary conditions is worthwhile. As discussed in Appendix C, climate boundary conditions can lengthen computational time, but astute input of climatic data as net fluxes (i.e., mathematical computations for climatic variations are done elsewhere first) may work. The boundary conditions for the HDPE pipes could also be improved. In the current study, the HDPE pipes were simulated as constant temperature elements that only changed between heating and cooling mode. Ideally, cyclic temperatures that represent when the ground loop is actually on or off would better simulate heat rejection and extraction to and from the ground. Furthermore, rather than simulating a simple cross-section of the ground loop, simulating the entire ground loop would provide information about the temperature distribution along the ground loop. However, SVOffice does not incorporate mass flow rate through nonporous materials well and computation fluid dynamic programs such as Fluent may be better options. Other suggestions that would improve the model include, but are not limited to, longer-term computation of heat exchanger operation to confirm the thermal stability of soil and reduction of model time steps to refine output files. Ultimately, a useful numerical model should have a balance between precision and detail of actual conditions and efficient computational time.

2) Experimental verification. The implementation of experimental testing is strongly recommended to provide validation and verification of the simulated models. Examples of experimental testing of shallow horizontal ground loops can be found in Demir et al. (2009), Pulat et al. (2009), Wu et al. (2010), and Naylor et al. (2011). In these studies, temperature and moisture sensors were installed in a grid around

ground loops to monitor the spatial and temporal variation of temperature and water content, which are the same results that can be obtained from the simulated models. Experimental verification of the numerical models would also be useful for evaluating how representative laboratory determined SWCCs and TCDCs translate to field conditions.

3) Comprehensive life cycle cost (LCC) and life cycle assessment (LCA). The numerical models used in this study provide information about subsurface properties necessary to size the ground loop. Knowledge of the length of ground loop leads to information about cost implications. A simple cost comparison analysis based on results of the models was provided in Section 4.3. However, a much more comprehensive cost perspective and LCC evaluation could be done to quantify monetary costs involved with both the ground loop and entire GSHP system. For example, the total cost of the ground loop could be compared to the total cost of the distribution and refrigeration loops. Furthermore, sensitivity analyses should be performed to determine which components have the greatest effect on the cost of the GSHP system. For example, in terms of the ground loop, trenching had the greatest unit cost (Table 4-3), which may suggest the length of the trench has the greatest influence on the total cost of the ground loop. If a LCC evaluation is conducted, a LCA should also be done to determine the lifetime environmental impact of the GSHP system. Both life cycle approaches require similar information and a combined LCC and LCA evaluation would lead to better quantitative measures of design methods and implications that are relevant to the barriers of the GSHP market.

4) Standardization of experimental methods for the determination TCDCs. A possible reason TCDCs have not been incorporated more in numerical modeling is that there are no internationally-recognized or industry-accepted standards (e.g., ASTM or IEEE) for experimental determination of TCDCs. However, the usefulness of coupling TCDCs with coupled heat and moisture flow modeling in this study indicates the need for a standardized document to allow for consistent and reliable data input. The numerous variables that influence λ_{soil} create challenges in determining TCDCs and known methods measure λ_{soil} under different conditions that yield TCDCs of varying resolution. Consistent forms of TCDCs need to be measured such that variations in experimental techniques do not influence the results of the model. The ASTM standard draft in Appendix A provides a foundation for such efforts.

REFERENCES

Abu-Hamdeh, N.H. (2001). "Measurement of the thermal conductivity of sandy loam and clay loam soils using single and dual probes." *Journal of Agricultural Engineering Research,* Vol. 80 (2): 209-216.

Abu-Hamdeh, N.H., and Reeder, R.C. (2000). "Soil thermal conductivity effects of density, moisture, salt concentration, and organic matter." *Soil Science Society of America Journal*, Vol. 64 (4): 1285-1290.

Agus, S.S., and Schanz, T. (2005). "Comparison of four methods for measuring total suction." *Vadose Zone Journal,* Vol. 4 (4): 1087-1095.

ASHRAE. (2007). Geothermal energy. *ASHRAE Handbook: HVAC Applications,* American Society of Heating, Refrigerating and Air Conditioning Engineers.

ASTM D5334 (2008). Standard Test Method for Determination of Thermal Conductivity of Soil and Soft Rock by Thermal Needle Probe Procedure, ASTM International.

ASTM D6836 (2008). Standard Test Methods for Determination of the Soil Water Characteristic Curve for Desorption Using Hang Column, Pressure Extractor, Chilled Mirror Hygrometer, or Centrifuge. ASTM International.

ASTM D698 (2012). Standard Test Methods for Laboratory Compaction of Soil Using Standard Effort (12,400 ft-lbf/ft^3 (600 kN-m/m^3)), ASTM International.

Benazza, A., Blanco, E., Aichouba, M., Rio J.L., Laouedj, S. (2011). "Numerical investigation of horizontal ground coupled heat exchanger." *Energy Procedia*, Vol. 6: 29-35.

Brandon, T.L., and Mitchell, J.K. (1989). "Factors influencing thermal resistivity of sands." *Journal of Geotechnical Engineering*, Vol. 115 (12): 1683-1698.

Bristow , K.L., White, R.D., and Kluitenberg, G.J. (1994). "Comparison of single and dual probes for measuring soil thermal properties with transient heating." *Australian Journal of Soil Research,* Vol. 32: 447-464.

Campbell, G.S. (2012). "Heat and water transport in soil." 2nd International Thermal Resistivity Workshop, Decagon Devices, Seattle, Washington.

Campbell, G.S. and Bristow, K.L. (2007). "Underground power cable installations: soil thermal resistivity." Application Note. Decagon Devices.

Campbell, G.S., Jungbauer Jr, J.D., Bidlake, W.R., and Hungerford, R.D. (1994). "Predicting the effect of temperature on soil thermal conductivity." *Soil Science,* Vol. 158 (5): 307-313.

Cane, R.L. and Forgas, D.A. (1991). "Modeling of ground source heat pump performance." *ASHRAE Transactions*. Vol. 97 (1): 909-925.

Caneta Research Inc. (1992). "Development of algorithms for ground source heat pump heat exchanger length prediction and energy analysis." Efficiency and Alternative Energy Branch, Natural Resources Canada, Ottawa, Canada.

Caneta Research (1999). "Global warming Impacts of ground-source heat pumps compared to other heating and cooling systems." Caneta Research Inc., Ottawa, Canada.

Carslaw, H.S. and Jaeger, J.C. (1947). Conduction of heat in solids. Oxford: Claremore Press.

Chiasson, A.D. (2010). "Modeling horizontal ground heat exchangers in geothermal heat pump systems." *Proceedings of COMSOL Conference*.

Chong, C.S.A., Gan, G., Verhoef, A., Garcia, R.G., and Vidale, P.L. (2012). "Simulation of thermal performance of horizontal slinky-loop heat exchangers for ground source heat pumps." *Applied Energy,* Vol. 104: 603-610.

Cooper Laboratory Testing. (2013). "Geotechnical/environmental and corrosion testing schedule of charges." Website: http://www.coopertestinglabs.com/pages/FeeSchedule.pdf.

Congedo, P.M., Colangelo, G., and Starace, G. (2012). "CFD simulations of horizontal ground heat exchangers: A comparison among different configurations." *Applied Thermal Engineering,* Vol. 33: 24-32.

Côté, J., and Konrad, J.M. (2005). "A generalized thermal conductivity model for soils and construction materials." *Canadian Geotech. J.,* Vol. 42 (2): 443-458.

Curtis, R., Lund, J., Sanner, B., Rybach, L., and Hellström, G. (2005). "Ground source heat pumps–geothermal energy for anyone, anywhere: current worldwide activity." In *Proceedings World Geothermal Congress,* Antalya, Turkey: 24-29.

Demir, H., Koyun, A., and Temir, G. (2009). "Heat transfer of horizontal parallel pipe ground heat exchanger and experimental verification." *Applied Thermal Engineering,* Vol. 29 (2): 224-233.

de Vries, D.A. (1963). Thermal properties of soils. *Physics of Plant Environment*. W.R. van Wijk (ed.). North Holland Pub. Co. Amsterdam: 210-235.

de Vries, D. A. (1987). The theory of heat and moisture transfer in porous media revisited. *International Journal of Heat and Mass Transfer*, Vol. 30 (7): 1343-1350.

Do, S.L. and Haberl, J.S. (2010). "A review of ground couled heat pump models used in whole-building computer simulation programs." In *Proceedings of the 17th Symposium for Improving Building Systems in Hot and Humid Climates*, Austin, Texas.

Esen, H., Inalli, M., and Esen, M. (2007). "Numerical and experimental analysis of a horizontal ground-coupled heat pump system." *Building and Environment*, Vol. 42 (3): 1126-1134.

Florides, G., and Kalogirou, S. (2007). "Ground heat exchangers—A review of systems, models and applications." *Renewable Energy*, Vol. 32 (15): 2461-2478.

Fredlund, D. G., Rahardjo, H., and Fredlund, M. D. (2012). Unsaturated soil mechanics in engineering practice. Hoboken, N.J.: John Wiley & Sons.

GeoComfort. (2013). "The geothermal process." Website: http://www.geocomfort.com/about/geothermal-process

Hansen, D., Breyer, W. H., and Riback, W. J. (1970). Steady state heat transfer in partially liquid filled porous media. *Journal of Heat Transfer*, Vol. 92 (3).

Hanson, J.L., Neuhaeuser, S., Yesiller, N. (2004). "Development and calibration of a large-scale thermal conductivity probe." *Geotechnial Testing Journal*, Vol. 27 (4): 1-11.

Hartley, J.G. and Black, W.Z. (1981). "Transient simultaneous heat and mass transfer in moist, unsaturated soils." *Journal of Heat Transfer*, Vol. 103: 376-382

Hiraiwa, Y., and Kasubuchi, T. (2000). "Temperature dependence of thermal conductivity of soil over a wide range of temperature (5–75 C)." *European Journal of Soil Science*, Vol. 51 (2): 211-218.

Hopmans, J.W., and Dane, J.H. (1986). "Thermal conductivity of two prous media as a function of water ctonent, temperature, and density." *Soil Science Society of America Journal*, Vol. 142 (4): 187-195.

Hughes, P.J. (2008). "Geothermal (ground-source) heat pumps: market status. Barriers to adoption, and actions to overcome barrier." Oak Ridge National Laboratory for US DOE, ORNL/TM, 232.

İnallı, M., and Esen, H. (2005). "Seasonal cooling performance of a ground-coupled heat pump system in a hot and arid climate." *Renewable Energy*, Vol. 30 (9): 1411-1424.

Incropera, F.P., DeWitt, D.P., Bergman, T.L., and Lavine, A.S. (2006). Fundamentals of heat and mass transfer. Sixth Edition. John Wiley and Sons, Inc.

Ingersoll, L.R., Zobel, O.J., and Ingersoll, A.C. (1954). Heat conduction with engineering, geological, and other applications. New York: Mcgraw-Hill.

Jorgensen, S.C. (2012). Geothermal considerations in electrical collector system design for wind energy facilities. *MSc Thesis*, Department of Geological Engineering, University of Wisconsin-Madison, Madison, Wisconsin.

Kavanaugh, S., Gilbreath, C., and Kilpatrick J. (1995). "Cost containment for ground-source heat pumps." *Tennessee Valley Authority*, Chattanooga, Tennessee.

Krishnapillai, S. H., and Ravichandran, N. (2012). "New soil-water characteristic curve and its performance in the finite-element simulation of unsaturated Soils." *International Journal of Geomechanics*, Vol. 12 (3): 209-219.

Leij, F.J., Alves, W.J., van Genuchten, M.T., and Williams, J.R. (1996). "The UNSODA unsaturated hydraulic database." U.S. Environmental Protection Agency, Cincinnati, Ohio.

Likos, W. J., Olson, H. S., and Jaafar, R. (2012). "Comparison of laboratory methods for measuring thermal conductivity of unsaturated soils." *GeoCongress 2012 State of the Art and Practice in Geotechnical Engineering*, ASCE: 4366-4375.

McQuay International. (2002). Geothermal heat pump design manual. Application Guide AG 31-008. McQuay International.

Mitchell, J.K., Boggs, S.A., Rodenbaugh, T.J., Chu, F.Y., Ford, G.L., Radhakrishna, H. S., and Steinmanis, J. (1979). "EPRI soils research program." *Transmission and Distribution Conference and Exposition*, IEEE: 108-116.

Mitchell, J.K. and Kao, T.C. (1978). "Measurement of soil thermal resistivity." *ASCE Journal of the Geotechnical Engineering Division*, Vol. 104 (GT10): 1307-1320.

Mitchell, J.K. and Soga, K. (2005). Fundamentals of soil behavior. John Wiley and Sons, Inc.

Naylor, S., Gustin, A., and Ellett, K.M. (2011). "Monitoring near-surface thermal properties in conjunction with energy and moisture budgets to facilitate the optimization of ground-source heat pumps in the glaciated Midwest." American Geophysical Union Fall meeting, San Francisco, CA.

Neher, J.H. and McGrath, M.H. (1957). "The calculation of the temperature rise and load capability of cable systems." *AIEE Transactions*, Vol. 76 (3): 752-772.

Philip, J.R. and de Vries, D.A. (1957). "Moisture movement in porous materials under temperature gradients." *Transactions, American Geophysical Union*, Vol. 38 (2): 222-232.

Reid, D. (2005). Guarded hot plate apparatus design and construction for thermal conductivity measurements. *MSc Thesis*, Program of Mechanical Engineering, Ryerson University, Toronto, Ontario, Canada.

Remund C. and Carda, R. (2009). Ground source heat pump residential and light commercial design and installation guide. Oklahoma State University and International Ground Source Heat Pump Assocation.

Roth, K. (2012). Soil physics lecture notes V2.2. Institute of Environmental Physics, Heidelberg University.

Pulat, E., Coskun, S., Unlu, K., and Yamankaradeniz, N. (2009). "Experimental study of horizontal ground source heat pump performance for mild climate in Turkey." *Energy*, Vol. 34 (9): 1284-1295.

Salomone, L.A. and Kovacs, W.D. (1983). "The use of index property tests to determine the thermal properties of soils." *ASTM Geotechnical Testing Journal*, Vol. 6(4): 173-180.

Salomone, L.A., and Kovacs, W.D. (1984). "Thermal resistivity of soils." *Journal of Geotechnical Engineering*, Vol. 110 (3): 375-389.

Sepaskhah, A.R., and Boersma, L. (1979). "Thermal conductivity of soils as a function of temperature and water content." *Soil Science Society of America Journal*, Vol. 43 (3): 439-444.

Smits, K.M., Sakaki, T., Limsuwat, A., and Illangasekare, T.H. (2010). "Thermal conductivity of sands under varying moisture and porosity in drainage–wetting cycles." *Vadose Zone Journal*, Vol. 9 (1): 172-180.

Smits, K.M., Sakaki, T., Howington, S.E., Peters, J.F., and Illangasekare, T.H. (2012). "Temperature dependence of thermal properties of sands across a wide range of temperatures (30-70 °C)." *Vadose Zone Journal*, Vol. 12 (1): 1-8.

Su, H. J. (1981). Heat transfer in porous media with fluid phase changes. *Ph.D. Thesis, University of California-Berkley,* Berkley, California.

Tarnawski, V.R., and Leong, W.H. (1993). "Computer analysis, design and simulation of horizontal ground heat exchangers." *International Journal of Energy Research*, Vol. 17 (6): 467-477.

Tarnawski, V.R., Leong, W.H., and Bristow, K.L. (2000). "Developing a temperature-dependent Kersten function for soil thermal conductivity." *International Journal of Energy Research,* Vol. 24 (15): 1335-1350.

Tarnawski, V.R., Leong, W.H., Momose, T., and Hamada, Y. (2009). "Analysis of ground source heat pumps with horizontal ground heat exchangers for northern Japan." *Renewable Energy,* Vol. 34 (1): 127-134.

Thode R. and Zhang J. (2009). "SVHeat 1D/2D/3D geothermal modeling software theory manual." SoilVision® Systems Ltd.

Tinjum, J.M. (2012). "The thermal dryout curve." Second International Thermal Resistivity Workshop, Decagon Devices, Seattle, WA.

Ultimate Green Energy. (2013). "Heat pumps." Website: http://uge.uk.com/wp-content/uploads/2012/08/ground-source-heat-pump1.jpg

US Environmental Protection Agency. (1993). Space Conditioning: The Next Frontier. US Environmental Protection Agency.

van Genuchten, M.T. (1980). "A closed-form equation for predicting the hydraulic conductivity of unsaturated soils." *Soil Science Society of America Journal,* Vol. 44 (5): 892-898.

Van, R.M., and Winterkorn, H.F. (1959). "Structural and textural influences on thermal conductivity of soils." *Highway Research Board Proceedings,* Vol. 38: 576-621.

Williams, G.P. and Gold, L.W. (1976). "Ground temperatures." *Canadian Building Digest*. National Research Council of Canada.

Woodward, N.R., and Tinjum, J.M. (2012). "Impact of moisture migration on thermal resistivity testing in unsaturated soil." *GeoCongress 2012 State of the Art and Practice in Geotechnical Engineering,* ASCE: 4426-4435.

Woodward, N.R., Tinjum, J.M., and Wu, R. (2013). "Water migration impacts on thermal resistivity testing procedures." *Geotechnical Testing Journal,* Vol. 36 (6): 1-9.

Wu, Y., Gan, G., Verhoef, A., Vidale, P.L., and Gonzalez, R.G. (2010). "Experimental measurement and numerical simulation of horizontal-coupled slinky ground source heat exchangers." *Applied Thermal Engineering,* Vol. 30 (16): 2574-2583.

6. APPENDIX A - ASTM STANDARD DRAFT FOR EXPERIMENTAL DETERMINATION OF THERMAL RESISTIVITY DRYOUT CURVES

Include Ballot Rationale Here (Required for all Ballots)

Standard Test Methods for Determination of Thermal Resistivity Dryout Curves of Soil Using Single-specimen, Multiple-specimen, Stage-drying, or Automated Hanging Column [1]

This standard is issued under the fixed designation X XXXX; the number immediately following the designation indicates the year of original adoption or, in the case of revision, the year of last revision. A number in parentheses indicates the year of last reapproval. A superscript epsilon (ε) indicates an editorial change since the last revision or reapproval.

1. Scope

1.1 These test methods cover the determination of thermal resistivity dryout curves (TRDCs) of soil. TRDCs describe the relationship between thermal resistivity and gravimetric water content, volumetric water content, or degree of water saturation.

1.2 This standard describes four methods (A-D) for determining the thermal resistivity dryout curve. Methods A, B, and C are applicable to coarse and fine soils whereas Method D is generally constrained to coarse soils with little fines (e.g., sands). These methods are appropriate only for isotropic materials.

1.3 Method A (single-specimen) is suitable for undisturbed and compacted specimens. Method B (multiple-specimen) provides a faster procedure for determining the thermal resistivity dryout curve and is applicable to compacted specimens. Both Method A and Method B measure thermal resistivity through the vertical axis of the specimen and determine the average-based water content of the specimen. Method C (stage-drying) is useful for observing moisture distribution throughout the specimen and is applicable to compacted specimens. Method C measures thermal resistivity at three locations perpendicular to the vertical axis and determines

[1] This test method is under the jurisdiction of ASTM Committee and is the direct responsibility of Subcommittee .

Current edition approved XXX. XX, XXXX. Published XX XXXX. DOI:10.1520/XXXXX-XX

water content directly at the location of the thermal resistivity measurements. Method D (automated hanging column) is advantageous for continuous measurements of water content, thermal resistivity, matric suction, and temperature. Method D provides simultaneous determination of the thermal resistivity dryout curve and soil-water characteristic curve.

1.4 The values stated in SI units are to be regarded as standard. No other units of measurement are included in this standard.

1.5 *This standard does not purport to address all of the safety concerns, if any, associated with its use. It is the responsibility of the user of this standard to establish appropriate safety and health practices and determine the applicability of regulatory limitations prior to use.*

2. Referenced Documents

2.1 *ASTM Standards:*

C 127 Test Method for Density, Relative Density (Specific Gravity), and Absorption of Coarse Aggregate

D 653 Terminology Relating to Soil, Rock, and Contained Fluids

D 698 Test Methods for Laboratory Compaction Characteristics of Soil Using Standard Effort (600 kN-m/m^3)

D 854 Test Methods for Specific Gravity of Soil Solids by Water Pycnometer

D 1587 Practice for Thin-Walled Tube Sampling of Soils for Geotechnical Purposes

D 2216 Test Methods for Laboratory Determination of Water (Moisture) Content of Soil and Rock by Mass

D 3404 Guide for Measuring Matric Potential in Vadose Zone Using Tensiometers

D 3740 Practice for Minimum Requirements for Agencies Engaged in Testing and/or Inspection of Soil and Rock as Used in Engineering Design and Construction

D 4643 Test Methods for Determination of Water (Moisture) Content of Soil by Microwave Oven Heating

D 4753 Guide for Evaluating, Selecting, and Specifying Balances and Standard Masses for Use in Soil, Rock, and Construction Materials Testing

D 5334 Test Methods for Determination of Thermal Conductivity of Soil and Soft Rock by Thermal Needle Probe Procedure

D 6026 Practice for Using Significant Digits in Geotechnical Data

D 6169 Guide for Selection of Soil and Rock Sampling Devices Used With Drill Rigs for Environmental Investigations

2.2 *IEEE Standard:*

IEEE Std 442 Guide for Soil Thermal Resistivity Measurements

3. Terminology

3.1 *Definitions:*

3.1.1 For common definitions of soil and rock terms in this standard, refer to Terminology D 653.

3.2 *Definition of Terms Specific to This Standard:*

3.2.1 *critical water content,* θ_{crit} – the knee of the thermal resistivity dryout curve where a further reduction in water content corresponds to a large increase in thermal resistivity.

3.2.2 *thermal resistivity,* ρ_T – a measure of the ability of a material to resist heat, the inverse of thermal conductivity.

3.2.3 *thermal resistivity dryout curve (TRDC)* – a graph of thermal resistivity versus water content (gravimetric or volumetric) or saturation.

4. Summary of Test Methods

4.1 *Methods A-D* – Methods A-D yield thermal resistivity dryout curves as a function of water content (gravimetric or volumetric) or saturation. Various techniques are used to measure thermal resistivity at varying water contents. In Method A, a saturated specimen is dried slowly via evaporation. In Method B, several specimens are compacted to various water contents. In Method C, specimens are dried in an oven for varying periods of time. In Method D, water is drained from a saturated specimen.

4.2 *Method A* – In Method A, a single cylindrical test specimen is saturated and weighed. A thermal probe is inserted through the vertical axis of the specimen to measure thermal resistivity. Additional weight and thermal resistivity measurements are taken over time as the specimen dries via evaporation. The final weight and thermal resistivity measurements are taken after the specimen is placed in a 110 °C oven and fully dried.

4.3 *Method B* – In Method B, thermal resistivity measurements are obtained for multiple specimens prepared to the same dry density but varying water contents. A single specimen is recompacted to new water contents after each thermal resistivity measurement, or multiple specimens at various water contents are used. Similar to Method A, a thermal probe is inserted through the vertical axis of the specimen to measure thermal resistivity. Thermal resistivity measurements are taken for a minimum of five specimens.

4.4 *Method C* – In Method C, three identical cylindrical test specimens are compacted to a specified density and water content. The specimens are weighed and a thermal probe is inserted horizontally into the top, middle, and bottom thirds of each specimen to measure initial thermal resistivity values. The three specimens are placed in a 50 °C oven to accelerate the drying time. One specimen is removed after 24 hours, 3 days, and 10 days of oven drying. Upon removal, the specimen is weighed and new thermal resistivity measurements are taken at the top, middle, and bottom thirds of the specimen. A soil sample is collected from each measurement location for water content determination.

4.5 *Method D* – Method D simultaneously yields a thermal resistivity dryout curve and soil-water characteristic curve from continuous collection of thermal resistivity, matric suction, and water content via data logging. Soil is packed into a modified Tempe cell embedded with a dielectric soil moisture sensor, tensiometer, temperature probe, and thermal probe. The specimen is saturated by a hanging column reservoir. Water content, matric suction, temperature, and thermal resistivity are continuously measured as pore water drains through the specimen. Once the specimen is dry, soil samples in the vicinity of the sensors are collected and weighed to verify soil water content.

5. Significance and Use

5.1 Soil thermal resistivity is critical in analyzing and designing buried utilities (e.g., high-voltage electrical cables, steam and hot water lines, and gas pipelines), thermally active geo-structures (e.g., heat-exchange piles, thermo-active tunnels, and geosynthetic heat exchanger systems), and heat exchange elements for shallow geothermal heating and cooling systems.

5.2 Thermal resistivity dryout curves are used in design practice to classify the thermal behavior of soil and to predict coupled heat and moisture flow. The critical water content is also determined from the dryout curve. Accurate knowledge of the relationship between moisture distribution and thermal resistivity can lead to more efficient and cost-effective designs of the aforementioned applications.

5.3 These methods can be used to evaluate the effect of different soil properties–particularly water content, density, temperature, and composition–on thermal resistivity.

6. Apparatus

6.1 *Methods A, B, and C*

6.1.1 *Mold Assembly* – The mold assembly used for compacted specimen preparation shall follow guidelines described in Test Method D 698.

6.1.2 *Manual Rammer* – The manual operated rammer used for compacted specimen preparation shall follow guidelines described in Test Method D 698.

6.1.3 *Specimen Holder (Method A and B)* – A cylindrical shaped container (i.e. compaction mold or bucket) having a minimum inner diameter of 51 mm and inner height of 200 ± 30 mm.

6.1.4 *PVC Cylinder (Method C)* – PVC pipes having an inner diameter of 152 mm and a height of 203 mm. The PVC pipes have three openings oriented 120 degrees radially from each other located at the top, middle, and bottom thirds of the cylinder. The PVC pipes are secured to an acrylic plate with epoxy and sealed with silicone sealant along the outer base of the cylinder. A PVC cylinder having the required features is shown in Fig. 1.

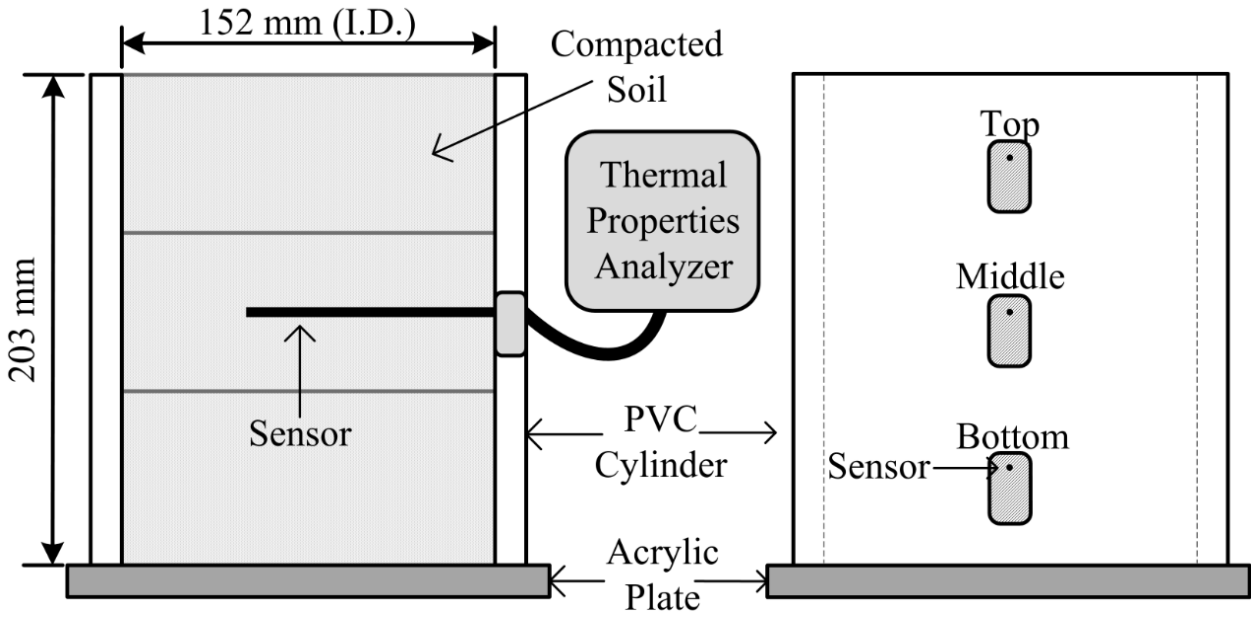

Fig 1. Schematic of PVC Cylinder used in Method C (Woodward et al., 2013).

6.2 *Method D*

6.2.1 *Modified Tempe Cell* – A Tempe cell modified with four sampling ports for placement of sensors. A modified Tempe cell having the required features is shown in Fig. 2.

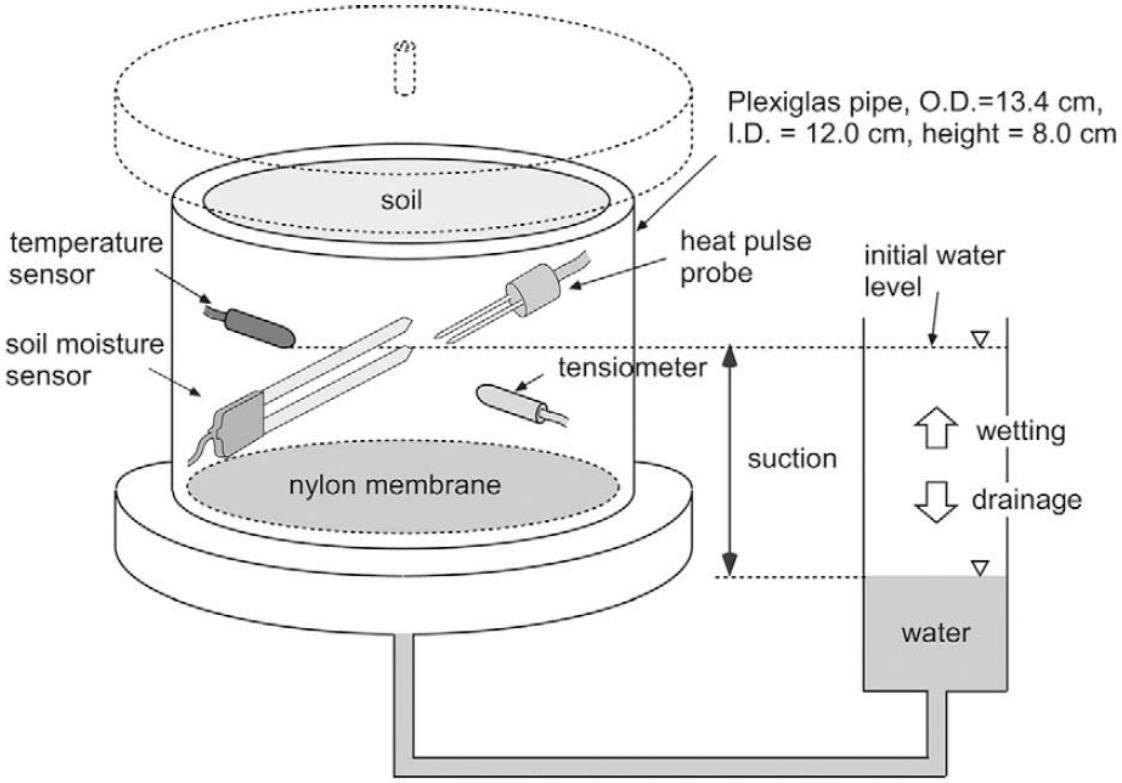

Fig 2. Schematic of modified Tempe cell used in Method D (Smits et al., 2010).

6.2.2 *Hanging Column Reservoir* – A long (i.e., greater than one meter) graduated cylindrical tube in which the water level can be gradually lowered or elevated (Fig. 2).

6.2.3 *Nylon Membrane Filter* – A hydrophilic nylon membrane filter with an equivalent diameter to the Tempe cell and air-entry pressure greater than atmospheric pressure.

6.2.4 *Dielectric Soil Moisture Sensor* – An instrument to determine the volumetric water content of the specimen by measuring the dielectric constant of the soil.

6.2.5 *Temperature Probe* – An instrument to determine the temperature of the specimen.

6.2.6 *Tensiometer* – An instrument to determine the matric suction of the specimen as described in Guide D 3404.

6.2.7 *Data Logger* – An instrument to record data from the dielectric soil moisture sensor, temperature probe, tensiometer, and thermal probe.

6.3 *Methods A-D*

6.3.1 *Thermal Probe* – A thermal probe meeting the specifications in Test Method D 5334 and IEEE Std 442. Methods A-C shall use a 100 mm long needle. Method D shall use a 30 mm long and 6 mm spacing dual-needle.

6.3.2 *Thermal Properties Analyzer* – A device capable of producing a constant heat source and measuring thermal resistivity as well as temperature.

6.3.3 *Thermal Grease* – A viscous fluid with high thermal conductivity (i.e., greater than 4 W/m-K) used to improve thermal contact between surfaces.

6.3.4 *Moisture Content Containers* – The containers used for determination of water content shall be in accordance with Test Method D 2216.

6.3.5 *Drying Ovens* – For Method C, a thermostatically controlled oven capable of maintaining a uniform temperature of 50 ± 5 °C shall be used. For determination of water content in Methods A-D, a thermostatically controlled oven capable of maintaining a uniform temperature of 110 ± 5 °C shall be used in accordance with Test Method D 2216.

6.3.6 *Balances* – For specimen weight measurements in Methods A, B, and C, a balance shall be used that has a minimum capacity of 20,000 g and a sensitivity of 0.1 g. For determination of water content in Methods A-D, a Class GP1 balance of 0.01 g readability shall be used for specimens having a mass of up to 200 g (excluding mass of specimen container). All balances shall meet the requirements provided in Specification D 4753.

6.3.7 *Drill* – Equipment capable of drilling a straight hole having a diameter and depth as close as possible to that of the thermal probe.

6.3.8 *Mixing Tools* – Scoops, trowel, mixing pan, airtight containers, and graduated cylinders (to add water).

6.3.9 *Miscellaneous Tools* – wire saw, beveled straightedge, spatula, and other small tools for trimming specimens, scotch tape, small buckets, pliers, hammer, screwdriver, tape measure, level, wrench, tampering hammer, plastic tubing, syringe, insulation.

6.3.10 *Laboratory Environment* – The laboratory temperature shall be maintained within ± 3 °C during the test. The apparatus and specimens shall be shielded from direct sunlight or other sources of heat that may cause variations in temperature.

7. Reagents and Materials

7.1 *Water* – For Method A, B, and C, potable tap water may be used to compact and saturate a specimen.

7.2 *Deaired Water* – For Method D, deaired water shall be used to pack and saturate a specimen. Water is usually deaired by boiling, spraying a fine mist of water into an evacuated vessel attached to a vacuum source, or by forceful agitation of water in a container attached to a vacuum source.

8. Preparation of Apparatus

8.1 *Specimen Holder, PVC Cylinder, or Modified Tempe Cell(Method A-D)* – Measure the inside diameter of the specimen holder, PVC cylinder, or modified Tempe cell to the nearest 0.1

mm at three locations and record the average of these measurements as the diameter. Measure the inside height of the specimen holder, PVC cylinder, or modified Tempe cell to the nearest 0.1 mm at three locations and record the average of these measurements as the height. Calculate the volume of the specimen holder, PVC cylinder, or modified Tempe cell using the diameter and inside height.

8.2 *Specimen Holder and PVC Cylinder (Method A, B, and C)* – Weigh the specimen holder or PVC cylinder and record the weight to the nearest 0.1 g.

8.3 *PVC Cylinder (Method C)* – Cover the three openings with a thin membrane (e.g., scotch tape) to prevent soil and water from escaping the cylinder.

8.4 *Modified Tempe Cell (Method D)* – Place the nylon membrane filter at the bottom of the cell. High vacuum grease may be used to provide a better seal. Connect the bottom of the Tempe cell to the hanging column reservoir. Saturate the tensiometer with deaired water (7.2). Place the thermal probe, temperature probe, dielectric soil moisture sensor, and tensiometer into the cell.

9. Specimen Preparation

9.1 *Undisturbed Soil Specimens (Method A)* – Prepare a specimen with minimum dimensions of 51 mm diameter and 200 ± 30 mm length by coring undisturbed soil using an appropriate method such as described in Practice D 1587 or Guide D 6169 .

9.2 *Compacted Soil Specimens (Methods A, B, and C)* – Compact specimens to the desired density, water content, and specimen dimensions (adhering to minimum specimen holder dimensions). For Method A, one specimen shall be made. For Method B, a single specimen

recompacted to new water contents after each measurement, or a minimum of five specimens at various water contents shall be made. For Method C, three identical specimens shall be made.

9.2.1 *Initial Water Content Determination* – If the initial water content of the soil sample is unknown, water content determination shall be done in accordance with Test Method D 4643.

9.2.2 *Desired Water Content* – Based on the initial water content of the soil, add the appropriate amount of water to reach the desired water content. Thoroughly mix the soil and water and leave the soil mixture in an airtight container for at least 24 hours.

9.2.3 *Water Content Verification* – Prior to compaction, determine the water content according to Test Method D 4643 to verify the water content is within ± 0.5% of the desired water content. If the water content is not within ± 0.5% of the desired water content, add or remove the proper mass of water. Place the soil in an airtight container for at least an additional 12 hours.

9.2.4 *Compaction* – The appropriate mold assembly and specimen holder or PVC cylinder for Methods A and B or C, respectively, shall be used. Compact the specimens to the desired dry density on a mass basis in three equal lifts using the manual rammer and Standard Proctor effort described in Test Method ASTM D 698. Use a consistent blow pattern to ensure even lifts. For Method A, the compacted specimen shall be carefully extruded from the specimen holder. For Methods B and C, the compacted specimens shall remain in the specimen holders or PVC cylinders.

9.3 *Specific Gravity* – The specific gravity of the soil is necessary to determine the degree of saturation from water content. The specific gravity may be assumed or measured in accordance to an appropriate test method, such as Test Method C 127 or Test Method D 854.

9.4 *Maximum Dry Unit Weight and Optimum Water Content* – If the maximum dry unit weight and optimum water content of the soil are unknown, a compaction curve denoting the maximum dry unit weight and optimum water content should be done in accordance to Test Method D 698.

10. Calibration and Standardization

10.1 Calibration and standardization for procedures related to the standard effort compaction of the specimen shall be done in accordance to Test Method ASTM D 698.

10.2 The thermal probe shall be calibrated before use in accordance to Test Method ASTM D 5334 and IEEE Std 442.

10.3 The dielectric soil moisture sensor shall be calibrated before use according to the method developed by Sakaki et al. (2008).

11. Procedure

11.1 *Sensor Holes Prior to Thermal Probe Insertion* – Methods A, B, and C require proper thermal probe insertion technique to obtain accurate thermal resistivity measurements and care to prevent damage to the probe. Prior to inserting the thermal probe into the specimen, a sensor hole of equal diameter and length to the thermal probe shall be made. The sensor hole facilitates proper insertion of the thermal probe. For dense soil or dry soil at low water contents, a drill may be necessary to create the sensor hole. If a drill is used, the thermal probe shall not be inserted until a sufficient cool-down period has dissipated the heat from drilling. The thermal probe should be inserted straight and completely into the specimen to ensure good thermal contact

between the thermal probe and the specimen. Thermal grease may be used to improve the thermal contact between the thermal probe and the specimen. The thermal probe has been properly inserted if the entire probe fits snugly into the sensor hole. Additionally, the thermal probe should be connected properly to the thermal properties analyzer.

11.2 *Thermal Resistivity Measurements* – Methods A, B, and C use the 100-mm-long thermal probe. After the thermal probe has been inserted into the sensor hole, at least five minutes shall be given for the probe to equilibrate within the specimen. Thermal resistivity measurements shall be done using a ten minute read time.

11.3 *Single-specimen (Method A)*:

11.3.1 *Specimen Saturation* – Place the prepared soil specimen (undisturbed or compacted) in a pan of water approximately 9 cm deep for at least 24 hours.

11.3.2 *Specimen Temperature Equilibration* – Remove the specimen from the pan, place it on a balance, and weigh the specimen. Allow the specimen to come to equilibrium with the laboratory room temperature prior to measuring thermal resistivity. Temperature equilibration is important as temperature drift causes error in the thermal resistivity measurements.

11.3.3 *Thermal Probe Insertion* – Create a sensor hole through the vertical axis of the specimen as described in 11.1. Insert the thermal probe.

11.3.4 *Thermal Resistivity Measurements* – Keeping the specimen on the balance, make simultaneous thermal resistivity and weight measurements at regular time intervals as the specimen dries from evaporation to the testing environment. Thermal resistivity measurements are taken for a 10-min read time (11.2) and given at least a 15 min cool-down period between measurements. In general, a frequency of two measurements per day is adequate.

11.3.5 *Oven Dry Specimen* – When the specimen reaches a sufficiently low water content (i.e., consecutive weight measurements are within one gram of each other), place the specimen in a 110 °C oven for at least 24 h or until the specimen is fully dry. Remove the dry specimen from the oven and allow it to cool to room temperature. Make the final weight and thermal resistivity measurements.

11.4 *Multiple-specimen (Method B)*:

11.4.1 *First Specimen Measurements* – Typically, the first specimen tested is with dry soil. Weigh the specimen after the specimen has been compacted to the desired density. Create a sensor hole through the vertical axis of the specimen as described in 11.1. Insert the thermal probe into the sensor hole and measure thermal resistivity as described in 11.2.

11.4.2 *Subsample for Water Content Determination* –Take a 50-100 g sample from the specimen for water content determination in accordance to Test Method D 2216.

11.4.3 *Recompacted Specimens for Subsequent Measurements* – Deconstruct the first specimen if the same soil in the first specimen is reused. Add additional soil and water to achieve the same density as the first specimen but new water content to create a new specimen. For each new specimen, create a sensor hole through the vertical axis of the specimen as described in 11.1. Insert the thermal probe into the sensor hole and measure thermal resistivity as described in 11.2. Determine water content as described in 11.4.2. Repeat this step (11.4.3) until at least five recompacted specimens at varying water contents are tested.

11.4.4 *Multiple Specimens for Subsequent Measurements* – If an abundant amount of the soil is available, multiple specimens similar to the first specimen may be prepared. Prepare a minimum of five additional specimens at the same density as the first specimen but at incremental water contents. Weigh each specimen. For each specimen, create a sensor hole

through the vertical axis of the specimen as described in 11.1. Insert the thermal probe into the sensor hole and measure thermal resistivity as described in 11.2. Determine water content as described in 11.4.2.

11.5 *Stage-drying (Method C)*:

11.5.1 *Initial Weight Measurements* – Weigh each specimen after three identical specimens are compacted to the desired water content and density. Variability in specimen preparation can be identified based on differences in specimen weights.

11.5.2 *Horizontal Sensor Holes* – For each specimen, create a horizontal sensor hole through the top half of the openings located at the top and middle thirds of the specimen as well as through the bottom half of the opening located at the bottom third of the specimen as described in 11.1.

11.5.3 *Thermal Resistivity Measurements* – Starting at the top opening, insert the thermal probe into the sensor hole and measure thermal resistivity as described in 11.2. Remove the thermal probe from the top opening, wipe the probe, and insert the probe into the sensor hole at the middle opening. Measure thermal resistivity as described in 11.2. Remove the thermal probe from the middle opening, wipe the probe, and insert the probe into the sensor hole at the bottom opening. Measure thermal resistivity as described in 11.2. Remove the thermal probe from the specimen.

11.5.4 *Initial Thermal Resistivity Measurements* – On the first day of testing, thermal resistivity measurements are necessary for all three specimens. Obtain thermal resistivity measurements for each cylinder as described in 11.5.3. A total of nine initial thermal resistivity measurements are made (i.e., three for each specimen).

11.5.5 *Oven Stage-drying* – Place the specimens in a 50 °C oven after initial thermal resistivity measurements are made at each top, middle, and bottom location for all three specimens. One specimen is removed after 24 hours, 3 days, and 10 days of oven drying.

11.5.6 *Thermal Resistivity Measurements after 24 hours, 3 days, or 10 days of Drying* – Remove only one specimen out of the oven after each drying period and allow the specimen to equilibrate to room temperature. Sufficient time for temperature equilibration is important to obtain accurate thermal resistivity measurements. Weigh the specimen. If the sensor holes have shrunk or collapsed, reopen the sensor holes using the technique described in 11.1. If the sensor holes are intact, proceed and measure thermal resistivity at the top, middle, and bottom thirds of the specimen as described in 11.5.3. Thermal grease may be necessary if the specimen develops cracks due to desiccation.

11.5.7 *Water Content Determination after 24 hours, 3 days, or 10 days of Drying* – Collect water content samples after obtaining thermal resistivity measurements from all three sensor locations of the specimen. Remove soil from the top of the specimen in small layers. Collect 50-100 g samples from each top, middle, and bottom sensor location. Water content shall be determined in accordance to Test Method D 2216.

11.6 *Automated Hanging Column (Method D):*

11.6.1 *Pack Specimen into Tempe Cell* – Pour soil into the cell in equal lifts to achieve the desired density. Moist soil may be used to facilitate packing. Greater densities are achieved by tamping the soil down after each lift and tapping the cell wall. Looser densities are achieved by slowly pouring soil through a funnel into the cell and minimizing disturbance after packing. Take care in packing around the sensors, but ensure good contact between the sensors and soil. Place the cell cover to enclose the specimen.

11.6.2 *Insulate Tempe Cell* – Place insulation around the cell to maintain a stable soil temperature within the cell.

11.6.3 *Saturate Specimen* – Saturate the specimen by allowing water from the hanging column reservoir to rise into the Tempe cell. Additional water may need to be added to the hanging column reservoir to keep the water level above the specimen elevation to ensure water flow into the Tempe cell.

11.6.4 *Establish Water Table* – Establish a water table at the middle elevation of the Tempe cell after the specimen has been fully saturated.

11.6.5 *Start Sensor Data Logging* – Connect the thermal probe, temperature probe, dielectric soil moisture sensor, and tensiometer to their respective data loggers. Record volumetric water content, matric suction, and temperature continuously at 1 minute intervals. Record thermal resistivity continuously every 15 minutes to allow sufficient time for thermal gradients to dissipate between measurements. Measure thermal resistivity with the 30-mm long and 6-mm spacing dual-needle thermal probe and two minute read time. Start all data loggers simultaneously so the data can be matched by the time of measurements.

11.6.6 *Dry Specimen* – Gradually (0.1 to 0.5 cm/hr) allow the pore water to drain from the Tempe cell (i.e., falling water table established in 11.6.4). Remove the cover off the Tempe cell to increase drying through evaporation when drainage becomes very slow.

11.6.7 *Water Content Determination* – Collect water content samples in the vicinity of the soil moisture sensor and thermal probe to verify the soil moisture conditions after the specimen has fully dried. Water content shall be determined in accordance to Test Method D 2216.

12. Calculation and Plotting

12.1 *Water Content Computation* – The horizontal axis of the thermal resistivity dryout curve may be expressed in terms of gravimetric water content, volumetric water content, or degree of saturation.

12.1.1 Gravimetric water content (*w*) of the specimen is calculated using the method in Test Method D 2216.

12.1.2 If the thermal resistivity dryout curve is to be reported in terms of volumetric water content (θ) rather than gravimetric water content, calculate the volumetric water content corresponding to each gravimetric water content using:

$$\theta = \frac{\rho_d}{\rho_w} w \tag{1}$$

where ρ_d is the dry density of the soil and ρ_w is the density of water.

12.1.3 If the thermal resistivity dryout curve is to be reported in terms of degree of saturation (*S*) rather than water content, compute the degree of saturation corresponding to each gravimetric or volumetric water content using:

$$S = \frac{w}{\frac{\rho_w}{\rho_d} - \frac{1}{G_s}} \tag{2}$$

$$S = \frac{\theta}{1 - \frac{\rho_d}{G_s \rho_w}} \tag{3}$$

where G_s is the specific gravity of the soil.

12.2 *Thermal Resistivity Dryout Curve* – Plot thermal resistivity and water content (gravimetric or volumetric) or degree of saturation. Thermal resistivity is often reported in units

of [cm-°C/W]. Draw the thermal resistivity dryout curve as a smooth curve through the points, for example Fig 3. From the thermal resistivity dryout curve, the critical water content can be located at the knee of the curve. The shape of the thermal resistivity dryout curve is typically flatter for fine soils. Appropriate scales should be used to capture the shape of the curve.

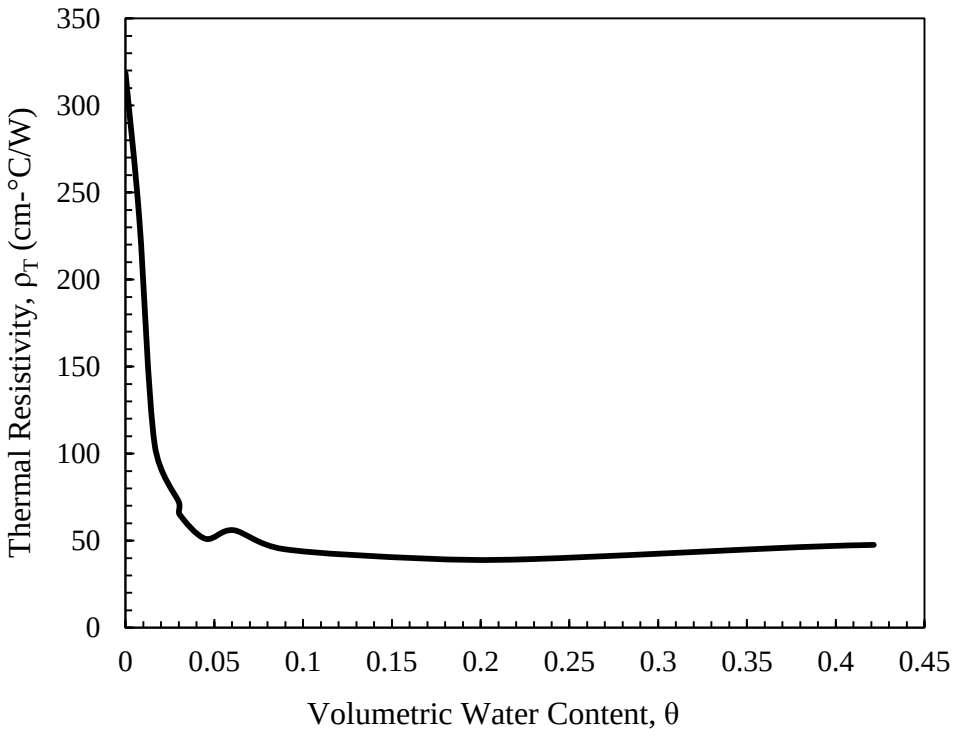

Fig 3. Thermal resistivity dryout curve for a poorly-graded sand using Method B.

12.3 *Soil-water Characteristic Curve* – For Method D, plot matric suction and water content (gravimetric or volumetric) or degree of saturation on the same thermal resistivity dryout curve graph (i.e., use one horizontal axis and have one vertical axis for thermal resistivity and a secondary vertical axis for matric suction). Draw the soil-water characteristic curve as a smooth curve through the points, for example Fig 4. From the soil-water characteristic curve, the

saturated water content (i.e., degree of saturations equals one) and residual water content located at the knee of the curve can be determined. In general, the residual water content and critical water content are proximal.

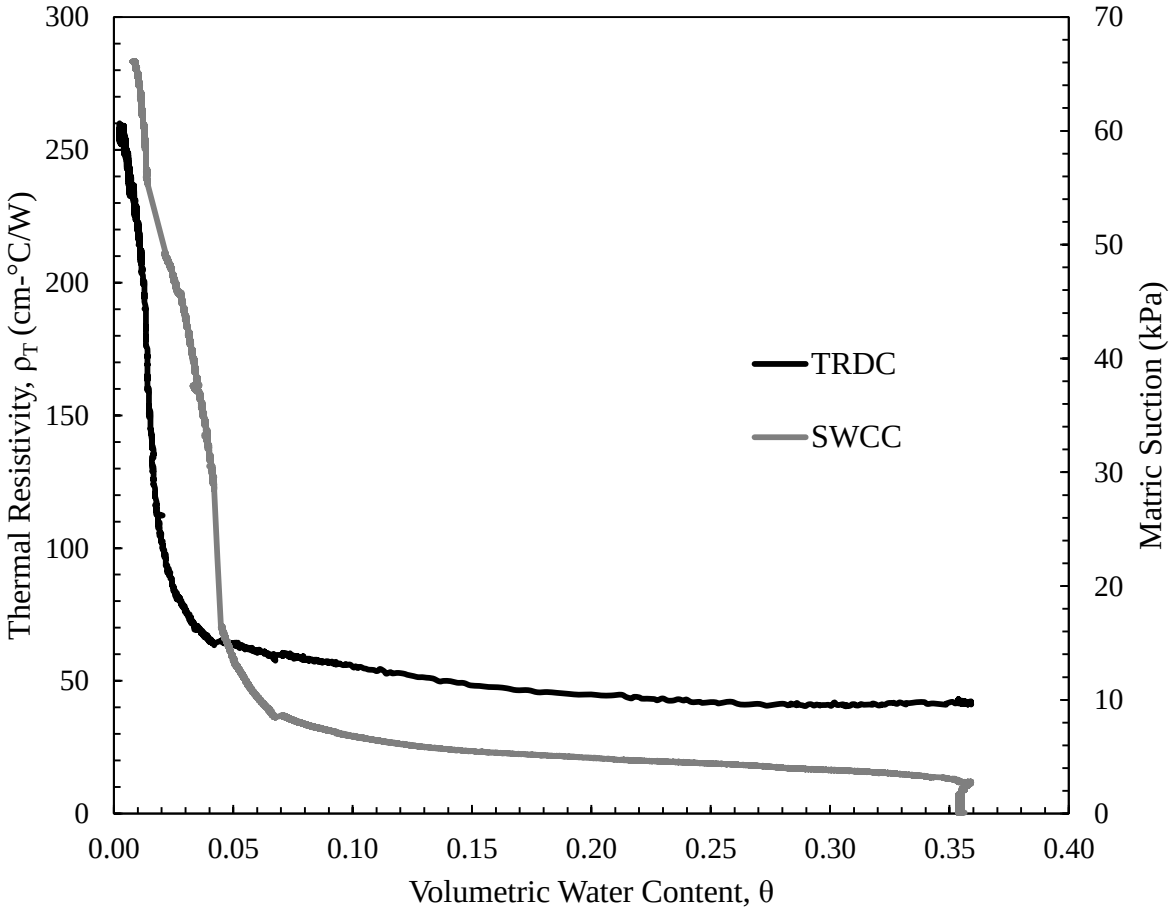

Fig 4. Thermal resistivity dryout curve and soil-water characteristic curve for a poorly-graded sand using Method D.

13. Report

13.1 The report shall include as a minimum the following information:

13.1.1 Specimen identifying information, such as United Soil Classification System (USCS) identification, Project No., Boring No., Sample No., Depth, etc.

13.1.2 The test method used (e.g., Method A, B, C, or D). For all methods, state the brand and model of thermal probe and thermal properties analyzer used. For Method D, state the brand and model of the dielectric soil moisture sensor, temperature probe, tensiometer, and nylon membrane filter used.

13.1.3 The preparation process used (e.g., undisturbed or compacted).

13.1.4 The dimensions of the specimen (e.g., the dimensions of the specimen holder).

13.1.5 The desired dry unit weight (percent of maximum) and water content the specimen was compacted to for testing.

13.1.6 The initial mass and water content of the prepared specimen.

13.1.7 The specific gravity of the soil and method of determination.

13.1.8 The maximum dry unit weight and optimum water content of the soil and method of determination.

13.2 The report shall include as a minimum the following testing data:

13.2.1 For Methods A, B, and C, a table reporting the time and date at which testing was performed, time for temperature equilibration, testing identification, thermal resistivity, error, specimen weight, and gravimetric water content corresponding to each thermal resistivity measurement. The use of thermal grease and observable changes in characteristics of the specimen (i.e. desiccation cracking) shall also be noted.

13.2.2 For Method D, a compiled table reporting data logged water content, matric suction, temperature, and thermal resistivity measurements at matched time intervals.

13.2.3 The thermal resistivity dryout curve showing thermal resistivity as a function of water content (gravimetric or volumetric) or degree of saturation with the critical water content labeled at the knee of the curve. For Method D, on the same thermal resistivity dryout curve graph, the soil-water characteristic curve (SWCC) showing matric suction as a function of water content (gravimetric or volumetric) or degree of saturation with labeled residual and saturated water content (gravimetric or volumetric) or degree of saturation shall also be plotted.

14. Precision and Bias

14.1 *Precision* – Ongoing experiments are being conducted at the University of Wisconsin-Madison to provide statistical measures on the repeatability of method results, comparisons of consistency between results from different methods, the effect of different oven temperatures for drying, and the effect of temperature equilibration time on the accuracy of thermal resistivity measurements. Additional work is also being done to determine correlations between the thermal resistivity dryout curve and soil-water characteristic curve. A comparison between thermal resistivity dryout curves in terms of degree of saturation determined from each method (A-D) is shown in Fig 6.

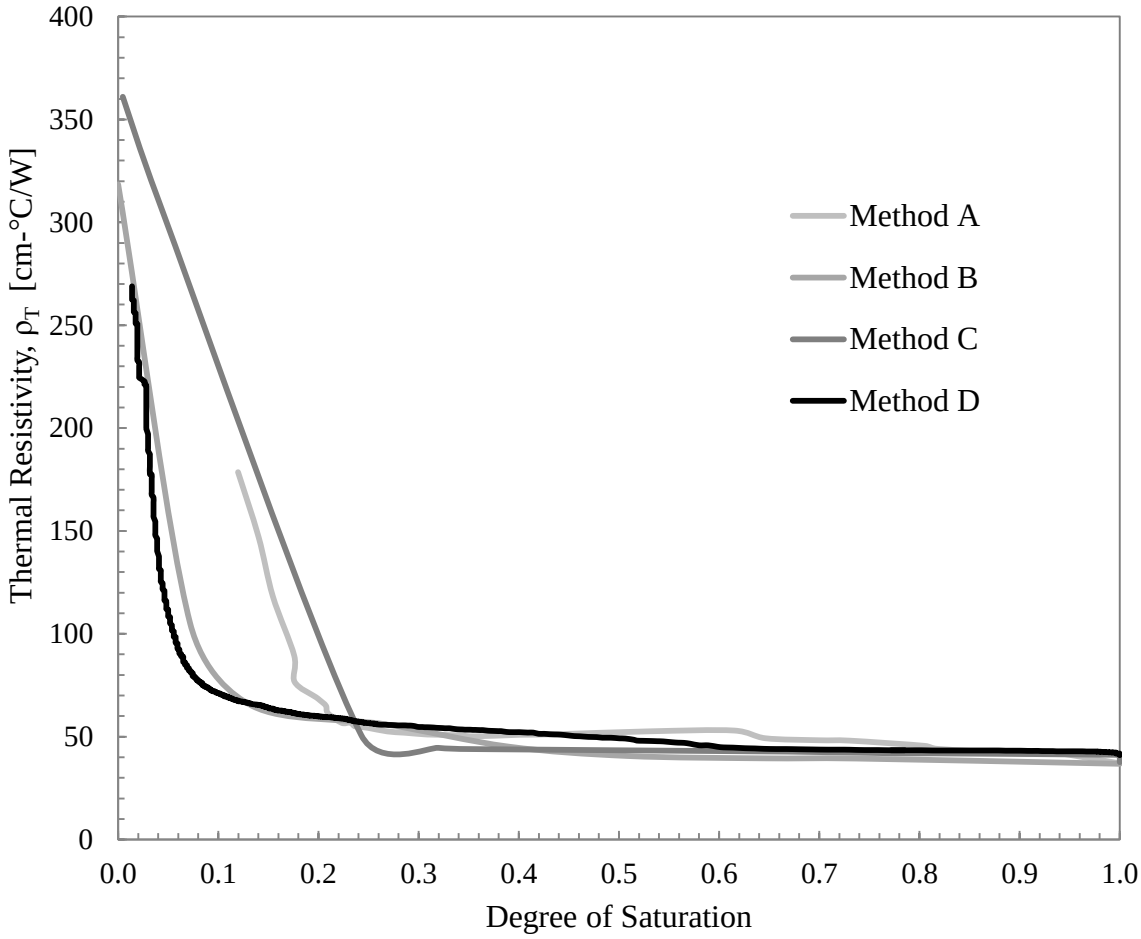

Fig 5. Thermal resistivity dryout curves for a poorly-graded sand using Methods A-D.

15. Keywords

15.1 thermal resistivity; thermal resistivity dryout curve; thermal conductivity; thermal probe; soil thermal properties; critical water content

ANNEX

(Mandatory Information)

A1.

A1.1

A1.1.1

APPENDIX

(Nonmandatory Information)

X1.

X1.1

X1.1.1

REFERENCES

(1) Bristow, K.L., "Measurement of Thermal Properties and Water Content of Unsaturated Sandy Soil Using Dual-Probe Heat-Pulse Probes," *Agricultural and Forestry Meteorology,* Vol 89, No. 2, 1998, pp. 75-84.

(2) Decagon Devices. "KD2 Pro Thermal Properties Analyzer Operator's Manual Version 8.A." Decagon Devices, Inc., Pullman WA. 2010.

(3) Decagon Devices. "Producing Thermal Dryout Curves for Buried Cable Applications." Application Note. Decagon Devices, Inc., Pullman WA. 2011.

(4) Likos, W. J., Olson, H. S., and Jaafar, R., "Comparison of Laboratory Methods for Measuring Thermal Conductivity of Unsaturated Soils," *Proceedings of GeoCongress 2012*, ASCE, Oakland, California.

(5) Sakaki, T., Limsuwat, A., Smits, K. M., and Illangasekare, T. H., "Empirical two-point α-mixing model for calibrating the ECH2O EC-5 soil moisture in sands," *Water Resources Research*, Vol 44, No. 4, 2008.

(6) Smits, K. M., Sakaki, T., Limsuwat, A., and Illangasekare, T. H., "Thermal Conductivity of Sands under Varying Moisture and Porosity in Drainage-Wetting Cycles," *Vadose Zone Journal*, Vol 9, No. 1, 2010, pp. 172-180.

(7) Smits, K. M., Sakaki, T., Peters, J. F., and Illangasekare, T. H., "Temperature Dependence of Thermal Properties of Sands across a Wide Range of Temperatures (30-70 °C)," *Vadose Zone Journal*, Vol 12, No. 1, 2013.

(8) Woodward, N. R., and Tinjum, J. M., "Impact of Moisture Migration on Thermal Resistivity Testing Unsaturated Soil," *Proceedings of GeoCongress 2012*, ASCE, Oakland, California.

(9) Woodward, N. R., and Tinjum, J. M., and Wu, R., "Water Migration Impacts on Thermal Resistivity Testing Procedures," *Geotechnical Testing Journal*, Vol. 36, No. 6, 2013, pp. 948–955.

7. APPENDIX B – SOIL THERMAL CONDUCTIVTY AT ELEVATED TEMPERATURES

Soil Thermal Conductivity at Elevated Temperatures

Abstract

Soil thermal conductivity (λ_{soil}) is a function of temperature. However, existing data on the temperature dependence of λ_{soil} at elevated temperatures is scarce and generally limited to specific soils. In this research, the thermal conductivity of two quartz sand and kaolinite clay mixtures were experimentally obtained using the stage-drying procedure at elevated temperatures. The 90% quartz sand and 10% kaolinite clay mixture was tested at 50 °C and 80 °C while the 50% quartz sand and 50% kaolinite clay mixture was tested at 50 °C, 60 °C, 70 °C, and 80 °C. For both soils, λ_{soil} generally appeared to increase at elevated temperatures. However, experimental issues encountered during testing, such as difficulty in heating the specimens to the desired temperature and specimen desiccation, resulted in scattered measurements that did not provide for effective comparisons between TCDCs generated at different temperatures.

Introduction

The thermal conductivity of soil (λ_{soil}) is often of interest because λ_{soil} reflects the ability of soil to conduct heat. Several studies have shown that λ_{soil} is a function of temperature and that λ_{soil} increases with increasing temperature within a certain range of soil water contents (Sepaskhah and Boersma, 1979; Hopmans and Dane, 1986). Quantifying the temperature dependence of λ_{soil} is important because several engineering applications involve heat transfer through soil operate at high temperatures. For instance, the maximum operating temperature is typically 90 °C in the case of underground medium-voltage, single-core cables used in wind energy facilities (Jorgensen, 2012). However, measuring λ_{soil} at high temperatures can be challenging due to the lack of suitable measurement devices and the potential for measurement-induced changes. As a result, the database of λ_{soil} at high temperatures is sparse and often limited

to coarse-grained soils. The purpose of this paper is to present measurements of λ_{soil} at elevated temperatures for quartz sand and kaolinite clay mixtures using the stage-drying procedure.

Background

One of the first theoretical estimates for λ_{soil} was proposed by de Vries (1963). Based on known information about the soil's mineral composition, porosity, and water content, the weighted average of the thermal conductivities of the various soil components (i.e., λ_{solids} = 1-5 W/m-K, λ_{water} = 0.6 W/m-K, and λ_{air} = 0.024 W/m-K (Côté and Konrad, 2005)) can be used to calculate the overall λ_{soil}. Furthermore, de Vries derived an expression to account for distillation effects induced from multiphase pore fluid movement. In short, the de Vries' model predicted that λ_{soil} would increase with increasing temperature from additional latent heat transfer in the soil pores. The work of de Vries provided the theoretical foundation for investigation of λ_{soil} as a temperature-dependent property. Within the past two decades, studies using different experimental techniques to determine λ_{soil} have improved the database of measured λ_{soil} at various temperatures.

Campbell et al. (1994) measured the effect of temperature on λ_{soil} using the single-specimen method on ten different soils containing a few percent to nearly 50% fines content. The λ_{soil} measurements were taken at 30 °C, 50 °C, 70 °C and 90 °C. Temperatures above 90 °C were not measured because above 90 °C the soil dries quickly and latent heat transport ceases to influence λ_{soil}. Experimental results indicated that λ_{soil} measured at 90 °C was generally three to five times greater than λ_{soil} measured at 30 °C in the intermediate range of volumetric water contents of the soils.

Hiraiwa and Kasubuchi (2000) conducted λ_{soil} tests on a clay loam and a light clay using the twin heat probe method over a temperature range of 5 °C to 75 °C. Similar results to

Campbell et al. (1994) were obtained. In the intermediate range of volumetric water contents, λ_{soil} measured at 75 °C was up to two times greater than the λ_{soil} measured at 5 °C (0.6 W/m-K to 0.8 W/m-K greater in terms of absolute difference). Hiraiwa and Kasubuchi also concluded that the thermal conductivity resulting from latent heat transfer could be determined by subtracting λ_{soil} measured at a temperature near 0 °C from λ_{soil} measured at a higher temperature.

Smits et al. (2012) obtained similar enhanced λ_{soil} behavior in quartz sands over a temperature range of 30 °C to 70 °C using the automated hanging column method. Between degrees of saturation of 0.1 to 0.6, the λ_{soil} measured at 70 °C was nearly twice the λ_{soil} measured at 30 °C. Significant conclusions from the study were that an increase in λ_{soil} became distinct at soil temperatures above 50 °C and the maximum enhancement of λ_{soil} occurred near the residual saturation for each sand. Smits et al. also presented results that compared λ_{soil} at loose and dense packing conditions. Loosely packed sands exhibited a noticeable decrease in λ_{soil} compared to tightly packed sands at comparable saturations.

Nikolaev et al. (2013) investigated the temperature dependence of λ_{soil} for an Ottawa sand and a fine sandy loam using the guarded hot-plate method for temperatures ranging from 2 °C to 92 °C. Again, similar enhanced λ_{soil} behavior with increasing temperature was observed. The λ_{soil} measured at 92 °C was two to four times the λ_{soil} measured at 2 °C in the intermediate range of volumetric water contents. Nikolaev et al. also noted that extending their investigation to measure λ_{soil} of silt, clay, loam, and peat in unfrozen and frozen states would be worthwhile.

Materials and Methods

Two different mixtures of quartz sand and kaolinite clay were tested. On a mass basis, one mixture consisted of 90% quartz sand and 10% kaolinite clay whereas the other mixture consisted of 50% quartz sand and 50% kaolinite clay. Standard Proctor tests according to ASTM

D698-12 were performed to determine the compaction curve of each mixture (Figure 7-1). As expected, the 50% quartz sand and 50% kaolinite clay mixture had a higher optimum water content (w_{opt}) than the 90% quartz sand and 10% kaolinite clay mixture. To determine the thermal conductivity dryout curve (TCDC) of each mixture using the stage-drying method outlined in Woodward et al. (2013), both mixtures were prepared at w_{opt} and 95% maximum dry unit weight ($\gamma_{d,max}$). The original PVC cylinder apparatus discussed in Woodward et al. (2013) was modified to a chlorinated polyvinyl chloride (CPVC) cylinder as a safety measure for elevated temperature testing. CPVC is PVC that has been chlorinated via a free radical chlorination reaction. The additional chlorine in CPVC increases the glass transition temperature (i.e., temperature at which a solid state transitions to a molten state) of PVC from approximately 80 °C to 110 °C for CPVC. The 50% quartz sand and 50% kaolinite clay mixture was tested at 50 °C, 60 °C, 70 °C, and 80 °C. The 90% quartz sand and 10% kaolinite clay mixture was only tested at 50 °C and 80 °C due to time constraints.

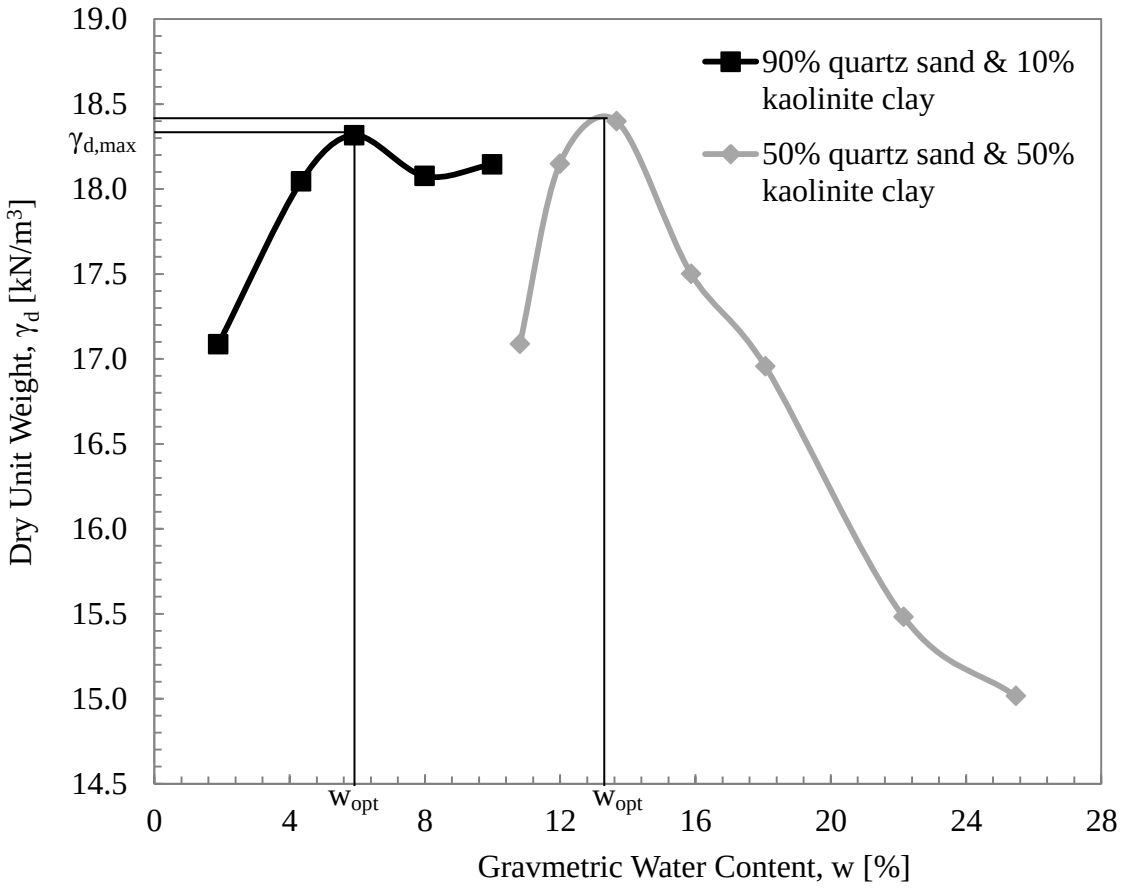

Figure 7-1. Standard Proctor compaction curves for 90% quartz sand and 10% kaolinite clay mixture as well as 50% quartz sand and 50% kaolinite clay mixture. The peak of the compactions curves correlate to maximum dry unit weight ($\gamma_{d,max}$) and optimum water content (w_{opt}).

Results and Discussion

The TCDCs for the two mixtures are shown in Figures 7-2 and 7-3. The general shape of the TCDCs exhibited expected behavior, but all the TCDCs had significant scatter and the anticipated results of lower λ_{soil} corresponding to lower volumetric water content (θ) was not always observed. One source of error for the large scatter was derived from specimen variability (e.g., specimens started at different water contents or densities when the specimens should have been prepared identically). Additional sources of error occurred at lower water contents where desiccation of the specimens caused poor thermal contact between the thermal probe and specimen. Furthermore, sensor holes had to be drilled to insert the thermal probe in specimens that were extremely dry and cemented from drying shrinkage. The use of a power drill to create the sensor holes could have caused additional drying of the soil due to heat dissipated from the drilling process.

For both mixtures, the range of λ_{soil} was between 1 and 3.5 W/m-K. In Figure 7-2, the TCDC measured at 80 °C appeared to be slightly higher than the TCDC measured at 50 °C. However, none of the λ_{soil} measurements overlapped at the same water content and comparisons between temperatures were not exact. Figure 7-3 provided similar results as Figure 7-2. In general, measurements obtained at higher temperatures appeared to have higher λ_{soil} than measurements obtained at lower temperatures, but the enhanced behavior of λ_{soil} was not as apparent as in previous studies. The advantage of using a higher oven temperature was that λ_{soil} measurements were obtained at lower water contents. However, the lack of λ_{soil} measurements within the intermediate range of θ for higher temperatures also indicated that different oven drying times or additional specimens were necessary for different oven temperatures to determine a complete TCDC.

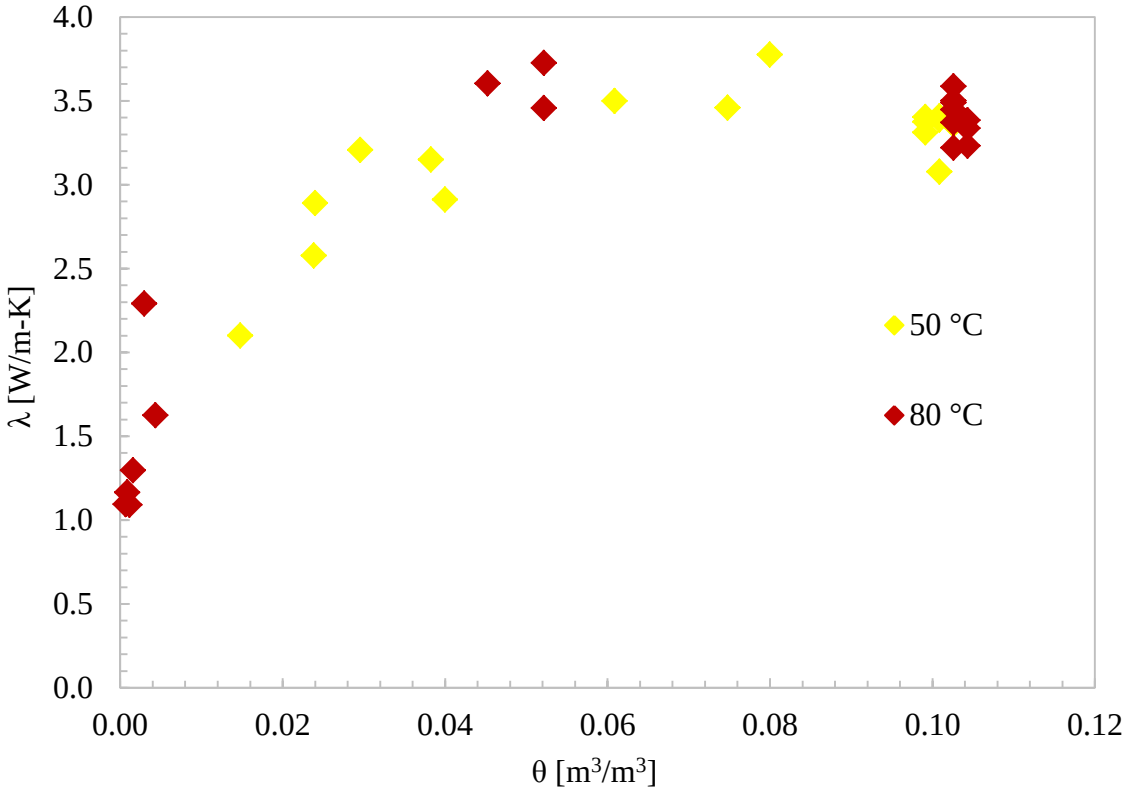

Figure 7-2. TCDC for 90% quartz sand and 10% kaolinite clay mixture.

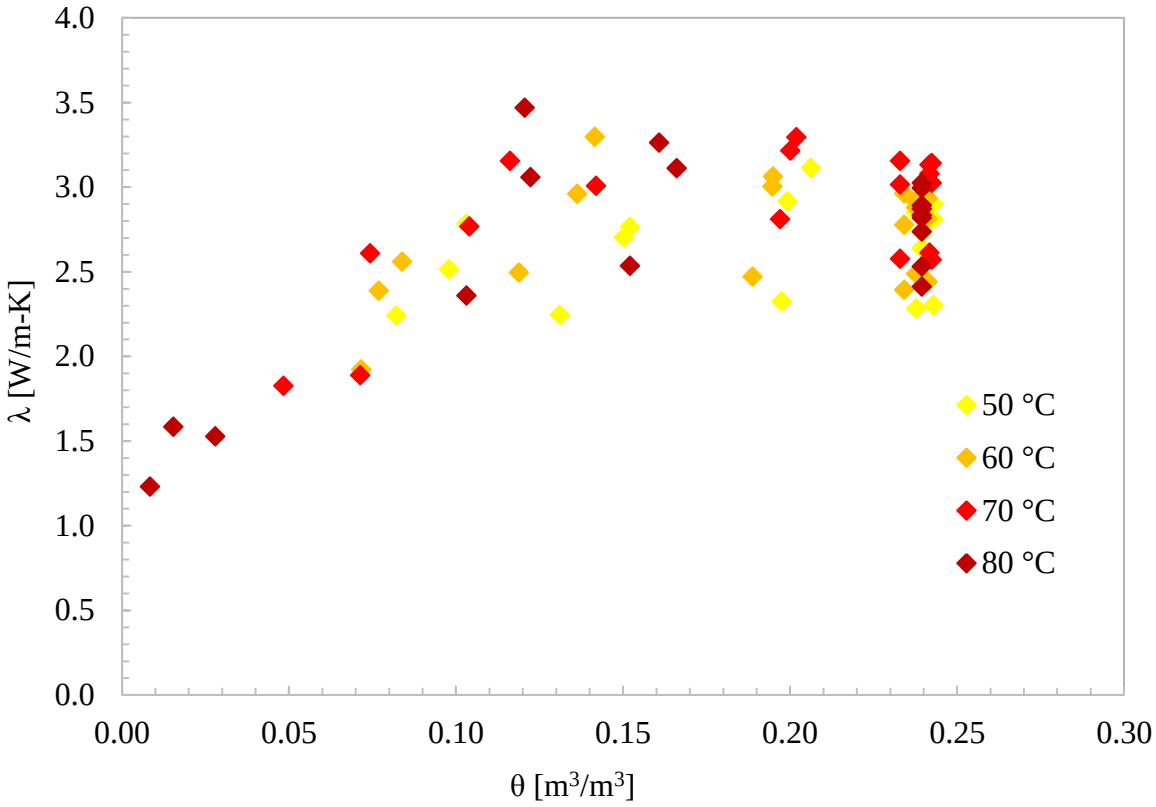

Figure 7-3. TCDC for 50% quartz sand and 50% kaolinite clay mixture.

Conclusions

Effective comparisons between λ_{soil} and elevated temperatures were not observed due to significant scatter and incomplete TCDCs. Specimen variability, desiccation, cementation, and shrinkage were significant issues that made determining the TCDCs of soils with high clay content challenging. However, there are several possible explanations for why the two-fold enhancement of λ_{soil} at elevated temperatures seen in previous studies was not observed in this research. Campbell et al. (1994) stated that λ_{soil} is temperature dependent because of latent heat of distillation across the pores of soil. For latent heat transfer to occur, pore water must be able to change phases and have space to migrate across the soil pores. Due to the clodding nature of compacted clay minerals (Benson and Daniel, 1990), vapor transport may have been hindered in the compacted sand-clay mixtures and latent heat transfer was suppressed.

Another possible source of discrepancy in the observed data with previous findings is the thermal inertia of the soil (i.e., the amount of time it takes for the soil to reach the desired testing temperature). Due to the relatively large sample of soil used in the staged-drying method to fill the CPVC cylinders, longer periods of time are necessary for the specimens to reach testing temperatures. Thermocouples used to verify internal specimen temperatures indicated that the 50% quartz sand and 50% kaolinite clay mixture required ten days to reach the 80 °C testing temperature. Thus, measurements taken on day one and three were not at 80 °C. In fact, at the time of measurements on day three, the temperatures at the top, middle, and bottom locations were only 61.6 °C, 65.1°C, and 68.7 °C, respectively. These measurements also indicated that a temperature gradient existed along the vertical axis of the specimen. Since thermal inertia and temperature gradient effects were present, direct comparisons between λ_{soil} measurements at different temperatures could not be made. For future testing, the use of smaller specimens to

address thermal inertia and gradient effects as well as keeping the thermal probe in the specimen during testing to avoid reinsertion issues are recommended to improve the quality of results. In general, a larger data set is necessary to make robust conclusions on the effect of elevated temperatures on λ_{soil}.

Acknowledgements

Special thanks are offered to Mr. Ben Ziomek for his efforts and perseverance in conducting thermal conductivity at elevated temperatures experiments in the laboratory.

References

Benson, C. H., and Daniel, D. E. (1990). "Influence of clods on the hydraulic conductivity of compacted clay." *Journal of Geotechnical Engineering*, Vol. 116 (8): 1231-1248.

Campbell, G.S., Jungbauer Jr, J.D., Bidlake, W.R., and Hungerford, R.D. (1994). "Predicting the effect of temperature on soil thermal conductivity." *Soil Science*, Vol. 158 (5): 307-313.

Côté, J., and Konrad, J.M. (2005). "A generalized thermal conductivity model for soils and construction materials." *Canadian Geotech. J.*, Vol. 42 (2): 443-458.

de Vries, D.A. (1963). Thermal properties of soils. *Physics of Plant Environment*. W.R. van Wijk (ed.). North Holland Pub. Co. Amsterdam: 210-235.

Hiraiwa, Y., and Kasubuchi, T. (2000). "Temperature dependence of thermal conductivity of soil over a wide range of temperature (5–75 C)." *European Journal of Soil Science*, Vol. 51 (2): 211-218.

Hopmans, J.W., and Dane, J.H. (1986). "Thermal conductivity of two prous media as a function of water ctonent, temperature, and density." *Soil Science Society of America Journal*, Vol. 142 (4): 187-195.

Jorgensen, S.C. (2012). Geothermal considerations in electrical collector system design for wind energy facilities. *MSc Thesis*, Department of Geological Engineering, University of Wisconsin-Madison, Madison, WI, 124 p.

Nikolaev, I.V., Leong, W.H., and Rosen, M.A. (2013). "Experimental investigation of soil thermal conductivity of soil over a wide temperature range." *International Journal of Soil Thermophysics*, Vol. 34 (6): 1110-1129.

Sepaskhah, A.R., and Boersma, L. (1979). "Thermal conductivity of soils as a function of temperature and water content." *Soil Science Society of America Journal*, Vol. 43 (3): 439-444.

Smits, K.M., Sakaki, T., Howington, S.E., Peters, J.F., and Illangasekare, T.H. (2013). "Temperature dependence of thermal properties of sands across a wide range of temperatures (30-70 °C)." *Vadose Zone Journal*, Vol. 12 (1): 1-8.

Woodward, N.R., Tinjum, J.M., and Wu, R. (2013). "Water migration impacts on thermal resistivity testing procedures." *Geotechnical Testing Journal*, Vol. 36 (6): 1-9.

8. APPENDIX C – FINITE-ELEMENT MODELING WITH SVOFFICE

Finite Element Modeling with SVOffice

Finite Element Method

The finite element method (FEM), also referred to as finite element analysis (FEA), is a numerical technique for determining approximate solutions of partial differential equations. For simple engineering problems, analytical solutions can be used to solve differential equations. However, for engineering problems that involve intricate geometries, material properties, boundary conditions, and nonlinearity, using FEM is more practical and efficient. Generally, advanced mathematical models, such as FEM, are necessary to accurately describe the behavior of unsaturated soil surrounding geothermal ground loops because of transient and coupled heat and moisture flow that exists during operation of the ground loop. In this study, SoilVision® Systems' SVOffice was used to simulate coupled heat and moisture transfer in unsaturated soils around a shallow horizontal ground loop. The governing differential equations for coupled heat and moisture flow are Eq. 2.3 and 2.4 (Section 2.1). The modified partial differential equations used in SVHeat and SVFlux are Eq. 3.14 and 3.15 (Section 3.2).

SVOFFICE

SVOffice is a finite-element software suite consisting of six modules that can be used to analyze slope stability (SVSlope), seepage and groundwater (SVFlux), conductive and convective heat movement (SVHeat), chemical transport (ChemFlux), stress state and deformations (SVSolid), and soil vapor extraction and infiltration (SVAirFlow) in saturated and unsaturated soils. The advantage of using SVOffice is that the simulation code is furnished for geotechnical and hydrological subsurface processes and the automated solver saves time from designing the finite element mesh. Models created in SVOffice can be done in one-dimension (1D), two-dimensions (2D), or three-dimensions (3D) as well as steady-state or transient.

Furthermore, individual modules can be coupled. For modeling of geothermal ground loops, coupled SVFlux and SVHeat were used. SVFlux was necessary to model groundwater flow and climatic effects (e.g., precipitation) as well as manage variable hydraulic properties of materials (e.g., input of material SWCCs). SVHeat was necessary to model conductive and convective heat transfer and manage variable thermal properties of materials (e.g., input of a material TCDCs).

General Modeling Procedure

The following procedure outlines general steps that can be taken to develop a numerical model specific to SVFlux and SVHeat. Personal learning experiences are also included to facilitate the learning curve for future SVOffice users. However, these modeling steps do not completely detail all the functionalities of SVFlux and SVHeat. Additional information on the modeling procedure, theory behind the modules, and example models can be found in the user and tutorial manuals provided with the software.

1. Create a New Model. In the SVOffice Manager pop-up menu (Figure 8-1), a new model must be created under a specific project folder chosen by the user. The user needs to specify the application (e.g., SVFlux or SVHeat), system (e.g., 1D, 2D, or 3D), type (e.g., steady-state or transient), units (e.g., metric or imperial), and time units (e.g, seconds, minutes, hours, days, or years). Since these settings cannot be changed once the model is created, the purpose and objectives of the model should be clearly defined prior to creating a new model. The user also needs to specify the dimensions of the model domain (world coordinate system) as well as the time-step increment and total model duration. Smaller time-step increments may help the model converge, but also increases the computational time. The world coordinate system and timing can be modified after creating the model. Once the model is created a blank

model domain appears. To couple SVFlux and SVHeat, the "add coupling" feature must be selected from the file tab (Figure 8-2). Coupling SVFlux and SVHeat will automatically require a new file to be saved.

2. Input Model Geometry. Closed shapes are required to define each material region (Figure 8-3). Each shape can only represent one type of material. Shapes can be drawn by selecting coordinates on the domain or typing in the coordinates. The order in which coordinate points are entered (e.g., clockwise or counterclockwise) are not important. Geometries may also be imported from other compatible software.
3. Specify Boundary Conditions. Boundary conditions are necessary to define how the model interacts with the flow of the system. Boundary conditions need to be applied to every geometry surface created in Step 2. Boundary conditions may be constant, an expression, or from tabulated data. Boundary conditions specific to SVFlux include total head, pressure head, excess pore pressure, surface pond, unit gradient, gradient, review by pressure, and geomembrane. Boundary conditions specific to SVHeat include temperature, resistance, and inner/outer insulation. Boundary conditions available in both SVFlux and SVHeat include flux, no boundary condition (no BC), continue (same boundary condition as previous node), and contact/jump. Definitions of each of these boundary conditions are provided in the SVOffice Help Manual. Boundary conditions other than zero flux and no BC will show up as different colored surfaces (Figure 8-4). If the model time units are set to days and a climate boundary condition is used, SVOffice enforces a maximum time-step increment of 0.2 (20% of a day). Thus, the use of a climate boundary condition can drastically increase the computational time of the model. If only precipitation is considered, an equivalent Y-flux boundary condition can be used.

4. Apply Material Properties. Each shape needs to be assigned a material type. In SVFlux, the hydraulic conductivity curve, SWCC, and volume-mass parameters (e.g., specific gravity) are required for each material (Figure 8-5a). These material properties may be input from experimentally measured data or built-in estimation models. Selection of the appropriate saturated and unsaturated hydraulic conductivity seems to have a significant effect on the ability of the model to converge. SVFlux provides a warning when the saturated hydraulic conductivity between materials is greater than five orders of magnitude apart. Likewise, SVFlux provides a warning if the unsaturated hydraulic is too low (i.e., below 1×10^{-10} m/s). While models can still run with these warnings, the models converge slower and may even terminate before completion.

   In SVHeat, the TCDC, volumetric heat capacity, soil-freezing characteristic curve (SFCC), and hydraulic permeability reduction are required as for each material (Figure 8-5b). The SFCC defines the relationship between unfrozen water content as a function of temperature below soil freezing point. The SFCC is used to calculate the unfrozen water content or ice content and the energy release in freezing or absorption in thawing. The hydraulic permeability reduction calculates the reduction of hydraulic conductivity due to the presence of ice in frozen soil and is only available when SVHeat is coupled with SVFlux. Again, these material properties may be input from experimentally measured data or built-in estimation models. If experimentally measured data is used, as many data points as possible should be input since SVOffice can only interpolate linearly between provided data.

5. Specify Initial Conditions. Initial conditions must be specified to provide a starting point for the model. In SVFlux, initial conditions can be derived from results of another SVFlux model, a water table, pore water pressure, or head conditions (Figure 8-6). In SVHeat, initial

conditions are chosen from results of another SVHeat model or temperature conditions. Initial conditions need to be reasonable and agree with specified boundary conditions. Physically unrealistic conditions can cause difficulties in converging. For example, both the singular diagonal block error and halt time-step error encountered during model simulation are usually related to setting inappropriate initial conditions that are not close enough to the actual transient solution the solver uses. Reducing the time-step, increasing the number of nodes, increasing the allowable error, or adjusting the initial conditions such that boundary values or fluxes do not change instantaneously can fix those errors. One method of obtaining appropriate initial boundary conditions is to perform the model simulation at steady-state conditions first and then use the results of the steady-state simulation as the initial conditions for the transient model.

6. Specify model outputs. Variables involved with analysis can be reported as contour (2D), elevation (2D), vector (2D), or surface (3D) plots for the entire domain or as history plots (i.e., variable vs. time) at specified points within the domain (Figure 8-7). These plots can be viewed and saved in four different manners: 1) display, 2) display and save, 3) write txt, and 4) plot off. In the display option, low-quality versions of the plots provide visibility of the solution at certain time intervals as the solver is solving. These plots are not saved and once the program is exited, the plots are lost. In display and save, the plots are saved, but the plots may take up significant storage space, especially if small time-steps are used, and extra time is required to save the plots to the computer. The write txt only option does not show any plots, but saves the raw data used to generate the plots. In plots off, plots are not recorded in any manner and only the final result is shown. The display and write txt options are

recommended because the display option provides insight about the results over time and the write txt option is necessary to create higher quality graphs in Microsoft Excel or SigmaPlot.

7. Analyze and Visualize. Once the model is setup properly and the desired output files are selected, the model can be analyzed. If the model is successfully solved, high-quality results can be visualized using the ACUMESH software (Figure 8-8).

The basic modeling procedure for SVFlux and SVHeat is straightforward and not overly-complicated. However, the most challenging and time-consuming aspects are related to obtaining and specifying material properties, troubleshooting errors that prevent the model from converging, and waiting for complete results. Drawing the expected model setup on paper first and organizing input parameters into the appropriate format can reduce time for setting up the model. Furthermore, understanding the limitations of the solver as well as selecting appropriate initial and boundary conditions can prevent model scenarios that result in terminating errors.

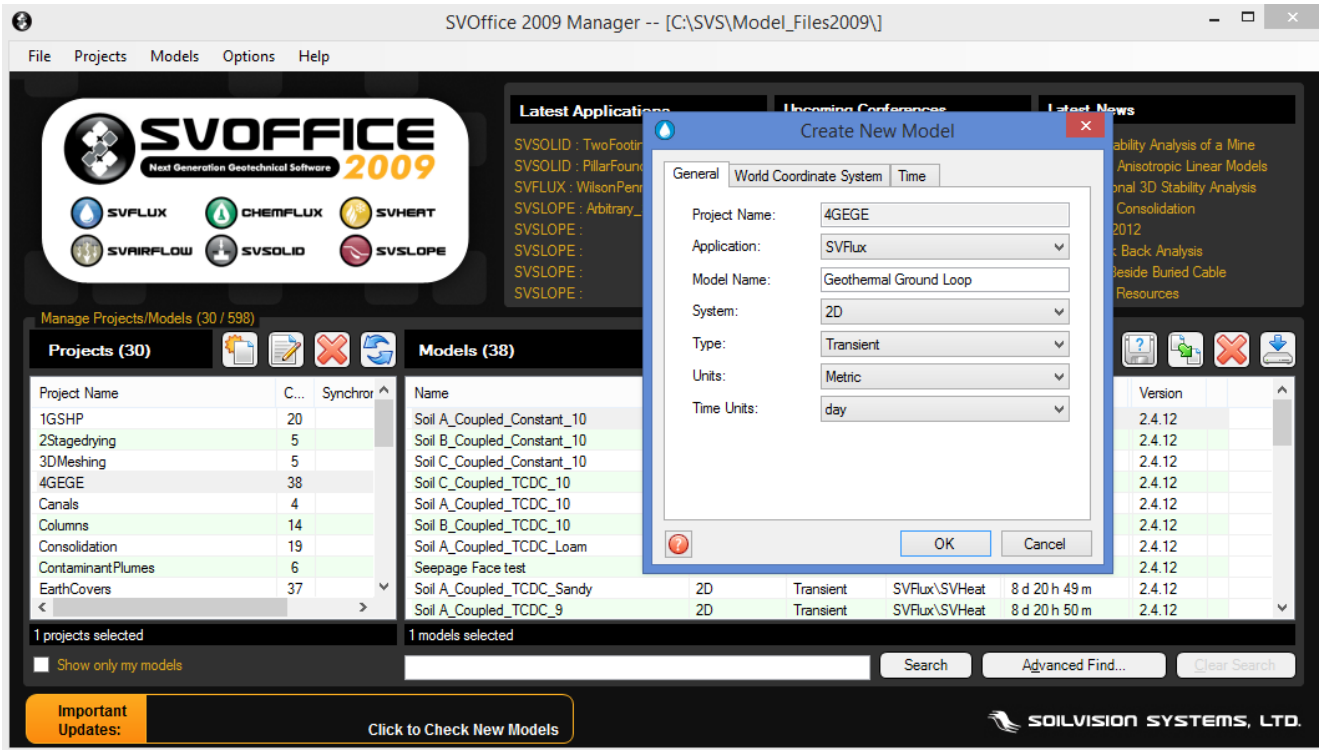

Figure 8-1. The first step is to create a new model in the SVOffice Manager menu. Once a new model is created, the available entries cannot be changed.

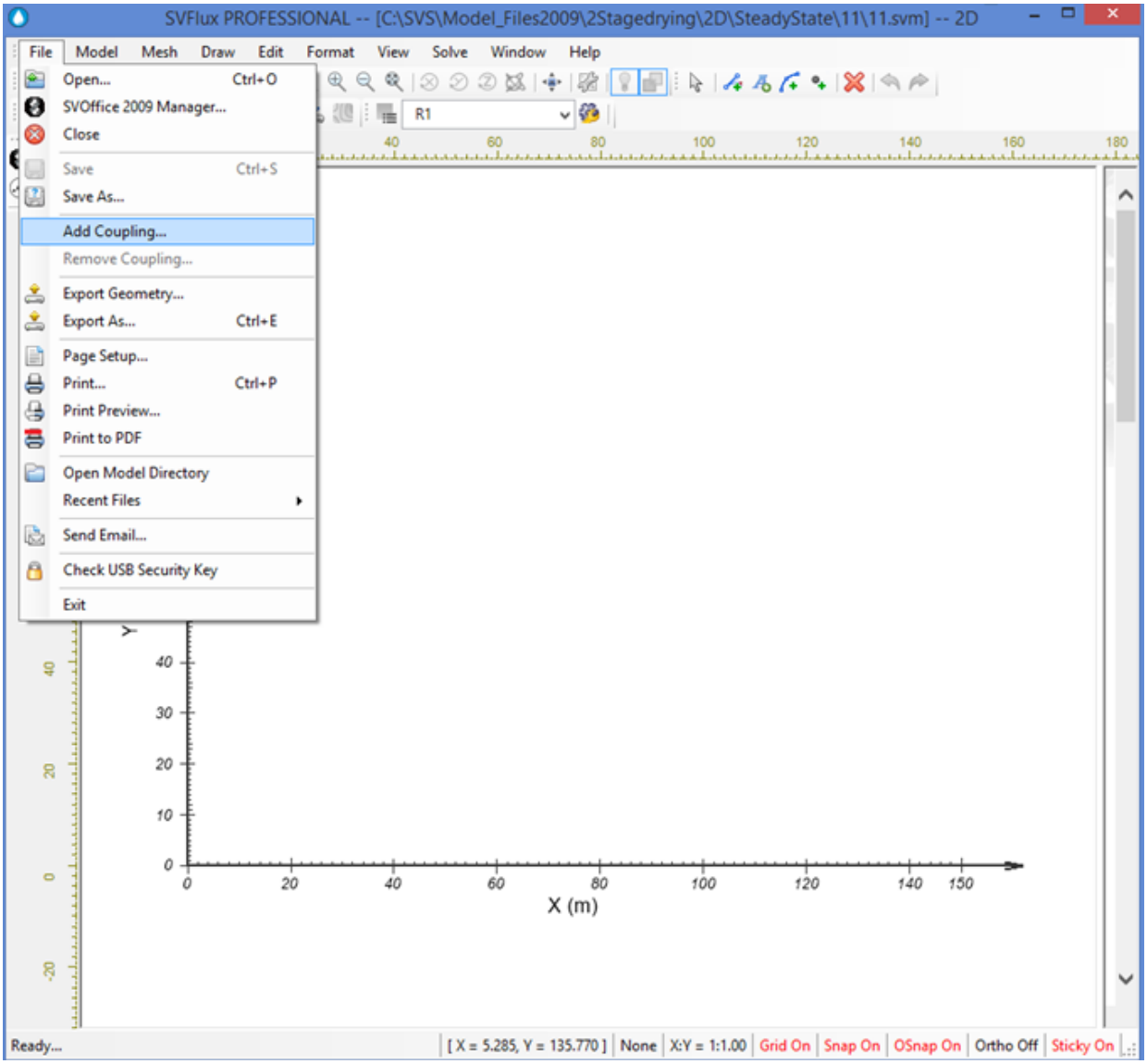

Figure 8-2. Coupling SVFlux and SVHeat occurs after a model is created in either SVFlux or SVHeat first.

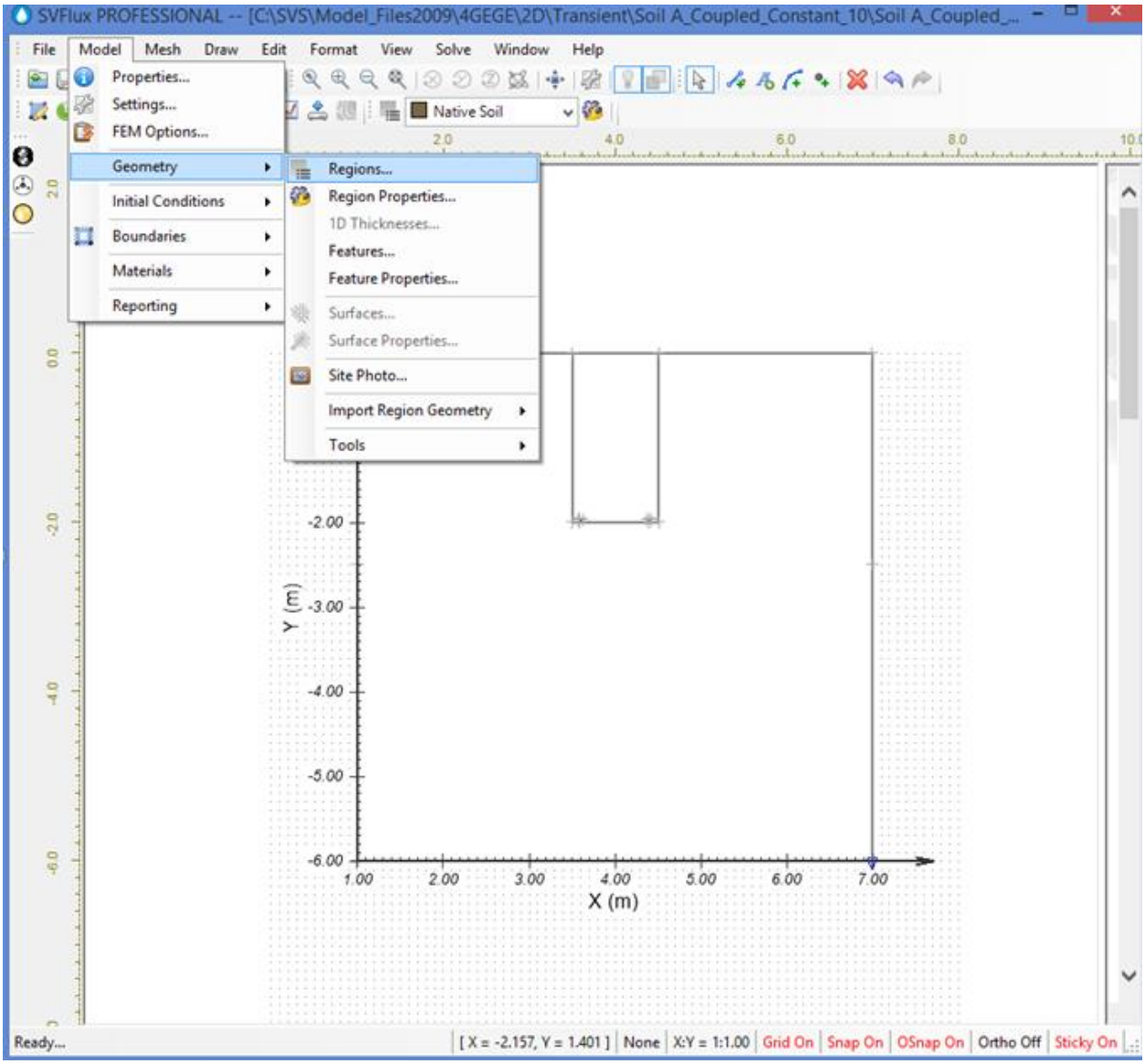

Figure 8-3. The second step is to draw shapes that define each material layer. Each shape can only represent one type of material.

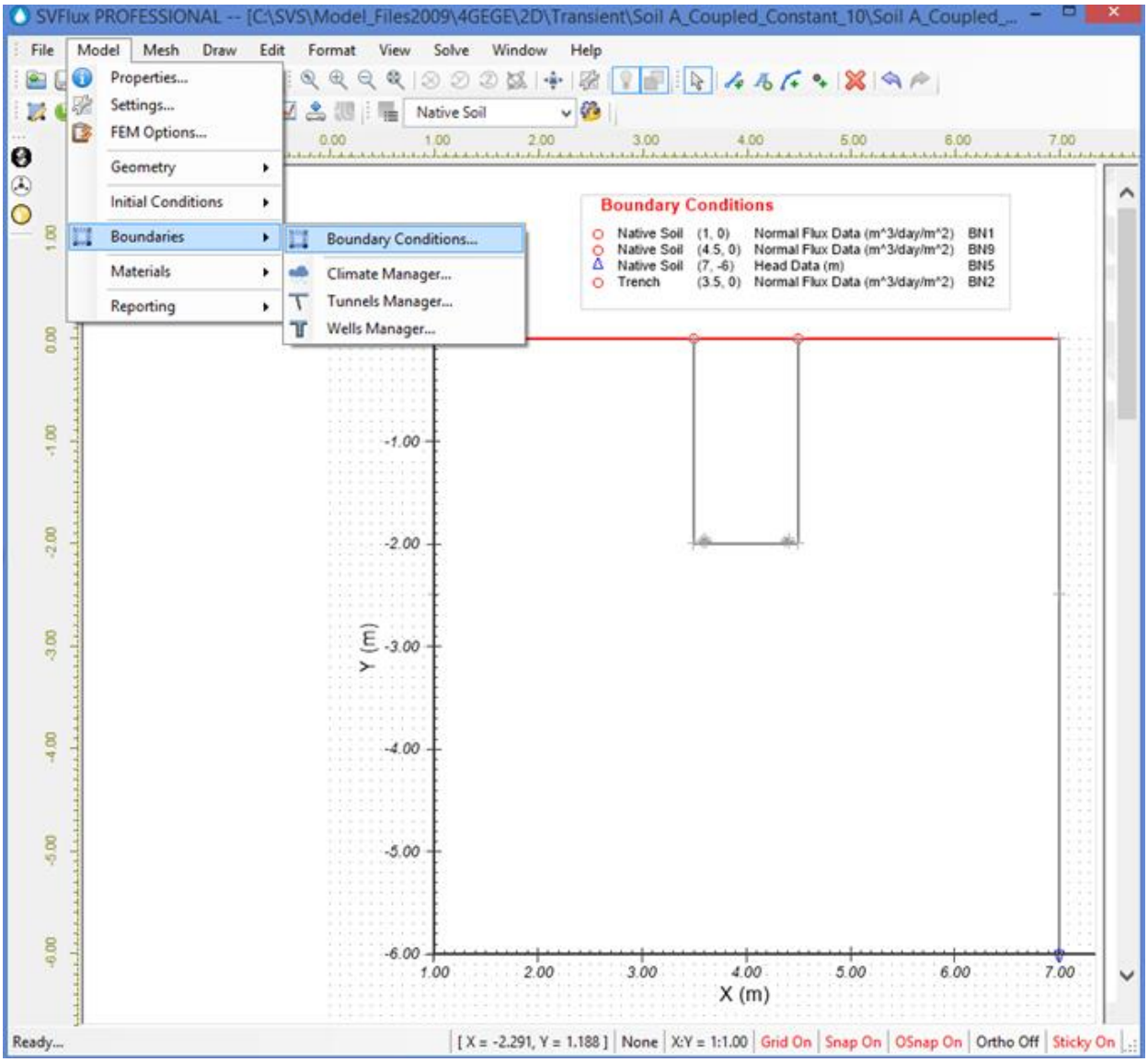

Figure 8-4. The third step is to specify boundary conditions for each geometry surface. Boundary conditions other than zero flux and no BC will show up as different colored surfaces.

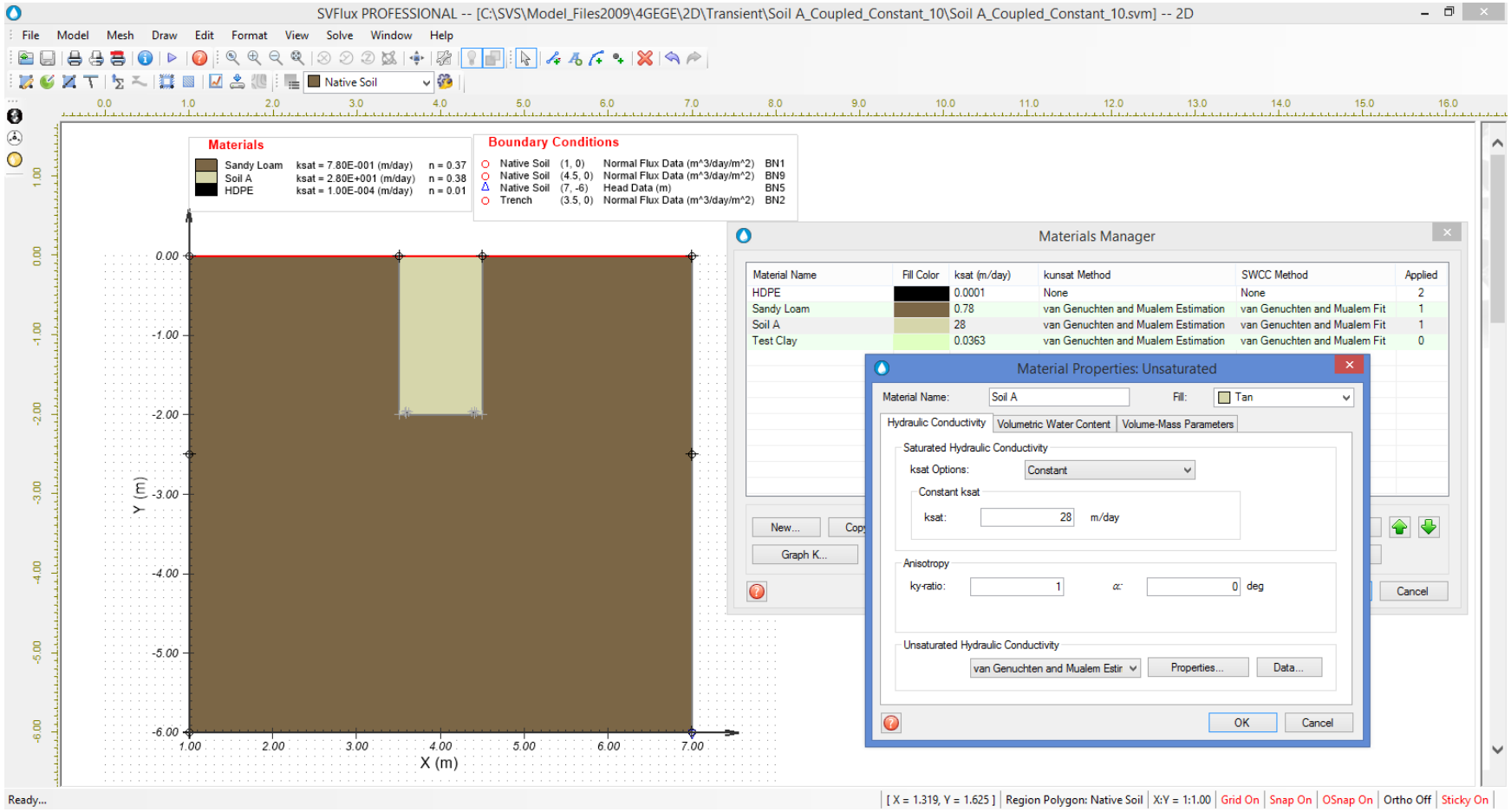

Figure 8-5a. The fourth step is to assign a material type to each shape. SVFlux requires information about the material's hydraulic conductivity as a function of volumetric water content, SWCC, and volume-mass parameters.

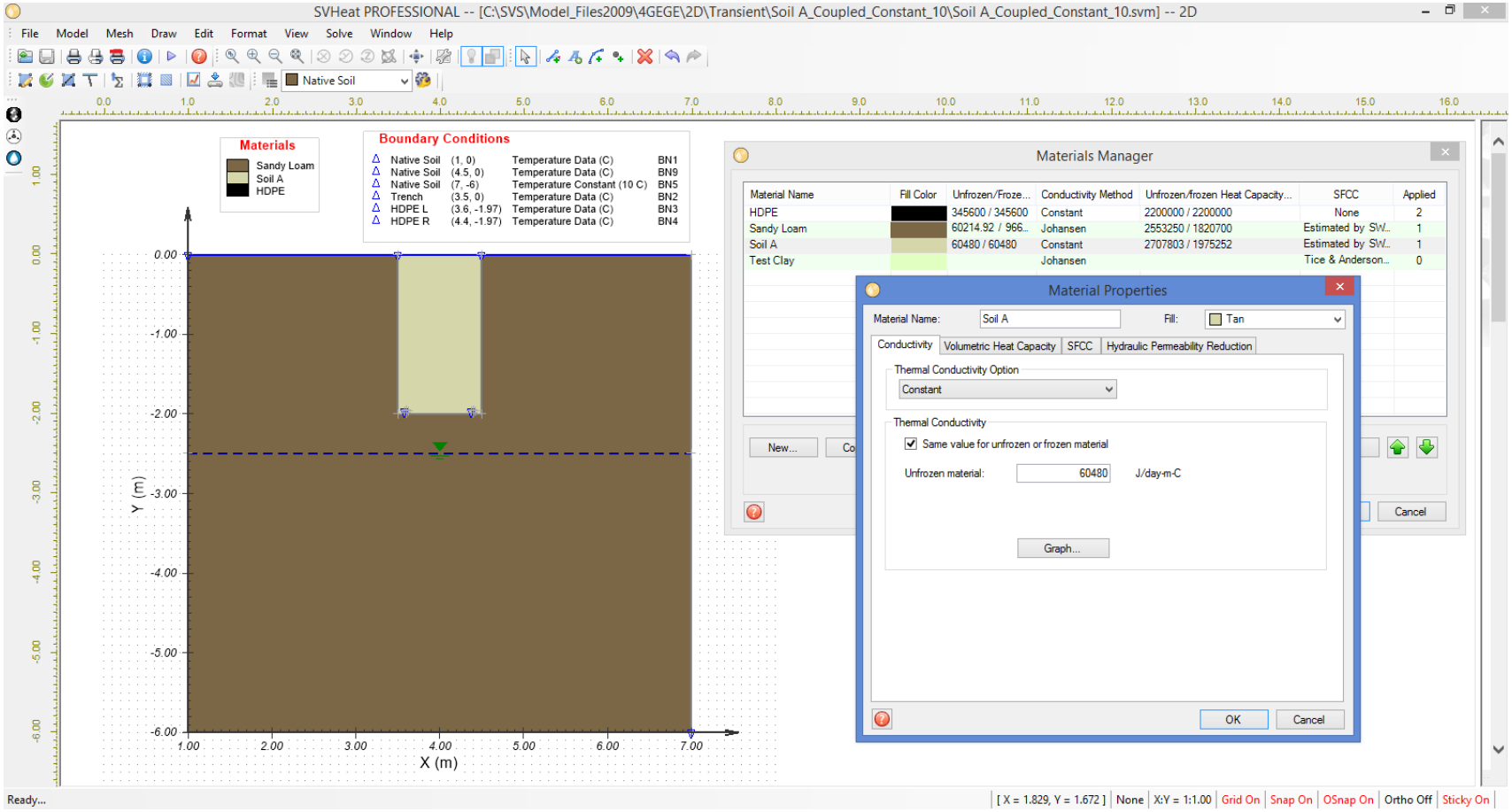

Figure 8-5b. The fourth step is to assign a material type to each shape. SVHeat requires information about the material's TCDC, volumetric heat capacity, SFCC, and hydraulic permeability reduction.

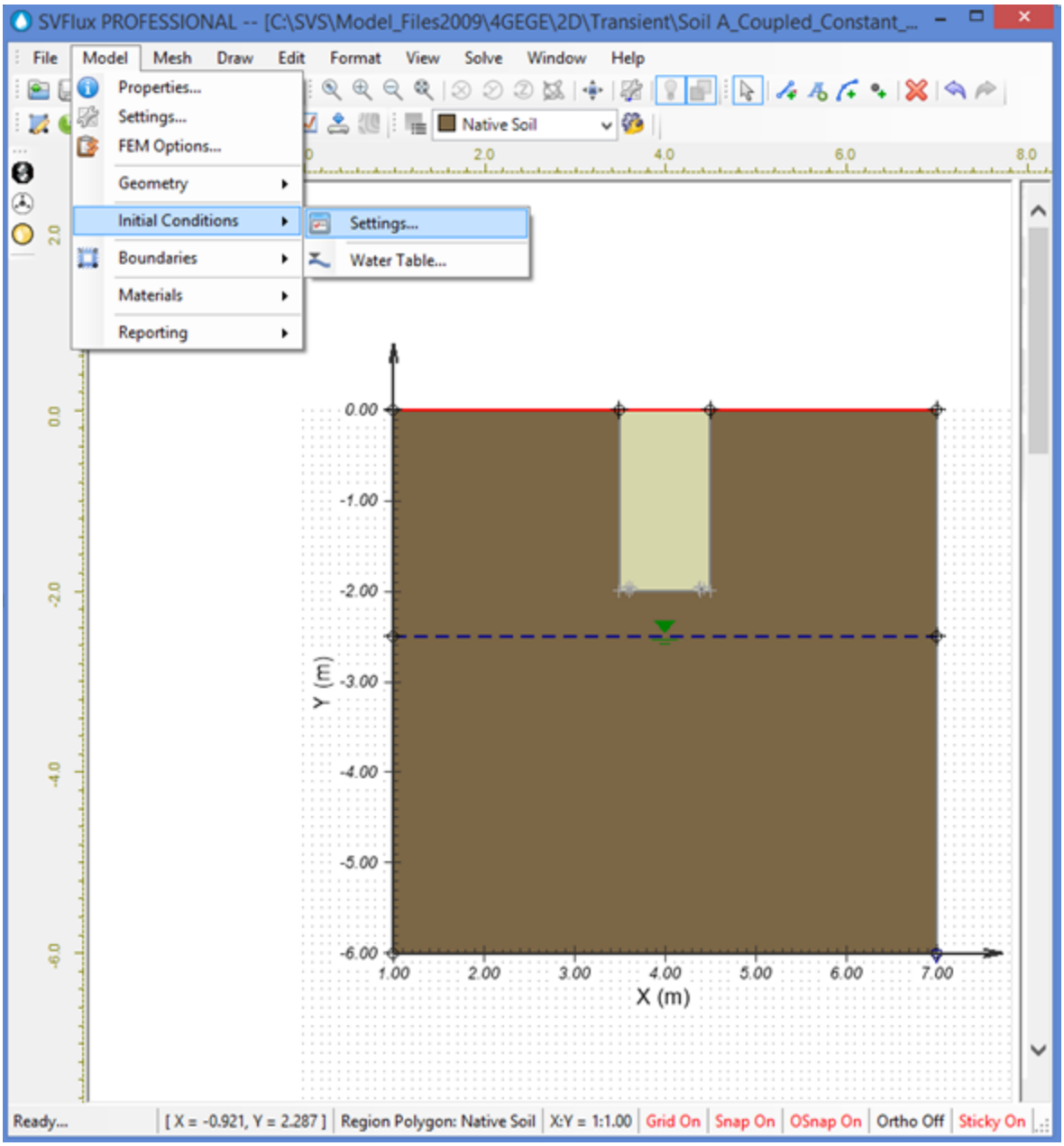

Figure 8-6. The fifth step is to specify initial conditions. The blue horizontally dashed line illustrates the location of an initial groundwater table. Physically realistic initial conditions are necessary for the model to converge.

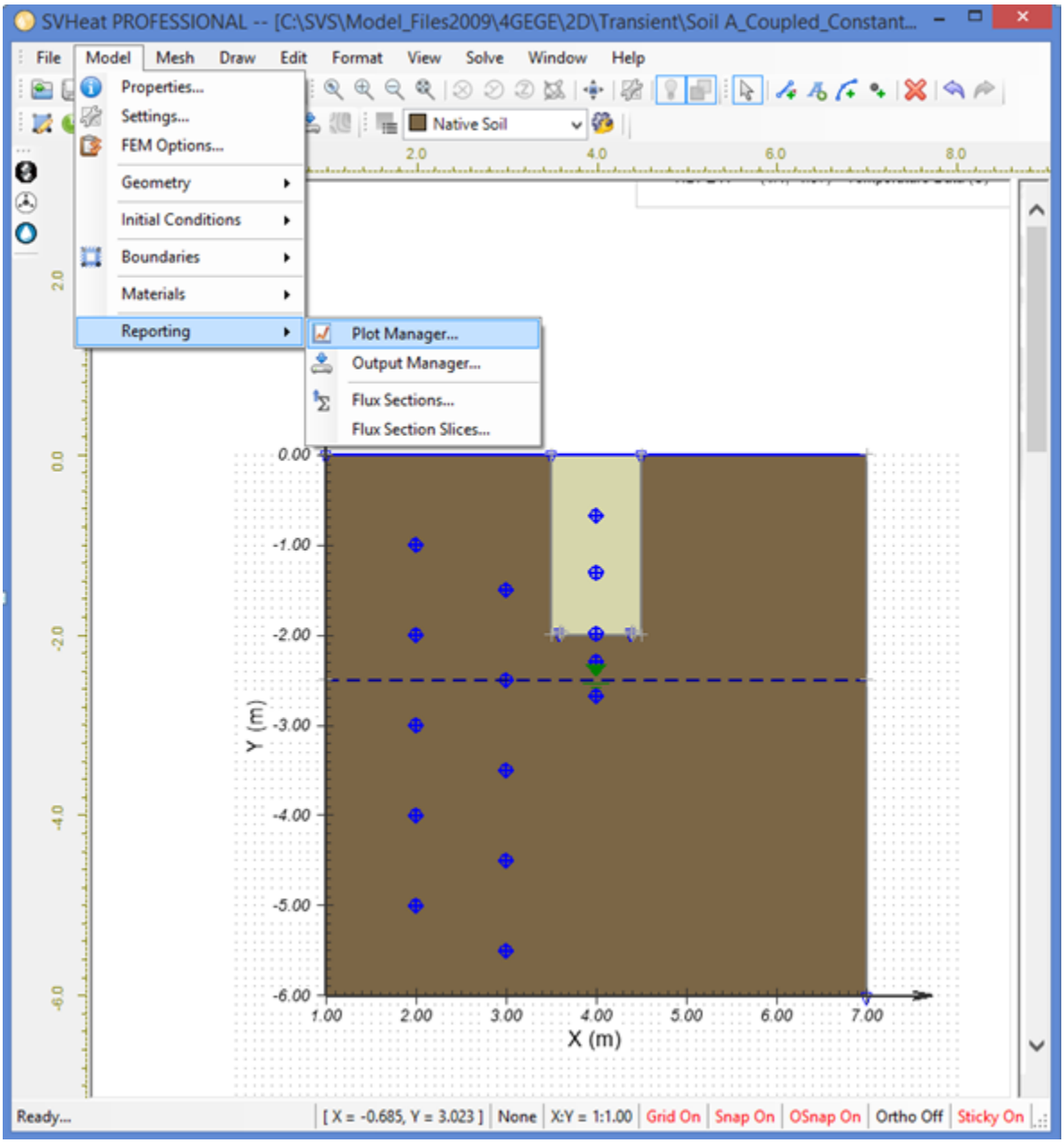

Figure 8-7. The sixth step is to specify model outputs. The blue crosshairs indicate observation points where temperature and volumetric water content measurements will be reported as a function of time (i.e, history plots).

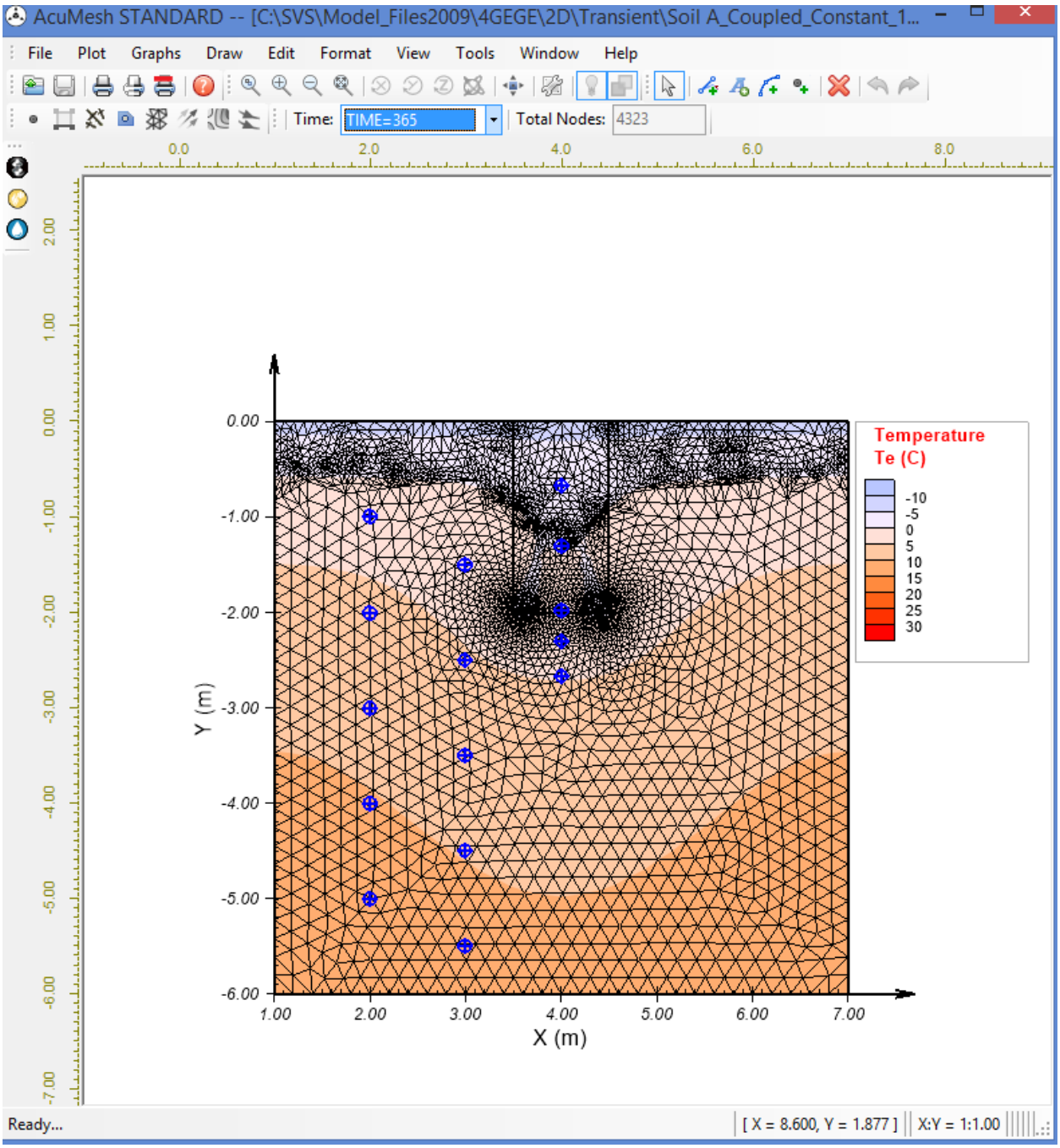

Figure 8-7. The seventh step is to analyze the model and visualize results. Simulation results are visualized using ACUMESH.